

## **NEUP Project 21-24152- Final Report**

Project Start Date: 10/1/2021  
Project End Date: 09/30/2024

Prepared for:  
U.S. Department of Energy - Nuclear Energy University Program  
NEUP Integration Office  
Center for Advanced Energy Studies  
P.O. Box 1625  
Idaho Falls, ID 83415

Technical Point of Contact: Piyush Sabharwal  
National Technical Director: John Jackson  
Federal Manager: Diana Li

Prepared by:  
Hitesh Bindra (Purdue University)  
Ketan Ajay  
Zayed Ahmed  
Broderick Sieh  
Caleb Brooks (University of Illinois)  
Timothy Grunloh  
Anshuman Chaube  
Dimitri Kalinichenko  
Alvin Lee

## **Executive Summary:**

Process heat is envisioned as an alternative application for nuclear reactors, but the supply of heat is always driven by the process coolant conditions and indirect heat transfer through a secondary or tertiary heat transfer fluid. This makes design and integration complex, and particularly uneconomical. Most of the thermally driven hydrogen generation processes or fertilizer production processes involve endothermic chemical reactions in a hot catalytic bed. The microreactors are uniquely suited for remote deployment to provide thermal or electrical energy needs. This project explored the technical and economic feasibility of these microreactors integrated with chemical processes for agricultural applications such as hydrogen to operate combines and other farm equipment, and ammonia for use as a fertilizer.

Microreactors are small sized nuclear reactors rated at power levels  $< 20$  MWth, which can be readily customized based upon the end use requirement. Reactor cooling systems are simplified and are designed to operate at much higher temperatures than most of the existing light water reactors. The reactor coolant system designs under development includes heat pipe design with Na-K fluid, and high temperature helium cooled micro-configuration of High Temperature Gas-Cooled Reactors (HTGRs).

Due to their smaller size, microreactors are uniquely positioned to act as a dependable distributed energy source. Their small size allows them to be deployed at remote locations or locations which have accessibility limitations for larger nuclear power plants. They are ideally suited for the unique process energy needs for energy-intensive remote operations such as those involved in mining and agriculture. Heavy machines involved in these industries are currently operated using gasoline or natural gas. The transportation or storage of conventional fossil fuels can be expensive or challenging for these remote operations. In addition, with the emphasis on clean environment and reduced carbon emissions, there is demand to replace them with hydrogen as a high power density fuel, without burning hydrocarbons. Microreactors can provide process heat to convert locally available raw materials such as water, agro or bio waste, naphtha feed- for generating hydrogen to operate heavy machines. The major advantage of microreactors in those applications is that they don't have continuous refueling needs and provide continuous heat and electricity for generating fuels like hydrogen or direct process heat in the form of hot process fluid. In agricultural applications, microreactors can help build a sustainable ecosystem by catering to the energy needs of agriculture machinery or providing process heat for producing fertilizers, and agriculture or farm waste can be processed using nuclear heat to generate hydrogen. Hydrogen can in turn power the combines and tractors. The core de-

sign of microreactors, including the primary reactor coolant system, is currently being investigated at DOE national laboratories and private companies. However, the integration of microreactors for different end-use applications needed more conceptual research to improve their deployment potential. Although nuclear power plants have been previously used to provide process heat for water purification, fertilizer production, and district heating, the process heat integration was retrofitted to the existing nuclear power plant and thus was not the optimal integration method to dispatch heat. In the case of microreactors, the design objective is to provide combined heat and power— therefore techno-economically more optimal integration strategy can be explored. The first task of this report reviews different microreactor designs and their constraints in delivering process heat.

The typical approach to tap into a nuclear reactor system for extracting process heat is done with the help of primary-to-secondary or secondary-to-tertiary medium heat transfer via fluid circuits. The use of multiple fluid and indirect heat exchange circuits to transfer energy from reactor primary coolant to the chemical process plant leads to higher destruction of exergy and increase in parasitic losses.

Moreover, in order to deliver process heat from microreactors with Na-K heat pipe design or Helium cooled micro-HTGR design, the final heat transport fluid (HTF) carrying the heat must be compatible with the chemical process. This is conventionally done by using steam or air as final HTF. In case of Na-K heat pipe type microreactor designs, the primary reactor coolant Na-K circulates within the large number of small pipes and exchanges heat with secondary medium indirectly through the tube surfaces. In micro-HTGRs, primary coolant helium transfers heat to an intermediate molten salt loop (e.g. in USNC design) or operates the Brayton cycle. With a conventional approach, the heat from these Na-K pipes or molten salt intermediate loops can be dispatched for chemical processes using air or steam but it is quite challenging because it can only be done at very high pressures and process endures substantial parasitic losses. In addition, due to the large volume of such heat transport systems, it can make the system bulky or incompatible with microreactors.

The process integration can be made techno-economically feasible if the integration is simple and does not involve additional intermediate heat transfer fluid circuits. During the last decade, use of particulate flows (flow of small solid particles as an HTF) or granular ceramic media to extract high temperature thermal energy from solar receivers has gained attraction, and Sandia National Laboratory successfully demonstrated the critical technological components. The direct benefit of heating granular ceramic media or solid particle flows is that the solid particles offer large thermal capacity and chemical inertness, thus making them

attractive for equipment design on the secondary side. One approach explored here directly heats catalyst particles, involved in the typical chemical process application, from the primary or secondary coolant and then uses the hot catalytic bed for chemical reaction. In this design, solid catalyst particles flow under gravity over the hot tubes containing high temperature coolant and exit the heat exchanger at high desirable temperature and enter into the chemical reactor. This equipment is called the Moving Packed Bed Heat Exchanger (MPBHX). After the chemical process is complete, the catalysts will be regenerated and re-circulated via conveyer belts over the MPBHX, and the cycle continues. The economic feasibility of integrating MPBHX, compared to conventional approaches, is analyzed.

Agriculture consumes a large fraction of energy resources for fertilizer production and operation of agriculture machinery. It is almost impossible to make agriculture self-sustaining given current agricultural practices, but with the efficient use of nuclear energy, it can be made more sustainable while reducing carbon emissions. Mobile reactors offer ample opportunities to produce energy savings and reduce greenhouse emissions; additionally, there is substantial interest in creating modular hydrogen and ammonia production in rural communities. Agriculture machines (e.g., tractors, combines) are currently operated using diesel or gasoline. The use of fossil fuel leads to large amount of CO<sub>2</sub> emissions and also makes agriculture dependent on transportation and storage of these fuel. By producing hydrogen from biomass as described in Task 4 using microreactors, these machines can be powered locally. There is more biomass available in the United States than is required for food and animal feed needs. With the anticipated improvements in agricultural practices, it is projected that up to 1 billion dry tons of biomass can be available for energy use annually. But growing more biomass requires energy, as mentioned earlier, for machines and fertilizers.

The Haber-Bosch process (400–500° C) process utilized to create ammonia consumes 1–2% of the world's total energy due to its low efficiency (i.e., 15%) and sustains 40% of the world's population. In 2017, 180 MT/year of ammonia were produced – 80% used to produce fertilizer – and production is expected to increase to 270 MT/year by 2050. Nuclear-based ammonia synthesis outperforms natural gas-fed steam methane reforming in most environmental categories (e.g., global warming potential, ozone depletion potential, acidification potential, etc.). The final task involved the technical and economical evaluation of using the microreactors for directly heating catalytic reactor beds in the Haber-Bosch process and compare this approach with existing methods. Fertilizer production and agricultural machines consume more than 70% of the total farm energy use. The final goal of this task was to perform an overall analysis on microreactor capabilities for providing agricultural energy needs by– generating hydrogen fuel from agrowaste to

power machines and supplying process heat for fertilizer production. Overall techno-economic assessment of clean microreactor driven agricultural ecosystem is conducted and presented.

<b>Table of Contents</b>	<b>Page</b>
Task 1: Microreactors for hydrogen generation review	1
Task 2: Heat exchanger integration options	10
Task 3: Hydrogen and ammonia generation pathways	22
Task 4: Economics of heat exchanger integration	36
Task 5: Techno-economic feasibility of sustainable agriculture using micro Reactors	45
Task 5 (Illinois): Coupling and economic analysis of nuclear microreactor enabled ammonia production – Demand side analysis	65

# Task 1: Microreactors for hydrogen generation review

## 1 Introduction

In an effort to mitigate climate change, low carbon energy solutions are being explored. One source of clean baseload energy is nuclear power, which is safe and reliable, has no direct emissions, and has median life cycle emissions (for instance, from plant construction; nuclear fuel mining, milling, and processing) lower than both solar photovoltaic and wind power sources [1–4]. The significance of nuclear power is also evidenced by its inclusion in near- and long-term emission reduction goals of nations such as the United States, China, France, and Japan [5–8]. However, nuclear power plants have seen an increase in construction costs and construction times in the United States, and building a conventional, large-scale nuclear power station is perceived as a high risk endeavor [9–12]. Therefore, there is renewed interest in smaller nuclear power plants that require lower capital costs [13].

One such nuclear power technology is microreactors, which can typically generate up to 20 MW<sub>th</sub> [14]. They are being developed for applications such as integration with remote microgrids, supporting key military infrastructure and disaster relief efforts, and for process heat [15–19]. Due to their smaller size, microreactors are uniquely positioned to act as a dependable distributed energy source. Additionally, the reduced footprint allows them to be deployed at remote locations or locations which have accessibility limitations for larger nuclear power plants. They are ideally suited for the unique needs of energy intensive remote operations such as mining and agriculture. Potential for global market demand has also been demonstrated, along with some significant challenges [20]. As a result, efforts are underway to deploy microreactors as early as 2027 [17, 21]. Microreactors offer not only distributed electricity sources but also localized sources of reliable heat and power without any short-term (< 2–3 year) refueling needs. The process heat applications may be important also from the perspective of maximizing the economic potential of a microreactor, as they are at a disadvantage due to economies of scale, high leakage and low power density, high operation and maintenance costs per unit energy output, and challenges associated with manufacturing, especially advanced fuel fabrication [22].

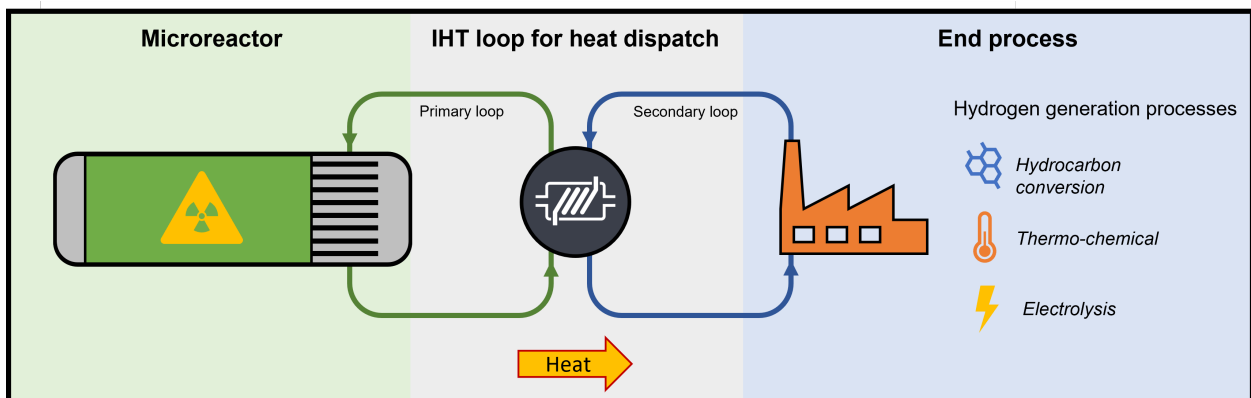


Figure 1. Integration of a microreactor with hydrogen generation processes.

Heavy machines involved in the process industries are currently operated using gasoline or natural gas. The transportation or storage of conventional fossil fuels can be expensive or challenging for these remote operations. In addition, with the emphasis on environment-friendly practices and reduced carbon emissions, there is demand to replace them with hydrogen as a high power density fuel, without burning hydrocarbons. Microreactors can provide process heat to convert locally available raw materials such as water, agro/bio waste, or naphtha feed to the compounds necessary for hydrogen production. If the existing hydrogen generation methods can be integrated with the microreactor design concepts, there is a potential for the widespread deployment of the microreactor technology (see Figure 1). But dispatching energy from microreactors for hydrogen generation involves process integration, which requires review of three main components: hydrogen generation processes, microreactor design concepts, and intermediate heat exchangers which deliver the reactor heat to the hydrogen generation process. Hydrogen cogeneration has long been considered as an option to utilize waste heat from nuclear power plants [23–25]. Hydrogen has been identified as a potentially impactful energy storage and conversion medium that could substantially reduce greenhouse gas emissions across multiple energy sectors, especially if generated from low carbon sources such as nuclear power or renewables [26–32]. Hence, it is imperative that hydrogen cogeneration and process heat utilization strategies should be assessed for compatibility with emerging microreactor designs. This review analyses microreactor designs and components such as intermediate heat exchangers from the perspective of process heat applications such as hydrogen cogeneration and industrial heat systems.

## 2 Microreactor designs review

An overview of currently available commercial microreactor designs is presented, based on data supplied largely from the reactor designers. Some data have been received through private communication with reactor manufacturers. In case specific operating pressures are not available in literature, the operating pressure of reactors with high boiling point-coolants has been assumed  $\approx 1$  atm. The salient features of each design are summarized in Table I. The relevant data may change as the reactors are presently undergoing rapid development.

The Westinghouse eVinci Reactor is a 0.2-5 MW<sub>e</sub>/2-20 MW<sub>th</sub> heat pipe reactor that is inspired by NASA's Kilopower and Megapower reactors [33–35]. The reactor has a solid core with fuel channels. Each fuel channel is located in the vicinity of at least two liquid sodium heat pipes for efficient heat transfer and safety through redundancy. A decay heat exchanger is present to remove decay heat through the heat pipes. The heat pipes obviate the need for a mechanical pump, valves, or other components of a typical LWR primary loop. The power conversion system is based on the Brayton cycle. Current candidate fuels include uranium in oxide, silicide, and metallic form moderated by metal hydride. Specifically, high-assay low-enriched uranium (HALEU) tri-structural isotropic (TRISO) fuel has been mentioned as the fuel of choice [13,20,36]. The predicted enrichment is 5-19.75% [35]. The refueling interval is over 3 years, with Westinghouse claiming the period between refueling to be as long as 10 years, after which the entire unit is replaced [33, 35, 36]. The reactor operates at less than 1 atm of pressure. The primary heat exchanger comprises of annular tubes around the ex-core condenser. Safety measures for major accidents are built into the design, and the solid core has strong negative temperature feedback. Westinghouse aims to be ready for commercial deployment by 2025.

X-energy's Xe-Mobile is a pebble bed HTGR capable of producing 7.4 MW<sub>e</sub>/20 MW<sub>th</sub> [21, 37]. The core is cooled by helium, and the power conversion system is based on the Rankine cycle [35]. The reactor is fueled by HALEU UCO in TRISO particle form with 19.7% enrichment. The lifetime of the core, which operates at full power for 3 years without refueling, is predicted to be approximately 40 years [35, 37]. It is

designed as a power source for military bases, disaster relief efforts, and remote communities.

BWX Technologies Inc. (BWXT) is developing a TRISO-fueled HTGR called BWXT Advanced Nuclear Reactor (BANR) [21]. The reactor is rated at  $17 \text{ MW}_e/50 \text{ MW}_{th}$ , is cooled by helium, and is moderated by graphite [36]. The proposed refueling interval is 5 years. Like many other microreactors, it is also designed to be easily transportable by rail, truck, or military aircraft. The UCO TRISO fuel is in a graphite matrix, and has an enrichment of 19.75% [38]. The reactor operates in either a power generation or cogeneration configuration, both based on a Rankine cycle system. The reactor has passive heat removal and a negative reactivity temperature coefficient. Reactivity control is achieved through mechanical means. BWXT is exploring the use of nitride fuel and the use of direct Brayton or combined cycle to improve core life and efficiency.

General Atomics' (GA) microreactor design, the GA Micro, is a 4-10  $\text{MW}_e$  HTGR [17]. The refueling period is projected to be greater than 10 years. The reactor can fit in a standard CONEX shipping container. The reactor concept promises the ability to utilize advanced fuel and materials to improve performance and safety as well as the ability to rapidly respond to large fluctuations in demand, as seen at military bases.

NuScale offers two reactor designs in the microreactor power range [17]. One is a heat pipe reactor in the sub-20  $\text{MW}_e$  range [36]. This reactor design is a liquid metal heat pipe option that utilizes metallic fuel and uses liquid metal as a moderator. The operating pressure is expected to be close to atmospheric pressure. The refueling interval is 10 years. The design proposes the utilization of minimal site infrastructure, rapid construction and deployment, and fully-automated operation. The second design is the NuScale Power Module (NPM), which is an LWR in the 10-50  $\text{MW}_e/40\text{-}160\text{MW}_{th}$  range [35]. The operating pressure is 12.7 MPa [39]. The design is an entirely self-contained module that encloses both the primary and secondary loop in a containment vessel, and can be transported to a site where multiple modules can be interconnected. The modules are situated underwater which serves as a heat sink. The core utilizes natural circulation, minimizing the chances of safety incidents associated with the malfunction of pumps and valves. The fuel assembly is a shorter variant of the  $17 \times 17$  pressurized water reactor (PWR) assembly. It can be fueled by less than 5%  $\text{UO}_2$  ceramic, 15-20% U-Zr Lightbridge, or HALEU fuel. The refueling interval is 10 years, and the overall lifetime of the power module is 60 years. The reactor offers passive safety with no need for operator action and it requires no offsite power.

The Ultra Safe Nuclear Corporation (USNC) micro modular reactor (MMR) is a 5  $\text{MW}_e/15 \text{ MW}_{th}$  HTGR design that is cooled by helium and moderated by graphite [40]. It is designed to use two reactors with an intermediate molten salt loop, which is coupled to a Brayton power cycle system [35]. The operating pressure is 3 MPa in the primary helium loop, and 0.5 MPa in the secondary molten salt loop [40]. It is fueled by a proprietary fuel element, named the Fully Ceramic Micro Encapsulated fuel, that is a type of pellet that encapsulates approximately 7644 TRISO particles. The fuel enrichment level is 19.75%. The reactor is operated for a lifetime 20 years without refueling. The plant has been designed for providing power to remote areas, serving as a backup power generator, desalination, process heating, and supporting military and critical infrastructure. Each plant is equipped with a secondary facility that uses molten salt thermal storage to extract process heat. The core inlet and outlet coolant temperatures are 300 °C and 630 °C, whereas the molten salt secondary loop's inlet and outlet temperatures are 275 °C and 565 °C. The power density is a relatively low  $1.24 \text{ W/cm}^3$ , the TRISO particles are extremely safe, and the specific heat capacity of the core is high, leading to thermal stability within the core. The reactor core is meltdown proof and has a variety of passive and active safety features. Much of the reactor is situated underground, and the reactor operation is fully autonomous [35]. USNC is planning to begin construction between 2023-2027.

The HolosGen Holos Quad microreactor is a 10-13 MW<sub>e</sub> reactor, with modules just as portable as the aforementioned microreactor designs [41]. It is comprised of sub-critical power modules that make the reactor critical when placed in proximity to each other within the core containment. It is fueled by 8-19% enriched TRISO particles encased in fuel cartridges, with the most likely enrichment being 10-15% [35]. The reactor can operate without refueling for 12-20 years. The overall lifespan of a single reactor unit is predicted to be 60 years. The reactor can utilize the Brayton power cycle, or a bottoming Rankine power cycle using organic working fluids to recover waste heat for efficiency enhancements and process heat applications. These systems also assist with decay heat removal in case of a shutdown. The Brayton cycle-based design is heavily influenced by a turbojet engine [35]. The efficiency of the overall system is 45-60%. The primary working fluid is either helium or CO<sub>2</sub>. The former requires inlet and outlet pressures of 70 and 35 bar, whereas the latter requires 200 and 70 bar respectively [41]. The targeted core outlet temperature is 850 °C, and the projected temperature available for process heat is approximately 620 °C. During decay heat removal, the reactor relies on being passively cooled by air. The reactor design has multiple passive safety features which enable it to withstand a variety of design basis accidents.

Oklo's Aurora microreactor is a 1.5 MW<sub>e</sub>/4 MW<sub>th</sub> sodium heat pipe reactor [35]. It can be fueled by metallic uranium-zirconium fuel with less than 20% enrichment or with HALEU fuel [17,35]. The refueling interval is 10 years. Heat from the core is transferred to a Brayton cycle power conversion system using sodium heat pipes. The reactor power is controlled by external reflectors and control rods. Due to its small size, the design can dissipate decay heat through conduction into structural materials and to its surroundings. The balance of plant system is based on a super-critical CO<sub>2</sub> power conversion system [42]. The reactor is encased in multiple layers, including a robust cask, and is housed underground for safety. The reactor is intended to serve remote communities in addition to military and industrial sites [17].

LeadCold's SEALER is a 3 MW<sub>e</sub> lead-cooled fast reactor design that has been designed in collaboration with the Swedish Royal Institute of Technology [43]. It is fueled by 19.75 wt% UO<sub>2</sub>, and is operated for 27 full power years in a sealed fashion to circumvent proliferation issues. The power conversion system is based on the Rankine cycle. The operating pressure of the primary loop is expected to be near atmospheric pressure, while the steam generator's internal pressure is at least 13 MPa. The steam generator has an outlet temperature of 417 °C. The designers intend to compete with diesel generators in remote areas, especially in the Arctic mining communities. Many passive safety features are built in, and some transient analyses are presented to demonstrate this.

Urenco's U-Battery is a helium-cooled HTGR rated at 4 MW<sub>e</sub>/10 MW<sub>th</sub> [44]. It is fueled by TRISO particles and moderated by graphite. The output heat is mentioned as 710 °C, which allows for some hydrogen cogeneration opportunities. The operational lifetime of the plant is mentioned as 30 years to 60 years, with the core's lifetime being 5 effective full-power years [13,35]. The design may be scaled up to 20 MW<sub>th</sub> [35]. The TRISO fuel has less than 20% enrichment. The designers are exploring the use of the thorium fuel cycle as well. The design is a dual-circuit primary loop with an indirect Brayton power cycle that uses nitrogen as the working fluid for power generation.

The Nugen Engine is a 1-3 MW<sub>e</sub> HTGR [36]. It is cooled by helium and fueled by TRISO fuel. Nugen is also working on a reactor of size 1-50 MW<sub>e</sub> [45]. The reactor claims to provide all the aforementioned microreactor applications such as load following, passive safety, and process heat. Additionally, the designers claim the reactor can be used for nuclear space propulsion and energy for extraterrestrial bases.

Radiant is designing a 1.2 MW<sub>e</sub>/3.5 MW<sub>th</sub> HTGR called Kaleidos Battery [36,46,47]. The coolant of choice is helium, and the reactor is fueled by TRISO fuel and moderated by graphite. [36] The refueling interval is 4-6 years.

Alpha-Tech Research Corp (ARC) Nuclear Generator is a 12 MW<sub>e</sub>/30 MW<sub>th</sub> molten salt reactor (MSR) concept fueled by low-enriched uranium (LEU) [48, 49]. The coolant is a fluoride salt and the reactor is moderated by yttrium hydride [36]. The manufacturers claim the reactor can provide process heat at temperatures upwards of 700 °C, which is intended for applications such as green hydrogen, water desalination, manufacturing, magnesium production, coal gasification, and coal pyrolysis [48]. The reactor's passive safety features stem from the use of molten salt, which does not boil at elevated temperatures at atmospheric pressure. The reactor is designed such that loss of power results in the salt freezing within the reactor, containing the fission products. Multiple units can be combined together, and each core and the necessary shielding material is transportable via semi-truck. The company has its own proprietary fuel reprocessing technology as well.

MicroNuclear's Micro Scale Nuclear Battery is a 5-10 MW<sub>e</sub>/10-20 MW<sub>th</sub> molten salt based heat pipe reactor [35, 49]. It is fueled by UF<sub>4</sub> dissolved in a FLiBe carrier salt, with an enrichment of 20% with 5% fuel loading in salt [36]. The use of molten salt suggests operating temperatures close to atmospheric pressure. The design proposes using a shipping cask confinement to transport the reactor to remote locations [35]. The reactor relies on natural circulation for circulating the molten salt in the core, and utilizes sodium or potassium heat pipes to transport heat to a helium Brayton-cycle. The refueling interval is estimated to be 10 years.

The Hydromine TL-X is a lead-cooled fast reactor with an output of 20 MW<sub>e</sub>/60 MW<sub>th</sub> [35]. The reactor operates at atmospheric pressure and has multiple active and passive safety features. The reactor does not require offsite power or operator intervention for passive shutdown or decay heat management. The reactor is intended for use in remote locations. The operating lifetime is 30 years, with refueling intervals of 8 years. The core is a "monolithic cylindrical bundle" in a triangular lattice, meant to be extracted as a whole for fuel replacement. This follows the model of transporting a finished unit on-site and using central facilities for fuel servicing. The candidate fuels under consideration include uranium oxide, nitride, and carbide, with enrichment less than 20%. In 2021, Hydromine's microreactor and small modular reactor concepts were acquired by Newcleo, Ltd. [50].

**Table I. Summary of microreactor designs**

Reactor	Design	Power	Max. Process Heat Temp.	Operating Pressure	Coolant	Power Conversion System
Westinghouse eVinci	Heat Pipe <sup>[33]</sup>	0.2-5MW <sub>e</sub> /2-20MW <sub>th</sub> <sup>[33,49]</sup>	600°C <sup>[33]</sup>	<1atm <sup>[34]</sup>	Na <sup>[36]</sup>	Brayton Cycle <sup>[35]</sup>
Xenergy Xe-mobile	HTGR <sup>[36]</sup>	7.4 MW <sub>e</sub> /20 MW <sub>th</sub> <sup>[36]</sup>	N/A	N/A	He <sup>[36]</sup>	Rankine Cycle <sup>[35]</sup>
BWXT BANR	HTGR <sup>[36]</sup>	17 MW <sub>e</sub> /50 MW <sub>th</sub> <sup>[36]</sup>	N/A	N/A	He <sup>[36]</sup>	Rankine/Brayton Cycle <sup>[38]</sup>
GA Micro NuScale	HTGR <sup>[36]</sup>	4-10 MW <sub>e</sub> <sup>[36]</sup>	N/A	N/A	Gas <sup>[36]</sup>	N/A
Microreactor NuScale NPM	Heat pipe <sup>[36]</sup>	≥20 MW <sub>e</sub> <sup>[36]</sup>	N/A	N/A	Liquid metal <sup>[36]</sup>	N/A
	LWR <sup>[35]</sup>	10-50 MW <sub>e</sub> /40-160MW <sub>th</sub> <sup>[35]</sup>	N/A	12.7 MPa <sup>[39]</sup>	Water <sup>[35]</sup>	Rankine Cycle <sup>[35,39]</sup>
USNC MMR	HTGR <sup>[40]</sup>	5 MW <sub>e</sub> /15 MW <sub>th</sub> <sup>[40]</sup>	565°C <sup>[40]</sup>	3MPa(1°), 0.5MPa(2°) <sup>[40]</sup>	He(1°), molten salt(2°) <sup>[40]</sup>	Rankine Cycle <sup>[35]</sup>
HolosGen Holos Quad	HTGR <sup>[36]</sup>	10-13MW <sub>e</sub> <sup>[41]</sup>	620°C <sup>[41]</sup>	70bar(1°)/35bar(2°) <sup>[41]</sup>	He, sCO <sub>2</sub> <sup>[41]</sup>	Brayton Cycle <sup>[35,41]</sup> /Organic Rankine Cycle <sup>[41]</sup>
Oklo Aurora	SFR Heat pipe <sup>[36,42]</sup>	1.5 MW <sub>e</sub> /4 MW <sub>th</sub> <sup>[36,42]</sup>	N/A	N/A	Na <sup>[36,42]</sup>	N/A
LeadCold SEALER	Lead-cooled <sup>[43]</sup>	3-10 MW <sub>e</sub> <sup>[43]</sup>	417°C <sup>[43]</sup>	N/A	Pb <sup>[43]</sup>	Rankine Cycle <sup>[43]</sup>
Urenco U-Battery	HTGR <sup>[44]</sup>	4MW <sub>e</sub> /10 MW <sub>th</sub> <sup>[44]</sup>	710°C <sup>[44]</sup>	N/A	He, N <sup>[44]</sup>	Brayton Cycle <sup>[35]</sup>
Nugen Engine	HTGR <sup>[36,45]</sup>	1-3 MW <sub>e</sub> <sup>[36,45]</sup>	N/A	N/A	He <sup>[36,45]</sup>	N/A
Radiant Kaleidos	HTGR <sup>[36]</sup>	1.2 MW <sub>e</sub> /3.5 MW <sub>th</sub> <sup>[46,49]</sup>	N/A	N/A	He <sup>[36]</sup>	N/A
ARC Nuclear Generator	MSR <sup>[36]</sup>	12 MW <sub>e</sub> /30 MW <sub>th</sub> <sup>[36]</sup>	700°C <sup>[48]</sup>	N/A	Fluoride salt <sup>[36]</sup>	N/A
Micro Nuclear Micro Scale Nuclear Battery	MSR heat pipe <sup>[36]</sup>	5-10 MW <sub>e</sub> /10-20 MW <sub>th</sub> <sup>[36,49]</sup>	N/A	N/A	UF <sub>4</sub> +FLiBe (1°), Na/K heat pipe + He(2°) <sup>[35]</sup>	Brayton Cycle <sup>[35]</sup>
Hydromine/Newcleo TL-X	Lead-cooled <sup>[35]</sup>	20 MW <sub>e</sub> /60 MW <sub>th</sub> <sup>[35]</sup>	N/A	N/A	Pb <sup>[35]</sup>	N/A

## References

1. Anil Markandya and Paul Wilkinson. Electricity generation and health. *The Lancet*, 370(9591):979–990, September 2007.
2. Staffan A. Qvist and Barry W. Brook. Environmental and health impacts of a policy to phase out nuclear power in Sweden. *Energy Policy*, 84:1–10, September 2015.
3. U.S. Energy Information Administration (EIA). Electric Power Monthly. Technical report, Department of Energy, 2021.
4. IPCC. *Climate Change 2014 Mitigation of Climate Change: Working Group III Contribution to the Fifth Assessment Report of the Intergovernmental Panel on Climate Change*. Cambridge University Press, Cambridge, 2014.
5. The White House. President Biden Sets 2030 Greenhouse Gas Pollution Reduction Target Aimed at Creating Good-Paying Union Jobs and Securing U.S. Leadership on Clean Energy Technologies, April 2021.
6. X. Jin Yang, Donghui Zhang, Mi Xu, and Jinying Li. China’s Nuclear Power Goals Surge Ahead. *Science*, April 2013. Publisher: American Association for the Advancement of Science.
7. AP News. France to build new nuclear reactors to meet climate goals, November 2021. Section: Climate.
8. Electricity Review Japan 2019. Technical report, The Federation of Electric Power Companies of Japan, 2019.
9. Jessica R. Lovering, Arthur Yip, and Ted Nordhaus. Historical construction costs of global nuclear power reactors. *Energy Policy*, 91:371–382, April 2016.
10. Fiona Caroline Saunders and Ellen A. Townsend. Delivering new nuclear projects: a megaprojects perspective. *International Journal of Managing Projects in Business*, 12(1):144–160, January 2018. Publisher: Emerald Publishing Limited.
11. Ioannis N. Kessides. Nuclear power: Understanding the economic risks and uncertainties. *Energy Policy*, 38(8):3849–3864, August 2010.
12. Lucas W. Davis. Prospects for Nuclear Power. *Journal of Economic Perspectives*, 26(1):49–66, February 2012.
13. Raffaella Testoni, Andrea Bersano, and Stefano Segantin. Review of nuclear microreactors: Status, potentialities and challenges. *Progress in Nuclear Energy*, 138:103822, August 2021.
14. Bahman Zohuri. *Nuclear Micro Reactors*. Springer International Publishing, Cham, 2020.
15. Ruairidh Macdonald and John E. Parsons. The Value of Nuclear Microreactors in Providing Heat and Electricity to Alaskan Communities. Technical report, MIT Center for Energy and Environmental Policy Research, 2021.
16. Hossam A. Gabbar, Muhammad R. Abdussami, and Md Ibrahim Adham. Micro Nuclear Reactors: Potential Replacements for Diesel Gensets within Micro Energy Grids. *Energies*, 13(19):5172, January 2020. Number: 19 Publisher: Multidisciplinary Digital Publishing Institute.

17. Marcus Nuclear Energy Institute. Roadmap for the Deployment of Micro-Reactors for U.S. Department of Defense Domestic Installations. Technical report, Nuclear Energy Institute, October 2018. Section: Technical Reports.
18. Molly Ross and Hitesh Bindra. Estimating energy storage size for nuclear-renewable hybrid energy systems using data-driven stochastic emulators. *Journal of Energy Storage*, 40:102787, 2021.
19. Molly Ross, T-Ying Lin, Isaiah Wicoff, Broderick Sieh, Piyush Sabharwall, Donald E McEligot, and Hitesh Bindra. Passive heat removal in horizontally oriented micro-htgrs. *Progress in Nuclear Energy*, 156:104530, 2023.
20. David E. Shropshire, Geoffrey Black, and Kathleen Araujo. Global Market Analysis of Microreactors. Technical Report INL/EXT-21-63214-Rev000, Idaho National Lab. (INL), Idaho Falls, ID (United States), July 2021.
21. US DOD. DOD Awards Contracts for Development of a Mobile Microreactor, 2020.
22. Kororush Shirvan, Jacopo Buongiorno, Ruairidh MacDonald, Bradley Dunkin, Sacit Cetiner, Earl Saito, Thomas Conboy, and Charles Forsberg. UO<sub>2</sub>-fueled microreactors: Near-term solutions to emerging markets. *Nuclear Engineering and Design*, 412:112470, October 2023.
23. S. Yalçın. A review of nuclear hydrogen production. *International Journal of Hydrogen Energy*, 14(8):551–561, January 1989.
24. Xing L. Yan and Ryutaro Hino, editors. *Nuclear Hydrogen Production Handbook*. CRC Press, Boca Raton, May 2011.
25. Sümer Şahin and Hacı Mehmet Şahin. Generation-IV reactors and nuclear hydrogen production. *International Journal of Hydrogen Energy*, 46(57):28936–28948, August 2021.
26. Anshuman Chaube, Andrew Chapman, Yosuke Shigetomi, Kathryn Huff, and James Stubbins. The Role of Hydrogen in Achieving Long Term Japanese Energy System Goals. *Energies*, 13(17):4539, January 2020. Number: 17 Publisher: Multidisciplinary Digital Publishing Institute.
27. Anshuman Chaube, Andrew Chapman, Akari Minami, James Stubbins, and Kathryn D. Huff. The role of current and emerging technologies in meeting Japan’s mid- to long-term carbon reduction goals. *Applied Energy*, 304:117669, December 2021.
28. Michael Ball and Martin Wietschel. The future of hydrogen – opportunities and challenges. *International Journal of Hydrogen Energy*, 34(2):615–627, January 2009.
29. Sonja van Renssen. The hydrogen solution? *Nature Climate Change*, 10(9):799–801, September 2020. Bandiera\_abtest: a Cg\_type: Nature Research Journals Number: 9 Primary\_atype: Special Features Publisher: Nature Publishing Group Subject.term: Carbon and energy;Climate-change mitigation;Hydrogen energy;Natural gas Subject.term\_id: carbon-and-energy;climate-change-mitigation;hydrogen-energy;natural-gas.
30. Roxanne Pinsky, Piyush Sabharwall, Jeremy Hartvigsen, and James O’Brien. Comparative review of hydrogen production technologies for nuclear hybrid energy systems. *Progress in Nuclear Energy*, 123:103317, May 2020.
31. Hitesh Bindra and Shripad Revankar. *Storage and Hybridization of Nuclear Energy: Techno-Economic Integration of Renewable and Nuclear Energy*. Academic Press, 2018.

32. Andrew Chapman, Kenshi Itaoka, Katsuhiko Hirose, F. Todd Davidson, Kazunori Nagasawa, Alan C. Lloyd, Michael E. Webber, Zeynep Kurban, Shunsuke Managi, Tetsuya Tamaki, Michael C. Lewis, Robert E. Hebner, and Yasumasa Fujii. A review of four case studies assessing the potential for hydrogen penetration of the future energy system. *International Journal of Hydrogen Energy*, 44(13):6371–6382, March 2019.
33. Arafat and Van Wyk. eVinci Micro Reactor. Technical report, Westinghouse Electric Company LLC, 2019.
34. Arafat. Westinghouse eVinci™ Micro Reactor Factsheet. Technical report, Westinghouse Electric Company, 2019.
35. Thomas Palmieri, Michael Corradini, and Paul Wilson. Analysis of the Case for Federal Support of Micro-Scale Nuclear Reactors to Provide Secure Power at U.S. Government Installations. Technical report, University of Wisconsin Institute for Nuclear Engineering Systems, 2021.
36. US DOE-NE. Microreactor Program Winter Review Meeting, March 2022.
37. X-energy. Reactor: Xe-Mobile — X-energy: HTGR | Nuclear Reactors (SMR) & TRISO Fuel.
38. Erik Nygaard. BWXT’s Advanced Nuclear Reactor, January 2021.
39. IAEA. NuScale Power Modular and Scalable Reactor - Design Description. Technical report, IAEA ARIS, 2013.
40. USNC. USNC Micro Modular Reactor (MMR™ Block 1) Technical Information. Technical report, 2021.
41. Claudio Filippone and Kelly Jordan. The Holos Reactor: A Distributable Power Generator with Transportable Subcritical Power Modules. Technical report, engrXiv, June 2017.
42. Oklo. Aurora NRC Application, 2020.
43. J. Wallenius, S. Qvist, I. Mickus, S. Bortot, P. Szakalos, and J. Ejenstam. Design of SEALER, a very small lead-cooled reactor for commercial power production in off-grid applications. *Nuclear Engineering and Design*, 338:23–33, November 2018.
44. URENCO. U-Battery Handout. Technical report.
45. NuGen. Nugen Engine Description.
46. Radiant. Radiant Nuclear.
47. Daniel Moneghan. Microreactors: Miniature Nuclear Energy Sources. Technical Report 000000003002023898, Electric Power Research Institute, 2022.
48. Alpha Tech Research Corp. Innovation for an Affordable, Clean-Energy Future | Alpha Tech Research Corp.
49. Advanced Nuclear Directory 2023. Technical report, Gateway for Advanced Innovation in Nuclear(GAIN), 2023.
50. Nuclear Engineering International. Nuclear technology company Newcleo acquires Hydromine - Nuclear Engineering International.

## **Task 2: Heat exchanger integration options**

### **1 Introduction**

Dispatching energy from a nuclear reactor to a chemical process plant is a crucial technological component for efficient coupling of nuclear reactors to end process use such as thermochemical hydrogen generation [1, 2]. One of the primary constraints for any nuclear reactor system including microreactors is that the primary loop is considered as a barrier for radioactivity, so it is expected to transfer heat to a chemical process plant via indirect heat exchange processes [3, 4]. This coupling requires efficient heat transport between the reactor and end application in an economic and safe manner. This is achieved through the Intermediate Heat Transport (IHT) loop that delivers the heat from the reactor to the end use.

The end use that requires the process heat sets design constraints on the intermediate heat transport loop by specifying a given heat load to be delivered at a given temperature. To efficiently deliver this given load of energy at a given operating temperature, the important considerations of the IHT loop include the choice of the coolant in the loop, the IHX design, and the operating parameters, like loop flowrates, pressures, etc. These considerations are aimed towards achieving the highest heat transfer performance with very low coolant transport requirements. The various hydrogen generation processes discussed in the previous section require process heat delivered at a high temperature for increased process efficiency and improved hydrogen production rates.

The following sections discuss the various considerations for dispatching the process heat along with the challenges of dispatching the heat at high temperatures. A metric to measure the suitability of a coolant, called figure-of-merit, is presented. Various IHX designs are presented along with the corresponding operating parametric range. This discussion aims to provide options to the designer with regards to the coolant selection and heat exchanger design. These sections should also inform the designer of the benefits and the expected challenges attributed to a particular design for dispatching heat supplied by a microreactor to the end use.

### **2 Challenges associated with high temperature heat dispatch**

Transporting heat at high temperatures imposes several unique engineering challenges, especially within the heat exchanger that is subjected to these high temperatures and large temperature gradients. The biggest challenge to be considered in designing high temperature heat exchangers is that of the structural integrity. It is important that the structure of the heat exchanger is able to handle the stresses induced in the material at such elevated temperatures. With temperature drastically increased, the yield strength of most of the commonly used materials decreases by orders of magnitude, especially above 800 °C [5]. This requires the use of thick tubing and excessive material for various components, adding to the high capital cost of the heat exchanger. At these high temperatures, the material used needs to have a good resistance to creep-fatigue due to cyclic temperature fluctuations, which can reduce the operational lifetime of the heat exchanger unit. The pressure drop needs to be low across the heat exchanger as the cost of additional work to pump the

coolant at such high temperatures may become prohibitive. The heat losses to the environment also become significant, thereby presenting the need for careful insulation and compact heat exchanger designs that have minimal surface area exposed to the surroundings [6].

In addition to these considerations, the permeation of hydrogen isotopes through materials is an important challenge. Hydrogen isotopes, especially tritium, can be produced in the reactor core in multiple ways: as a fission products, through the reaction of lithium and boron in graphite components, and He-3 fractions of the helium coolant. Tritium can permeate through the IHX walls into the secondary loop and can end up in the produced hydrogen [7, 8]. Therefore, the indirect heat transfer loops should not allow tritium migration from primary side to secondary side.

### **3 Material selection**

There are three main categories of materials for the heat exchanger structure in high temperature application: iron-based alloys, nickel-based alloy, and ceramics.

Iron based alloys have good mechanical properties up to temperatures of 600 °C but experience high corrosion rates at high temperatures. In atmospheres of high fission neutron irradiation, high ferrite steels have shown good performance up to 750 °C. [9] Therefore there are not many iron-based alloy options for the heat exchangers considered here.

Nickel based alloys have demonstrated potential at high temperatures, specifically for helium and molten salts environments with temperatures up to 750 °C [10]. Amongst the nickel-based-alloys, the top candidates are alloy 617 and alloy 230 [6]. These are relatively new materials and current research is focused on material characterization of physical properties, like resistance to corrosion due to helium impurities, and mechanical properties, like hardness, tensile strength, creep fatigue, oxidation rates, etc [11]. Another nickel-based alloy called Hastelloy XR, which is developed by Mitsubishi for the Japanese HTTR, has very limited open source databases available. This material has a higher corrosion resistance in helium environments than alloy 617, but has inferior creep resistance compared to alloy 617 [12]. Hastelloys, the Nickel-Molybdenum based superalloys are considered as preferred material candidate for handling alkali molten salts due to high corrosion resistance.

While metallic heat exchangers are easier to manufacture and display high strength, the performance of these instruments is limited to temperatures up to 750 °C. For high temperatures, ceramics have shown good performance and high corrosion/creep resistance at a low material cost. However, ceramics are rated for a limited operating pressure due to brittleness [5]. Silicon carbide-based ceramics have shown to be a suitable material for heat exchangers operating at temperatures near 1000 °C. However, oxidation becomes an issue at temperatures beyond 1000 °C. The use of Ceramic matrix composites, which utilize two phases of ceramics have been under development to improve the structural stability at high temperatures. Ceramics have a good potential to be widely used in high temperature applications, but the challenges associated with the manufacturability still remains an issue for heat exchanger applications.

#### **3.1 Secondary or tertiary coolant selection**

The choice of the secondary or tertiary coolant to be used in the heat recovery from the primary or secondary loop poses additional considerations on the system design. The choice of coolants typically used with ad-

vanced nuclear reactors is between water, molten salts, liquid metals, and gases. In selecting a coolant, several considerations need to be addressed that vary from application to application. A good coolant has the following characteristics: low pumping power, high heat transfer rate, low coolant volume for compactness, and low heat loss. A method to compare coolants and characterize heat transfer fluids have been proposed by Kim et al. based on several figures-of-merits (FOMs) which account for the mentioned coolant characteristics [13]. The FOMs facilitate the decision between various coolants based on their metrics, whose importance varies across various applications. These FOMs are calculated based on the thermophysical properties of the fluid under consideration. These FOMs characterize Heat Transfer Performance ( $FOM_{HT}$ ), Pumping Factor ( $FOM_P$ ), Coolant volume factor ( $FOM_{CV}$ ), and Heat loss factor ( $FOM_{HL}$ ).  $FOM_{HT}$  compares the heat transfer rate at the same pumping power for a given geometry.  $FOM_P$  compares the pumping power for a given coolant temperature rise.  $FOM_{CV}$  compares the volume of coolant required for a given heat transfer duty and pumping power. This is particularly useful when the volume occupied by the coolant is restricted.  $FOM_{HL}$  compares the heat loss incurred in the coolant for a same heat duty and pumping power. This metric is useful when the heat transfer loop is required to transfer the heat over very long distances, one that can be expected in nuclear-hydrogen plant coupling [14].

The FOM is calculated using only the thermophysical properties and has the general form: [13]

$$FOM = \frac{k^a \rho^b C_p^c \mu^d}{R_0} \quad (1)$$

where  $k$  is the thermal conductivity,  $\rho$  is the density,  $C_p$  is the specific heat capacity, and  $\mu$  is the dynamic viscosity of the coolant. The corresponding exponents for each FOM are summarized in Table I below. These exponents establish the relationship between a certain thermophysical property and the performance metric. A positive exponent implies that the FOM increases with an increase in the property and a negative exponent implies the contrary. The value of the exponent relates the sensitivity of the FOM to the property. High absolute values suggest a high dependence of the property on the FOM and low absolute values suggest less dependence.

**Table I. Exponents used in FOM calculations**

	$a$	$b$	$c$	$d$
$FOM_{HT}$	0.6	0.58	0.4	-0.47
$FOM_P$	0	2	2.8	-0.2
$FOM_{CV}$	0	0.84	1.16	-0.1
$FOM_{HL}$	-0.6	-0.34	-0.06	-0.44

The FOMs of various coolants are shown in Figure 1. These FOMs include the performance of various coolants with respect to water at 25 °C and 1 atm. The thermophysical properties of the coolant at 7 MPa are evaluated for gases and water. For liquid metals and molten salts, properties are evaluated at atmospheric pressures.

For coolant selection, the higher values of FOMs are preferred. High FOMs lead to high heat transfer capability, low pumping requirements, low coolant volume, and low heat losses to the environment. This metric lays out a guideline for selection of coolants. The optimum coolant can change depending on the specific application.

Liquid metals have very high heat transfer performance while gases have the poorest performance. The pumping performance of gases is also the lowest, while molten salts have the highest pumping performance

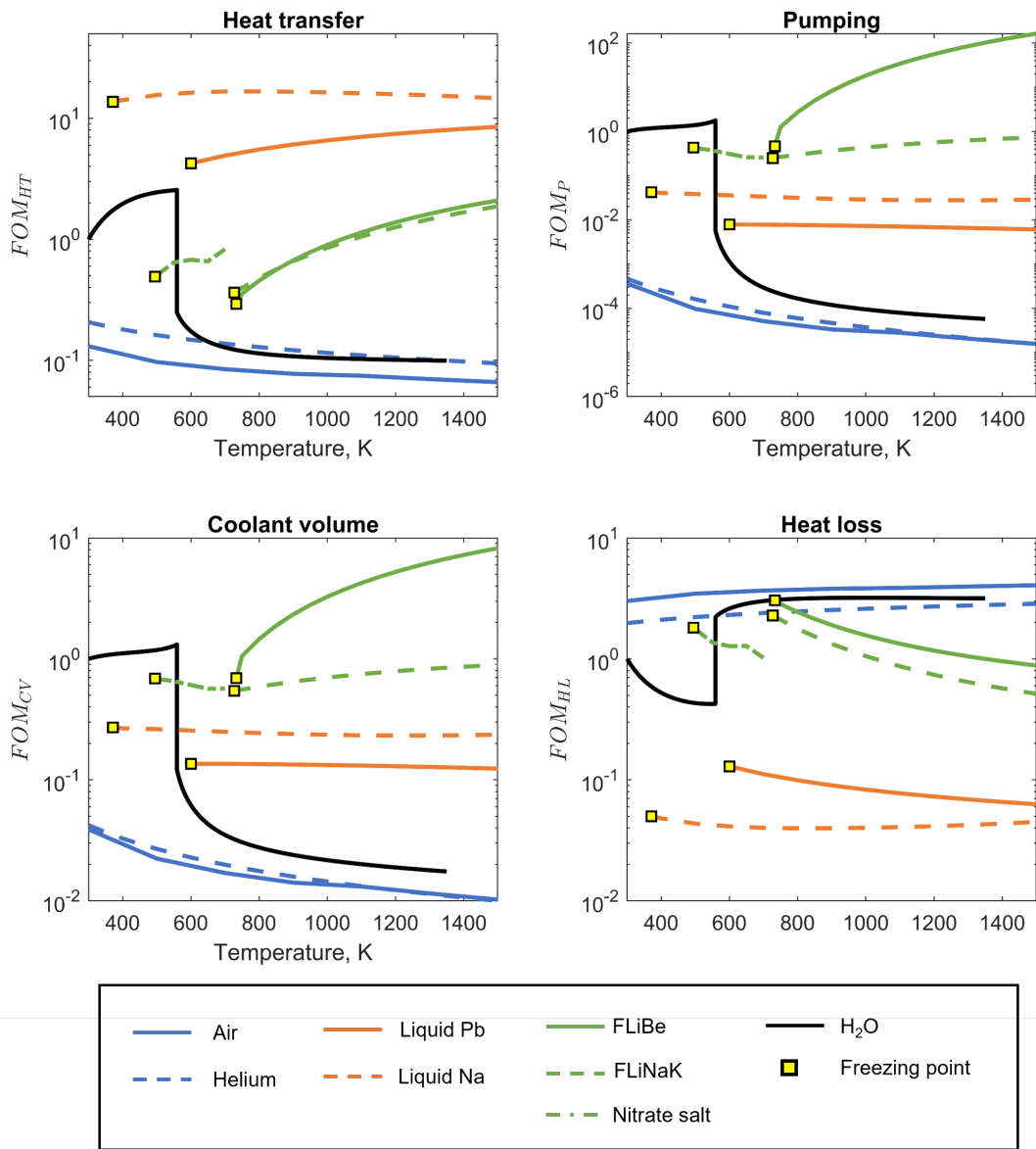


**Figure 1. Figures of Merits of various coolants (Air, Helium and H<sub>2</sub>O at 7 MPa and others at 0.1 MPa).**

due to their low density. Liquid metals have the highest heat loss and therefore the lowest FOM with regards to heat losses, thereby making them less desirable for energy transmission over long distances.

For hydrogen production using nuclear heat, helium and molten salts have been deemed the top candidates [15]. Helium and molten salts have also been considered for dual purpose nuclear plants with hydrogen and electricity cogeneration. It has been shown that the use of low pressure helium as a heat transfer fluid is a viable option, but not for a single-purpose facility dedicated to hydrogen production. Significant benefits can be obtained if the pressure of helium in intermediate heat transport loop is increased. Increasing the pressure from 2 MPa to 7 MPa would decrease the size of the loop by 30% and reduce pumping power by 20% for a single purpose hydrogen generation facility. However, the high pressure and high temperature

pose constraints on the material used in the loop, as the traditional materials exhibit reduced yield strengths at such temperatures. With the use of a molten salt as the coolant, the intermediate loop can be operated at low pressures. Thus, the metallic volume of the intermediate heat transport loop can be reduced by up to 70%, as compared to helium, along with a 40% reduction in pumping power. The use of a molten salt in a single-purpose plant is estimated to increase the overall plant efficiency up to 6% when compared to helium coolant [16]. However, molten salts have several disadvantages including material incompatibility challenges, high cost due to the addition of auxiliary system for coolant handling, etc.

## **4 Process Heat Dispatch Options**

For dispatching the process heat at high temperatures, the nuclear energy system designs have considered few potential IHX candidates for NR-HPP integration (see Table II). These are namely shell and tube heat exchangers, helical shell and tube heat exchangers, plate heat exchangers, printed circuit heat exchangers (PCHE), and some advanced designs including foam heat exchangers, capillary heat exchangers, etc [17]. This section discusses the various heat exchanger designs considered in nuclear industry for dispatching high temperature heat for process application.

### **4.1 Shell and tube heat exchangers**

Shell and tube heat exchangers are the most common type used in energy industry. These are the most versatile exchangers for a broad range of operating pressures and temperatures. They can handle pressures ranging from high vacuum to ultra high fluid pressures of 30 MPa on the shell side and 140 MPa on the tube side. The allowed temperature of operation for shell and tube heat exchangers is limited only by the material used. These heat exchangers are used for gas, liquid, and phase change-applications. However, these heat exchangers have very low heat transfer surface area for a given volume and, therefore, are not economical for high temperature applications. A shell and tube design is useful where space considerations are not important. This design has high technological maturity with a TRL level of 9, and can be used for a variety of fluids, temperatures, and pressure conditions. Due to its simplistic design, a variety of materials can be used with well established manufacturing procedures [18]. Several techniques have been established to increase the heat transfer efficiency. These methods involve the utilization of baffles, fins, surface enhancement techniques, etc.

### **4.2 Helical coil shell and tube heat exchangers**

The helical coil shell and tube design is an improved shell and tube heat exchanger that consists of a bundle of helical tubes enclosed in a shell. The flow of coolant within the tubes undergoes secondary circulation across the circular cross section. This gives an advantage of the flow transitioning to turbulence at a low Reynolds's leading to higher heat transfer rates. A higher heat transfer surface area per unit volume compared to the straight shell and tube heat exchanger is possible in a helical shell and tube heat exchanger [19]. This heat exchanger has been developed to deliver 5-30 MW of heat at high temperatures up to 950 °C. Such a heat exchanger has been deployed in the HTTR in Japan and in the HTR-10 in China for helium-helium heat exchange at 7 MPa [20]. The design also poses an advantage of being a simplistic design which can be manufactured using well established manufacturing methods. The configuration also allows for in-service inspection of the heat transfer tubes, however, cleaning a helical coil heat exchanger to get rid of the fouling can be a difficult endeavor. Helical shell and tube heat exchangers have reached a high technological

maturity with a TRL level of 6 for high-temperature, high-duty applications as compared to other competing designs for cogeneration plant integration [21]. However, certain thermal hydraulic and thermo-mechanical issues exist that need to be taken into consideration when using this design. These issues include the gyration effects causing higher pressure drop, flow induced vibrations due to high turbulence, creep buckling, and fatigue of the tubes [22].

### **4.3 Plate frame heat exchangers**

Plate frame heat exchangers contain plates that are stacked together and joined through gaskets, welds, or diffusion bonding. The fluids flow between the plates in a parallel, cross, or counter current flow arrangement. The plate heat exchanger has a number of advantages over the traditional shell and tube heat exchangers and are commonly used in gas to gas applications with high pressure differential.. These designs have a substantially greater surface area to volume ratio than an equivalent shell and tube heat exchanger operating under the same thermal constraints. This heat exchanger can be designed to have high heat transfer coefficients, allowing for a reduced heat transfer area that is nearly one-third of an equivalent shell and tube heat exchanger. These heat exchangers are easy to manufacture and have operational benefits such as reduced fouling, ease of cleaning, and design flexibility. The number of plates utilized can be varied for specific design. However, this design has limited versatility due to the pressure and temperature limitations imposed by the gaskets between the plates. They also use less material and are about one-sixth the weight of an equivalent shell and tube heat exchanger, implying low capital cost and installation cost. A special hybrid plate Bavex heat exchanger has been reported to be operable at pressures of 6 MPa at a maximum temperature of 900 °C [18, 23].

Another variation of the plate heat exchanger design is a plate-fin heat exchanger. Plate-fin heat exchangers consist of plates stacked with triangular or rectangular fins between the plates. The plates separate the fluid streams and the fins form the individual flow passages. For gas-liquid applications, the fins are generally placed only on the gas side and in certain applications, fins on the liquid side are added for structural strength, especially for high pressure application. For nuclear hydrogen application, McDonald [24] proposed a plate-fin design with additional features to reduce the helium and tritium leakage from the flow channels. This design has been constructed and tested for high temperature applications up to 950 °C, giving it a TRL level of 6. This design has been under consideration for advanced reactors, and the path forward to integrating this design with 1000 MW high temperature reactor in a steel pressure vessel has been explored by McDonald [24].

### **4.4 Compact heat exchangers**

Compact heat exchangers have been of interest to the nuclear community due to their large heat transfer area to volume ratio, which results in reduced space, weight, support structure, and material cost. The high ratio allows for easier integration with advanced high temperature reactors. However, the increased heat transfer area to volume ratio leads to high frictional losses in the coolant. To compensate for the high frictional losses, these compact heat exchangers operate in the laminar flow regime, requiring low pressure drops and minimal operational energy for coolant circulation. Several agencies have been considering compact heat exchangers for various applications. Currently, these IHX are in the design stage and are at a low technological readiness level [21].

Amongst the compact heat exchangers, printed circuit heat exchangers (PCHE) are of considerable interest

to the nuclear engineering community. These heat exchangers utilize advanced manufacturing techniques to create very low volume heat exchangers with high heat transfer surface area. PCHE is a relatively novel technology, manufactured by Heatrix [25]. These heat exchangers are fabricated by chemically etching the flow paths on a flat plate. These plates are then formed into the core geometry by stacking them and joining them through the diffusion bonding process. Diffusion bonding allows an interface-free joint between the plates giving a high yield strength, thus enabling operation at a high pressure. The flow paths in PCHE can be zig-zagged, straight, s-shape, or airfoil shape. These flow channels have a semi-circular cross sectional flow area with the hot and cold fluids flowing in between alternate plates in a counter-current flow arrangement. These PCHEs can handle high temperatures and pressures of 1000 °C and 50 MPa, respectively, making them a very attractive option for IHX for advanced reactors. Various studies exist in literature where the optimum geometry of a PCHE is proposed based on the operating conditions and coolants. These studies have investigated various geometries in addition to various coolant combinations like He-He, He-Fluoride salts, etc. Studies have shown that PCHEs are an economically viable option with helium circulated in the laminar regime. However for liquid sodium, a PCHE operating in the turbulent regime was deemed economic. Recent studies with regards to SFRs have shown that an economic design consists of a PCHE with 80° zig-zag channels using carbon dioxide as the working fluid. When nitrogen is used, an airfoil design is the most economic option considering the capital and operational costs for a given heat load [26, 27].

Based on the material, novel ceramic design types consist of two categories: monolithic and ceramic matrix composites (CMC). The use of ceramic microchannels with a platinum catalyst in S-I hydrogen production processes offers potential for superior performance when compared to traditional designs. The extremely high thermal conductivity of monolithic SiC exhibits good thermal performance, but issues related to the mechanical stability of the ceramic, particularly under high pressure applications, are still a concern [28–30]. The leakage between the primary and secondary fluid under high pressure differential is also significant [31]. Monolithic ceramics except SiC cannot resist large thermal gradients and therefore suffer from a lack of reliability [32]. Although SiC ceramics are chemically inert, they are susceptible to oxidation at high temperatures. [33] CMCs consist of two different phases, a reinforcement phase embedded in a matrix phase. This material has improved mechanical properties as compared to monolithic [32], however, several fabrication challenges still exist. [34] .

Several novel heat exchanger concepts exist. Such concepts include foam heat exchangers, capillary heat exchangers, moving packed bed heat exchangers, etc. These heat exchangers can prove to be economically viable options once they reach elevated technological readiness levels.

Foam heat exchangers utilize stacked plates combined with a metallic foam. The stacked, separated plates create a barrier that contains the foam through which the fluid flows [35]. The temperature and pressure limitations are defined by the properties of the foam. Typical values of yield strength are 100 psi for uncompressed metallic foams and are beyond 1000 psi for compressed foams. Experiments have been performed with nickel foam heat exchangers at temperatures near 750 °C [36]. Very limited studies exist on high temperature application using this design. Future work includes characterizing the temperature and pressure limits of this heat exchanger type. This heat exchanger design has a high heat transfer effectiveness, but several concerns have been identified for practical application. A few of the major concerns include high pressure loss in the foam, loss of small fragments of foam, and clogging of foam through solid impurities in the coolant [15].

Another novel concept, called the capillary heat exchanger, has been developed for molten salt - helium heat transfer purpose. This design uses capillary tube bundles with 2-3 mm diameter tubes for the molten salt coolant, enclosed in a conventional cylindrical containment. This design can sustain large pressure

differentials between the primary and secondary side of the heat exchanger. The small size of the tubes adds to the compactness gain, but presents several concerns including vibration risk and complexity in manufacturing [37].

A moving packed bed heat exchanger that utilizes flowing ceramic particles that are coated with catalyst material has also been proposed. In this heat exchanger concept, these ceramic particles serve multiple purposes by acting as a heat transfer fluid, energy storage medium, and as a chemical catalyst, leading to possible economic feasibility of coupling microreactors to hydrogen generation methods [38].

For selecting the appropriate heat exchanger for a process use, several criteria need to be evaluated. The thermal performance is the primary criteria in selecting a heat exchanger since effective heat transfer is the primary objective and is greatly affected by the heat exchanger type. For effective heat transfer for long-term operation, the effect of fouling needs to be considered in the design along with establishing cleaning strategies. For continuous operation of the heat exchanger at increased temperatures and pressures, the maintenance of structural integrity is very important as joints and connections are subjected to the most static and dynamic loading during heat exchanger usage. Therefore the effect of mechanical stresses, thermal stresses, and flow induced vibration on the joints need to be carefully assessed to facilitate sustained, reliable operation.

**Table II. Summary of various heat exchanger designs**

<b>Heat Exchanger Design Type</b>	<b>Compactness (m<sup>2</sup>/m<sup>3</sup>)</b>	<b>Maximum Temp. (°C)</b>	<b>Maximum Pressure (bar)</b>	<b>Process Fluids</b>	<b>Material of Construction</b>	<b>TRL</b>
Shell&Tube [18]	~100	~900	~300	Gas/Gas, Gas/Liquid, Liquid/Liquid	S/S, Ti, Ni alloys, Hastelloy	9
Helical Coil Shell&Tube [20, 22]	~100	~900	~200	Liquid/Liquid, Gas/Gas	Hastelloy, Alloy 617	6
Plate-Fin [18, 24]	~500	~900	~200	Gas/Gas	S/S, Ti, Ni alloys	6
Plate-Frame [18]	120 - 660	-200 to 900	~50	Gas/Gas, Liquid/Liquid	S/S	9
Printed-Circuit (PCHE) [26, 27, 39]	500 - 5000	~950	~400	Gas/Gas, Gas/Liquid, Liquid/Liquid	Ni alloys	4
Foam HX [35, 36]	+3000	750	-	Gas/Gas, Gas/Liquid, Liquid/Liquid	Al, Cu, Ni foam	3
Capillary HX [37]	+1500	-	-	Liquid/Liquid	-	3
Ceramic HX [34, 40–42]	600	1370	5	Gas/Gas, Gas/Liquid, Liquid/Liquid	Monolithic, CMCs	4

## References

1. Hitesh Bindra and Shripad Revankar. *Storage and Hybridization of Nuclear Energy: Techno-Economic Integration of Renewable and Nuclear Energy*. Academic Press, 2018.
2. Roxanne Pinsky, Piyush Sabharwall, Jeremy Hartvigsen, and James O'Brien. Comparative review of hydrogen production technologies for nuclear hybrid energy systems. *Progress in Nuclear Energy*, 123:103317, May 2020.
3. Jacob Edwards, Hitesh Bindra, and Piyush Sabharwall. Exergy analysis of thermal energy storage options with nuclear power plants. *Annals of Nuclear Energy*, 96:104–111, 2016.
4. Graham Wilson, Sudhansu Sahoo, Piyush Sabharwal, and Hitesh Bindra. Packed bed thermal storage for lwrs. In *Storage and Hybridization of Nuclear Energy*, pages 229–248. Elsevier, 2019.
5. Michael Ohadi, Xiang Zhang, Hadi Keramati, Martinus Arie, Farah Singer, Ratnesh Tiwari, and Amir Shooshtari. Recent developments in high temperature heat exchangers: A review. *Frontiers in Heat and Mass Transfer (FHMT)*, 11, 2018.
6. K Natesan, A Moisseytsev, and S Majumdar. Preliminary issues associated with the next generation nuclear plant intermediate heat exchanger design. *Journal of nuclear materials*, 392(2):307–315, 2009.
7. Hirofumi Ohashi and Steven R Sherman. Tritium movement and accumulation in the ngnp system interface and hydrogen plant. Technical report, Idaho National Lab.(INL), Idaho Falls, ID (United States), 2007.
8. Xiaodong Sun, Richard Christensen, and John P Saving. Tritium mitigation/control for advanced reactor system. Technical report, The Ohio State Univ., Columbus, OH (United States), 2018.
9. Bengt Sundén. High temperature heat exchangers (hthe). In *Proceedings of the 5th International Conference on Science, Engineering and Technology*, 2005.
10. Jill K Wright. Next generation nuclear plant steam generator and intermediate heat exchanger materials research and development plan. Technical report, Idaho National Lab.(INL), Idaho Falls, ID (United States), 2010.
11. Kun Mo, Gianfranco Lovicu, Hsiao-Ming Tung, Xiang Chen, and James F Stubbins. High temperature aging and corrosion study on alloy 617 and alloy 230. *Journal of engineering for gas turbines and power*, 133(5), 2011.
12. Nariaki Sakaba, Hirofumi Ohashi, and Tetsuaki Takeda. Hydrogen permeation through heat transfer pipes made of hastelloy xr during the initial 950° c operation of the httr. *Journal of nuclear materials*, 353(1-2):42–51, 2006.
13. Eung Soo Kim, Piyush Sabharwall, and Nolan Anderson. Development of figure of merits (foms) for intermediate coolant characterization and selection. Technical report, Idaho National Lab.(INL), Idaho Falls, ID (United States), 2011.
14. Mohamed S El-Genk and Jean-Michel P Tournier. Reliable and safe thermal coupling of generation-iv vhttr to a hydrogen fuel production complex. *Thermal Science and Engineering Progress*, 3:164–170, 2017.

15. Ronald Eugene Mizia. Next generation nuclear plant intermediate heat exchanger acquisition strategy. Technical report, Idaho National Lab.(INL), Idaho Falls, ID (United States), 2008.
16. CB Davis, CH Oh, RB Barner, and DF Wilson. Thermal-hydraulic analyses of heat transfer fluid requirements and characteristics for coupling a hydrogen production plant to a high-temperature nuclear reactor. Technical report, Idaho National Lab.(INL), Idaho Falls, ID (United States), 2005.
17. N Bartel, M Chen, VP Utgikar, X Sun, I-H Kim, R Christensen, and P Sabharwall. Comparative analysis of compact heat exchangers for application as the intermediate heat exchanger for advanced nuclear reactors. *Annals of Nuclear Energy*, 81:143–149, 2015.
18. Ramesh K Shah and Dusan P Sekulic. *Fundamentals of heat exchanger design*. John Wiley & Sons, 2003.
19. Bahman Zohuri. *Nuclear Energy for Hydrogen Generation: Through Intermediate Heat Exchangers*. Springer, 2016.
20. Daisuke Tochio and Shigeaki Nakagawa. Thermal performance of intermediate heat exchanger during high-temperature continuous operation in htr. *Journal of nuclear science and technology*, 48(11):1361–1368, 2011.
21. John Collins. Next generation nuclear plant project technology development roadmaps: The technical path forward for 750–800 c reactor outlet temperature. Technical report, Idaho National Lab.(INL), Idaho Falls, ID (United States), 2009.
22. AREVA NP. Ngnp with hydrogen production ihx and secondary heat transport loop alternatives. Technical Report 12-9076325-001, AREVA, 2008.
23. DL Fisher and RL Sindelar. Compact heat exchanger manufacturing technology evaluation. *Savannah River Nuclear Solutions*, 2008.
24. Colin F McDonald. Compact buffer zone plate-fin ihx—the key component for high-temperature nuclear process heat realization with advanced mhr. *Applied Thermal Engineering*, 16(1):3–32, 1996.
25. Home - diffusion bonded heat exchangers and support.
26. Su Won Lee, Seong Min Shin, SungKun Chung, and HangJin Jo. Evaluation of thermal-hydraulic performance and economics of printed circuit heat exchanger (pche) for recuperators of sodium-cooled fast reactors (sfrs) using co2 and n2 as working fluids. *Nuclear Engineering and Technology*, 2021.
27. Zhongchao Zhao, Xiao Zhang, Kai Zhao, Pengpeng Jiang, and Yuping Chen. Numerical investigation on heat transfer and flow characteristics of supercritical nitrogen in a straight channel of printed circuit heat exchanger. *Applied Thermal Engineering*, 126:717–729, 2017.
28. Qunxiang Gao, Ping Zhang, Wei Peng, Songzhe Chen, and Gang Zhao. Structural design simulation of bayonet heat exchanger for sulfuric acid decomposition. *Energies*, 14(2):422, 2021.
29. Valery Ponyavin, Yitung Chen, Taha Mohamed, Mohamed Trabia, Anthony E Hechanova, and Merrill Wilson. Design of a compact ceramic high-temperature heat exchanger and chemical decomposer for hydrogen production. *Heat Transfer Engineering*, 33(10):853–870, 2012.
30. Vijaisri Nagarajan, Yitung Chen, Qiuwang Wang, and Ting Ma. Hydraulic and thermal performances of a novel configuration of high temperature ceramic plate-fin heat exchanger. *Applied Energy*, 113:589–602, 2014.

31. Donald Quentin Kern. *Process heat transfer*, volume 5. McGraw-Hill New York, 1950.
32. C Luzzatto, A Morgana, S Chaudourne, T O'Doherty, and G Sorbie. A new concept composite heat exchanger to be applied in high-temperature industrial processes. *Applied Thermal Engineering*, 17(8-10):789–797, 1997.
33. RA Penty and JW Bjerklie. Silicon carbide for high-temperature heat exchangers. In *1981 New England Section Topical Meeting on Nonoxide Ceramics*, volume 26, page 120. John Wiley & Sons, 2009.
34. Xiang Zhang, Hadi Keramati, Martinus Arie, Farah Singer, Ratnesh Tiwari, Amir Shooshtari, and Michael Ohadi. Recent developments in high temperature heat exchangers: A review. 2018.
35. Kevin Boomsma, Dimos Poulikakos, and F Zwick. Metal foams as compact high performance heat exchangers. *Mechanics of materials*, 35(12):1161–1176, 2003.
36. Pakeeza Hafeez, Sanjeev Chandra, and Javad Mostaghimi. Heat transfer during high temperature gas flow through metal foam heat exchangers. *Journal of Heat Transfer*, 139(12), 2017.
37. Per F Peterson. Capillary tube and shell heat exchanger design for helium to liquid salt heat transfer. Technical report, Report UCBTH-07-003, University of California–Berkeley, 2007.
38. Kevin J Albrecht and Clifford K Ho. Design and operating considerations for a shell-and-plate, moving packed-bed, particle-to-sco2 heat exchanger. *Solar Energy*, 178:331–340, 2019.
39. N Bartel, M Chen, VP Utgikar, X Sun, I-H Kim, R Christensen, and P Sabharwall. Comparative analysis of compact heat exchangers for application as the intermediate heat exchanger for advanced nuclear reactors. *Annals of Nuclear Energy*, 81:143–149, 2015.
40. AV Soudarev, AA Souryaninov, and BV Soudarev. Compact tubular ceramic heat exchangers for micro gas turbine engines. *WIT Transactions on Engineering Sciences*, 46, 2004.
41. M Ferrato and Bernard Thonon. A compact ceramic plate-fin heat exchanger for gas turbine heat recovery. In *Compact Heat Exchangers for the Process Industries*. Begel House Inc., 1997.
42. Jürgen Haunstetter, Volker Dreißigacker, and Stefan Zunft. Ceramic high temperature plate fin heat exchanger: Experimental investigation under high temperatures and pressures. *Applied Thermal Engineering*, 151:364–372, 2019.

## Task 3: Hydrogen and ammonia generation pathways

### 1 Introduction

This section offers an overview of hydrogen and ammonia generation pathways. A variety of hydrogen generation methods are described, along with a comparison of the respective temperature requirements, efficiencies, costs, and global warming potential (GWP) based on life cycle analysis, depending on the technological maturity of the process and availability of data.

### 2 Hydrogen generation methods

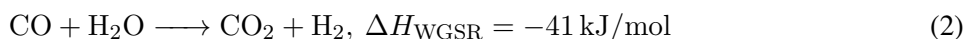
This section presents hydrogen production processes that may be compatible with existing microreactor designs. The feedstock, chemistry, and technological readiness of the production methods are discussed. Efficiency values are compiled, with a preference for higher heating values if available [1]. The relative cost of producing hydrogen and life-cycle emissions in the form of GWP are presented, along with the relevant context from sources in literature. However, both the cost and GWP values can vary depending on factors such as the scale of hydrogen production, technological readiness of the hydrogen generation method, the carbon-intensity of the power and manufacturing materials used, and geographical location. Note that the costs are presented exactly as they are reported in the cited sources, and have not been harmonized to a single currency from one year, or adjusted for inflation. The most important features of these hydrogen generation processes that are relevant to hydrogen production using process heat are summarized in Table I.

#### 2.1 Hydrocarbon conversion

At elevated temperatures and pressures, hydrocarbons can be converted into hydrogen and lighter hydrocarbons. The use of fossil fuels for such processes produces 95% of the world's hydrogen, with natural gas, heavy oil and naphtha, and coal accounting for 48%, 30%, and 18%, respectively [2, 3]. The most common example of such a method is steam methane reforming (SMR). Light hydrocarbons such as natural gas and naphtha are broken down into hydrogen and CO and CO<sub>2</sub> using 850 - 900 °C steam at 2.5-5 MPa in the presence of catalysts such as nickel, platinum, and ruthenium [3, 4]. The process begins with steam reforming [4]



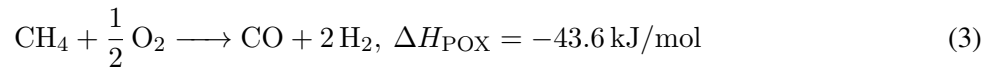
which is followed by the water-gas shift reaction [4]



In practice, the steam-to-carbon ratio is between 2.5-3 [4]. A nickel catalyst loaded to an alumina base at 10-15 wt% is typically used. Further purification steps result in a hydrogen purity of over 99%. Syngas, can also

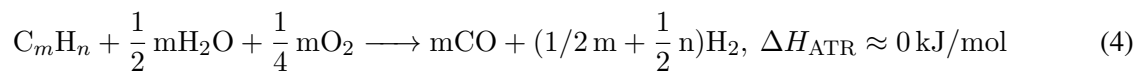
be utilized for the production of substitute natural gas, ammonia, or methanol. The overall efficiency is 70-85% for large-scale reforming (150-300 MW) and around 51% for small-scale reforming (0.15-15 MW) [5]. The latter is also less technologically mature than the widely commercialized large-scale reforming. A small-scale test facility has been proposed in Japan for use in conjunction with the high-temperature gas-cooled reactor (HTGR) [6]. The steam-to-carbon ratio is in the range of 3-4. In the steam reformer, the inlet temperatures of the process gas and helium gas are at 450 °C and 880 °C, and at the outlet 600 °C and 650 °C, respectively. The mass flow rate of the helium is set to 327.6 kg/h and the natural gas feed is 43.2 kg/h. The facility is capable of producing 120 Nm<sup>3</sup>/h of hydrogen. For steam reforming in general, the capital costs associated with large-scale reforming are between 400-600 USD/kW, whereas small-scale reforming costs around 3000-5000 USD/kW [5]. The estimated costs of hydrogen using this method are 2.08 USD/kg H<sub>2</sub> without CCS and 2.27 USD/kg H<sub>2</sub> with CCS [3]. The GWP, is 12.13 kg CO<sub>2</sub>-eq/kg H<sub>2</sub> [7]. The direct emissions of approximately 9 kg CO<sub>2</sub>-eq/kg H<sub>2</sub> could be mitigated up to 70% using CCS [8].

Partial oxidation (POX) can be used for generating hydrogen from heavier hydrocarbons such as oil or coal. It can be implemented at smaller power scales as low as 10 kW [4]. The reaction, with methane as the feedstock, is given by [9]



This is often followed by the water-gas shift reaction. As shown, this reaction is exothermic. The oxygen required is obtained through an air separation plant [4]. With catalysts, the process requires temperatures of 950-1100°C, instead of 1200-1450 °C [3]. However, these temperatures are still challenging to realize through microreactors. The conversion efficiency is 60-75%, which is lower than that of large-scale steam methane reforming. In a simulated reactor for catalytic partial oxidation of methane, an input feed rate of 5583.78 Nm<sup>3</sup>/h with an oxygen-to-methane ratio of 0.598 produced syngas with hydrogen produced at 5985 Nm<sup>3</sup>/h and carbon monoxide at 3036 Nm<sup>3</sup>/h [10]. The GWP is 10.8 kg CO<sub>2</sub>-eq/kg H<sub>2</sub>, which reduces to 4.8 kg CO<sub>2</sub>-eq/kg H<sub>2</sub> if using biological methane [11].

Autothermal reforming (ATR) combines elements of steam methane reforming and partial oxidation by using the exothermic partial oxidation to improve the hydrogen yield of the endothermic steam reforming reaction, reducing the temperatures required to as low as 575 °C [12]. The typical reaction is given by [3, 12]:



Hydrogen yield can be improved by the water-gas shift reaction. Ideally, the reaction is thermoneutral, however in practice, side reactions cause deviation from this behavior. The steam-to-carbon ratio is typically between 1-3. Bioethanol has been proposed as a feedstock to make this process sustainable [13]. An industrial autothermal reformer for producing syngas utilizes a methane feed rate of 3483 Nm<sup>3</sup>/h, with oxygen-to-methane and steam-to-methane ratios of 0.598 and 1.4, respectively [10]. This results in a hydrogen and carbon monoxide output of 6976 Nm<sup>3</sup>/h and 2444 Nm<sup>3</sup>/h, respectively. In general, the efficiency of ATR is comparable to partial oxidation and its reactions can be rapidly initiated and ceased. [12]. The purity of the hydrogen obtained is 55% [4]. While typical hydrogen output capacities range between 4000-35,000 Nm<sup>3</sup>/h, smaller units with an output of approximately 150 Nm<sup>3</sup>/h are being developed. The process can also be stopped and restarted more rapidly than steam reforming [12]. However, experience with commercial-scale hydrogen generation using this technology is limited [12, 13]. The GWP for ATR employing bioethanol, biological-methane, and fossil-membrane has been reported as 8.8 kg CO<sub>2</sub>-eq/kg

H<sub>2</sub>, 4.9 kg CO<sub>2</sub>-eq/kg H<sub>2</sub>, and 10.8 kg CO<sub>2</sub>-eq/kg H<sub>2</sub>, respectively [11]. With carbon capture, the GWP of bioethanol-based ATR may reduce to 1.9 kg CO<sub>2</sub>-eq/kg H<sub>2</sub> [14]. The estimated costs of hydrogen using this method are 1.48 USD/kg H<sub>2</sub> including CCS [3].

Coal gasification is performed in the presence of a gasification agent. Commonly, steam is used at temperatures exceeding 800 °C [4]. This process is also used for synthetic natural gas, ammonia, and methanol synthesis. For hydrogen generation, the coal is heated initially to expel its volatile content, after which the following reaction takes place [4]



Similar to the previous reactions, the carbon monoxide can be used in the water-gas shift reaction to obtain additional hydrogen. The coal conversion rate is roughly 95% and the efficiency is approximately 70%. Practical experience with coal gasification for hydrogen cogeneration with nuclear power has been gained from a small-scale project operated for over 26,000 hours in Germany [15]. The thermal power output has been reported as 1.2 MW with an operating pressure of 4 MPa. The helium inlet temperature and gasification temperatures were 950 °C and 700-850 °C, respectively. The helium flow rate was 1.1 kg/s, the coal input rate was 233 kg/h, and the steam velocity was 1.13 m/s. The resultant coal conversion rate was 83% with a raw gas production rate of 816 Nm<sup>3</sup>/h. The hydrogen content of the gas produced was over 50%. The GWP is extremely high at 24.2 kg CO<sub>2</sub>-eq/kg H<sub>2</sub> [7]. Plasma gasification or pyrolysis have the potential to mitigate CO<sub>2</sub> emissions, however these processes require temperatures above 1500 °C and up to 1000 °C, respectively [16, 17]. The estimated costs of hydrogen using this method are 1.34 USD/kg H<sub>2</sub> without CCS and 1.63 USD/kg H<sub>2</sub> with CCS [3].

Biomass gasification has the potential to utilize biomass in regions where it is abundant. Commonly considered feedstock includes plant waste, wood chips, and sawdust [4]. The high moisture content requires a significant amount of energy to dehydrate the feedstock [12]. High temperature steam of approximately 750 °C is required to carry out the gasification reactions. The chemical reactions for woody biomass lie within the range of the following reactions [4].



The former is representative of a process where no carbon dioxide is formed, whereas the latter is a process where all of the carbon monoxide formed is used to recover additional hydrogen. In a dual-gas-flow gasification scheme, biomass of dried cedar with a higher heating value of 20.0 MJ/kg, and a lower heating value of 18.6 MJ/kg can be used in a reactor to produce syngas [4]. With a feed of 100 kg of this biomass at 25 °C, 14.1 kg O<sub>2</sub> at 25 °C, 22.5 kg steam at 750 °C, and 513.36 MJ of high temperature heat from an HTGR, 217 Nm<sup>3</sup> of syngas with a lower heating value of 111.4 MJ is produced. The composition of the syngas is 11 kg of hydrogen, 74.4 kg of carbon monoxide, and 69.3 kg of carbon dioxide. Typical efficiency of hydrogen production from biomass is around 35-55%, and life-cycle emissions are estimated to be around 2.67 kg CO<sub>2</sub>-eq/kg H<sub>2</sub> [7, 12]. However, this number may vary depending on the transportation costs of the feedstock. The estimated costs of hydrogen using this method are 1.77-2.05 USD/kg H<sub>2</sub> [3].

Aqueous phase reforming can use hydrogenated hydrocarbons from biomass or carbohydrates to produce hydrogen at 2.9-5.6 MPa and 220-270 °C [18]. With glycerol and platinum-based catalysts, for instance [19]

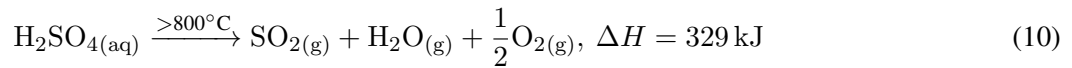
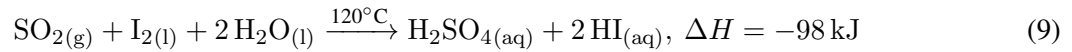


Efficiencies as high as 55% have been reported at lab-scale, but catalyst longevity needs to be improved for reaction sustenance and stability [12].

## 2.2 Thermochemical water decomposition

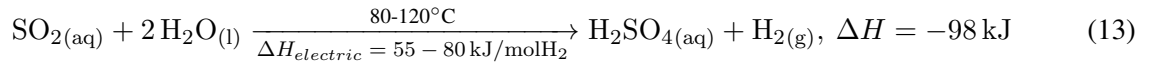
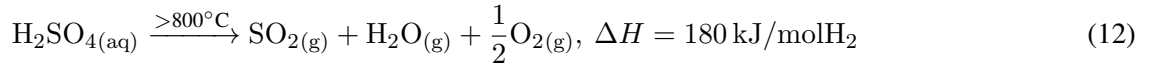
Thermochemical processes that utilize water as feed decompose water at elevated temperatures in the presence of catalysts in order to generate hydrogen with less energy than that required to decompose water directly. Typically, the efficiency of the processes is calculated as the ratio of formation enthalpy of water (286 kJ/mol) to the ratio of the heat and electric input to the process [20].

The sulfur iodine (SI) cycle is one of the most commonly studied thermochemical processes. The principles of this process were proposed as early as 1966 [21]. It was developed by General Atomics specifically for hydrogen production using HTGRs [22]. In this process, sulfuric acid and hydroiodic acid are used to break water down at temperatures around 800 °C. The main reactions are [4, 23]



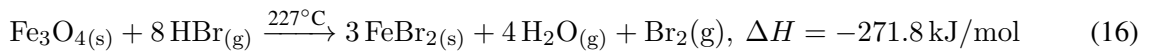
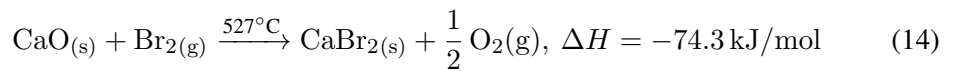
Other estimates of heat requirement provide a range between 391.3-432.9 kJ/mol-H<sub>2</sub> [20]. Its efficiency has been reported in the range of 35-57% [1, 4, 24, 25]. Experience with this process is demonstrated in the tests conducted by General Atomics and Japan Atomic Energy Agency (JAEA) [4], and more recent efforts by Sandia National Laboratories, French Alternative Energies and Atomic Energy Commission, and General Atomics [26, 27]. While the overall reaction is well-understood relative to other thermochemical processes, this process has still not reached the commercial stage, due to the lack of key experimental data regarding the formation of sulfur and hydrogen sulfide, vapor-liquid equilibria of the HI/I<sub>2</sub>/H<sub>2</sub>O system, kinetics and the potential need for a catalyst, and the need for economical materials that withstand the highly-corrosive reagents at high temperatures [27]. The GWP of nuclear-based SI cycle, taking life cycle emissions into account, has been reported as 0.5 kg CO<sub>2</sub>-eq/kg H<sub>2</sub> [28]. The cost of hydrogen from this process, in conjunction with nuclear power, has been estimated as 2.45-2.63 USD/kg H<sub>2</sub> [3].

The hybrid sulfur (HyS) cycle was developed by Westinghouse in 1975 [29]. It is an electrochemical process where the sulfuric acid decomposition reaction and the sulfur dioxide-polarized electrolysis of water are combined in a polymer electrolyte membrane (PEM) electrolyzer to produce hydrogen [4]. The two-step process is given by [4, 30]



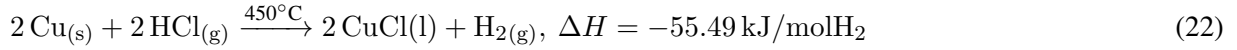
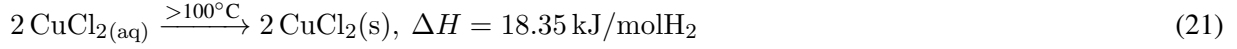
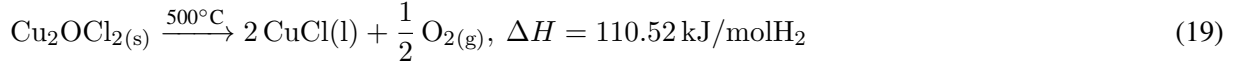
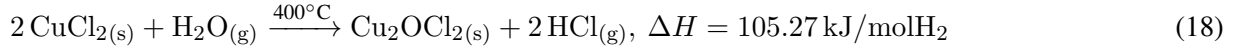
According to engineering scale models of a cell designed to produce 1 kmol-H<sub>2</sub>/s, a high temperature heat input of 340.3 kJ/mol-H<sub>2</sub>, low temperature heat of 76.8 kJ/mol-H<sub>2</sub>, and electricity input of 120.9 kJ/mol-H<sub>2</sub> is required [4]. 200 of such cells are necessary to produce 38 kg/h of hydrogen, equivalent to 1.5 MW of hydrogen. 182 of such modules are needed for a 500 MW<sub>th</sub> HTGR dedicated for hydrogen production, providing 950 °C outlet temperatures. The maximum temperatures obtained reach 850 °C [31]. The process has been mentioned favorably in multiple assessments as an excellent fit for hydrogen cogeneration with an HTGR, and is somewhat superior to the SI cycle due to its utilization of fewer steps (two steps compared to three in the SI cycle), more abundant reagents, and simpler reactions [31, 32]. Unlike the SI cycle, where heat loss minimization requires that the chemical plant be located in the vicinity of the nuclear plant, the hybrid sulfur cycle allows the possibility of conducting the thermal decomposition and electrolysis at separate locations [23]. The maximum theoretical efficiency has been estimated as 67% [1], whereas a more realistic range of predicted values is 31-49% [1, 4, 33]. The main drawbacks include a lack of commercial experience, low efficiency due to the acid electrolyzer, material degradation under extreme physical and chemical conditions [4, 34], and challenges associated with preventing back reaction in the thermal decomposition step [35]. The reported GWP is estimated to be 0.5 kg CO<sub>2</sub>-eq/kg H<sub>2</sub>, similar to the SI cycle [36]. The cost of hydrogen from this process using a dedicated nuclear reactor was estimated to be 1.64 USD/kg H<sub>2</sub> [1].

The UT-3 or Ca-Br-Fe cycle, developed at University of Tokyo, requires a lower temperature (750 °C) than the SI cycle [31, 37]. This process consists of the following main reactions [38, 39].



The predicted efficiency of 45% has been found to be closer to 13% [1, 40]. The reaction is complex, difficult to sustain, and utilizes reagents such as CaBr<sub>2</sub>, Br<sub>2</sub>, and Fe<sub>3</sub>O<sub>4</sub>. As a result, demonstrations beyond lab-scale have been challenging to achieve [41]. Other challenges include solid handling and the sintering of the solid reactants [40].

The hybrid Cu-Cl process was developed by Argonne National Laboratory, University of Ontario Institute of Technology, and Atomic Energy of Canada Limited [42]. It uses electrolysis in the presence of copper chloride and gaseous hydrochloric acid to produce hydrogen. The process has three, four, and five step variants, with small differences in the theoretical efficiencies of each variant [43]. The five step process is given by [44]

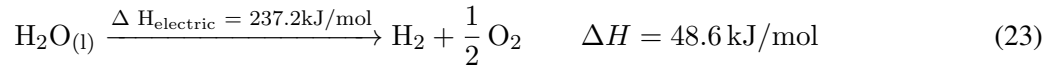


The inlet energy is 44% electricity and 56% heat [44]. The maximum operating temperature of the Cu-Cl process is nearly 530 °C, which is lower than many other processes. The maximum predicted thermodynamic efficiency is 49% [1]. Proof of concept experiments have demonstrated efficiencies of 40%, whereas a cogeneration system design coupled with a super-critical water reactor (SCWR) was estimated to have an efficiency of 31.6% [45]. Commercial scale experience is lacking, and improvements to the stability and efficiency of the reaction are necessary [46], especially with regards to corrosion and preventing Cu-crossover [23]. There are plans for a pilot plant that utilizes a >10 MW<sub>th</sub> source to generate hydrogen with a production rate of 36,000 Nm<sup>3</sup>/day, and a full scale plant that uses approximately 600 MW<sub>th</sub> heat to generate hydrogen at 3,000,000 Nm<sup>3</sup>/day [47]. The GWP has been reported as approximately 2 kg CO<sub>2</sub>-eq/kg H<sub>2</sub>, but another study [48] indicates a range of 0.55-0.63 kg CO<sub>2</sub>-eq/kg H<sub>2</sub>, depending on the operational parameters of the generation facility in question [36]. Further assessment with respect to different nuclear reactors are necessary to obtain a more precise value for its carbon intensity. The cost of hydrogen from this process, in conjunction with nuclear power, has been estimated as 2.17 USD/kg H<sub>2</sub> [3].

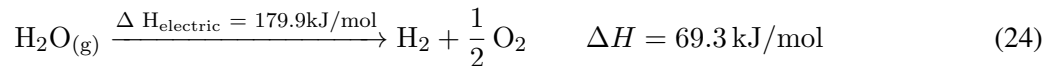
## 2.3 Electrolysis

Electrolysis is one of the most well-researched methods of producing hydrogen. Around 4% of the global hydrogen supply comes from electrolysis [2]. The basic process utilizes water or steam in an electrolyzer cell, where it breaks down due to the electric potential between the electrodes into oxygen and hydrogen, usually in the presence of a catalyst. Alkaline, polymer electrolyte membrane, and solid oxide electrolyzer cells are discussed below. In general, the cost of hydrogen from nuclear electrolysis has been estimated as 1.84-7.00 USD/kg H<sub>2</sub> [3, 49]. For reference, the cost of hydrogen generation from wind and solar has been estimated as 2.5-6 USD/kg H<sub>2</sub> [50].

A typical electrolysis reaction involves splitting water molecules in liquid state to hydrogen and oxygen molecules in gaseous form, and requires electric input of 237.2 kJ/mol and heat input of 48.6 kJ/mol to produce 1 mole of hydrogen gas, as given by [51]



Alkaline and polymer electrolytic membrane electrolyzers generate the heat required for this reaction using internal resistance, so a total of 285.8 kJ of electricity is required at 25 °C to produce 1 mole of hydrogen [51]. However, high temperature electrolysis, as carried out in solid oxide electrolyzer, relies on the following reaction [51]



Alkaline electrolyser cells (AECs) utilize nickel or nickel-coated cathodes in a strong potassium hydroxide solution, serving as an electrolyte, to break water down into hydrogen and oxygen [4]. It is the most mature electrolyzer technology, with operational lifetimes of 60,000-90,000 hours [5, 52]. The operational temperature range is between 50-80 °C [53]. The cold start-up time has been reported as 15 minutes [54]. The efficiency varies within the range of 60-82% [5, 53]. The main drawback of the method is the lack of scalability [5]. The costs are reported as 850-1500 USD/kW [5]. The GWP, when using electricity from wind power, has been reported as 0.60-0.97 kg CO<sub>2</sub>-eq/kg H<sub>2</sub> [54, 55].

Polymer electrolyte membrane electrolyser cell (PEMEC) utilize a polymer-based, highly acidic cation exchange membrane [53]. These electrolyzers provide high purity hydrogen and remove the risks associated with using highly alkaline electrolytes. The devices are more versatile, as they can be used for automobiles, or the instruments can be scaled up to utility-size systems as large as 1 MW [5]. The size of the largest operating PEM electrolyzer stack is 20 MW [56]. The device efficiency is similar to alkaline electrolyzers, in the range of 67-82%, and the operational temperatures are 50-80 °C [5, 53]. The cold start-up time is less than 15 minutes [54]. The main drawbacks are the cost and the operational lifetime of 20,000-60,000 hours [5, 52]. The costs are predicted to be 1500-3800 USD/kW, but the price is expected to reduce in the future [5, 57]. The GWP of these cells, when used with renewables alone, has been estimated as 2.21-3.3 kg CO<sub>2</sub>-eq/kg H<sub>2</sub> [7, 58]. These figures may evolve as cleaner electricity is used for manufacturing and electrolysis, more commercial experience is gained, and operational lifetimes improve.

Solid oxide electrolyzer cells (SOECs) are used for high temperature electrolysis (HTE), which electrolyzes steam at temperatures of 700-1000 °C [12]. The efficiency of these cells has been reported as high as 90% [5]. Unfortunately, they are the least developed of the three technologies, with most demonstrations being at lab scale, with operational lifetimes around 1000 hours [5, 52, 53]. The costs are higher than that of PEM electrolyzers, as expected from a less-developed technology, but they can be expected to reduce as more stable prototypes are developed [52, 57]. The GWP of an SOEC in combination with renewables has been reported to be around 5.1 kg CO<sub>2</sub>-eq/kg H<sub>2</sub>, but this value may change as more stable electrolyzers are built [7].

### **3 Nuclear hydrogen generation review**

Most nuclear-hydrogen cogeneration concepts currently rely on nuclear reactors larger than microreactors. Peak steam temperatures of most light water reactors (LWRs) are limited to 260-320 °C. Hydrogen generation has been proposed as a load-leveling method to divert excess electricity at times of low demand from the nuclear plant into electrolysis or hybrid thermochemical plants [4]. The steam temperature may be elevated using counter-current heat exchangers, waste heat from electrolysis units, and electrical heating [59]. Similar systems have been proposed for geothermal power. [60] High temperature electrolysis using a light water reactor was predicted to have an efficiency of 33% [61]. The AP1000 design has been assessed as a potential HTE-compatible candidate [62]. A cogeneration system comprising of an SCWR design along with a Cu-Cl process-based plant has been proposed as well [45].

Sodium-cooled fast reactor (SFR) designs typically cite outlet temperatures of 550 °C, making them suitable for hybrid cycles like Cu-Cl and low temperature electrolysis [4]. A new process, named hybrid hydrogen process in lower temperature range (HHLT), was recently proposed specifically for a sodium-cooled design as a lower temperature (500 °C) version of the hybrid sulfur cycle [63]. The process was experimentally demonstrated for 5 hours. Researchers estimated the efficiency to be in the range of 35-55%. Another process was proposed to lower the temperature of steam reforming to approximately 500 °C using a hydrogen

separation membrane [64]. A more recent process, named Na-O-H by its creators, was proposed with a theoretical hydrogen production rate of 1.321 kg H<sub>2</sub>/s, and temperatures that are potentially lower than 400 °C [65]. Unfortunately, many of these lower temperature hybrid thermochemical process are still in varying stages of development.

High temperature reactors such as HTGRs are considered the most versatile, since they can facilitate nearly all forms of hydrogen cogeneration due to the high temperature process heat they can provide. The high-temperature test reactor in Japan has been able to demonstrate temperatures above 930 °C [4]. An HTGR based system with four 600 MW<sub>th</sub> reactors used to produce hydrogen through high temperature electrolysis was conceptualized at Idaho National Laboratory, with hydrogen costs estimated as 2.22 USD/kg H<sub>2</sub>. In Germany, test facilities were constructed to demonstrate steam reforming using HTGR process heat at Forschungszentrum Jülich [66]. The JAEA has proposed detailed designs for an HTGR plant that can be used for electricity and hydrogen generation or dedicated solely to producing hydrogen [4]. It uses an intermediate heat exchanger to deliver high-temperature process heat to an SI cycle-based plant. The efficiency of the device was predicted as 45%. Load-following was also simulated. A hybrid cycle-based cogeneration plan was proposed by GA and INL, which they expect to be cheaper than HTE [67]. Brown et al [68], performed a transient analysis using a model of a high-temperature reactor coupled to a hydrogen production plant from the perspective of safety, highlighting the need for holistic safety assessments of nuclear hydrogen generation plants.

## 4 Ammonia generation method

The ammonia synthesis is based on the Haber-Bosch (HB) process, an exothermic equilibrium reaction between N<sub>2</sub> and H<sub>2</sub>, as represented by Eq 25.



The H<sub>2</sub> utilized for this process can be sourced from the any process described in the preceding section, while the N<sub>2</sub> is acquired through a system utilizing pressure swing adsorption (PSA) technology. Within the PSA, surrounding air is directed through a bed of adsorbent material, notably carbon molecular sieves, and then desorbed by altering the pressure. The cavities and pores of the absorber bed facilitate a more rapid diffusion of oxygen than nitrogen. This characteristic plays a pivotal role in achieving the successful separation of nitrogen during the absorption phase. The PSA unit is estimated to consume around 0.11 kWh/kg N<sub>2</sub> [69].

The ammonia synthesis through the H-B process is conventionally executed within the temperature range of 400 to 500 °C and under a pressure ranging from 150 to 200 bar in the presence of an iron-based catalyst. These high operating conditions represent a balance between achieving faster reaction rates and adhering to Le Chatelier's principle, which states that a system in equilibrium shifts to counteract changes in pressure or temperature. In this case, while lower temperatures favor ammonia production, higher temperatures are needed for faster reaction rates. As a result, only 20-30% of the H<sub>2</sub> is converted to ammonia in each pass. To enhance the yield, a recycle loop is implemented, facilitating the reintroduction of unreacted components and promoting further reactions to maximize ammonia production.

**Table I. Nuclear hydrogen generation processes**

Process	Temperature	Efficiency	Fully mature
SMR	850-900°C [4]	51-85% [5]	Yes [5]
POX	950°C [3]	60-75% [3]	Yes [23]
ATR	575°C [12]	60-75% [12]	No [12]
Coal Gasification	800°C [4]	70% [4]	Yes [4]
Biomass	750°C [12]	35-50% [12]	Yes [12]
Aqueous Reforming	220-270°C [70]	35-55% [12,23]	No [12]
SI	800°C [4,31]	33-57% [4]	No [4]
HyS	850°C [31]	31 [4]-49 [11]%	No [4]
UT-3	750°C [31]	13-45% [1]	No [4]
Cu-Cl	530°C [42]	31 [45]-49% [1]	No [46]
AEC	50-80°C [53]	60-82% [5]	Yes [5]
PEMEC	50-80°C [53]	67-82% [5]	Yes [56]
SOEC	700-1000°C [5]	85-90% [5]	No [5]

## References

1. Rachael Elder and Ray Allen. Nuclear heat for hydrogen production: Coupling a very high/high temperature reactor to a hydrogen production plant. *Progress in Nuclear Energy*, 51(3):500–525, April 2009.
2. Havva Balat and Elif Kırtay. Hydrogen from biomass – Present scenario and future prospects. *International Journal of Hydrogen Energy*, 35(14):7416–7426, July 2010.
3. Pavlos Nikolaidis and Andreas Poullikkas. A comparative overview of hydrogen production processes. *Renewable and Sustainable Energy Reviews*, 67:597–611, January 2017.
4. Xing L. Yan and Ryutaro Hino, editors. *Nuclear Hydrogen Production Handbook*. CRC Press, Boca Raton, May 2011.
5. A Körner, C Tam, S Bennett, and J Gagné. Technology Roadmap - Hydrogen and Fuel Cells – Analysis. Technical report, IEA, 2015.
6. Y. Miyamoto, S. Shiozawa, M. Ogawa, Y. Inagaki, T. Nishihara, and S. Shimizu. Research and development program of hydrogen production system with high temperature gas-cooled reactor. July 2000.

7. Andi Mehmeti, Athanasios Angelis-Dimakis, George Arampatzis, Stephen J. McPhail, and Sergio Ulgiati. Life Cycle Assessment and Water Footprint of Hydrogen Production Methods: From Conventional to Emerging Technologies. *Environments*, 5(2):24, February 2018. Number: 2 Publisher: Multidisciplinary Digital Publishing Institute.
8. Cormos Ana-Maria, Szima Szabolcs, Fogarasi Szabolcs, and Cormos Calin-Cristian. Economic assessments of hydrogen production processes based on natural gas reforming with carbon capture. *Chemical Engineering Transactions*, 70:1231–1236, 2018.
9. D.H. Lee. Hydrogen production via the Kvaerner process and plasma reforming. In *Compendium of Hydrogen Energy*, pages 349–391. Elsevier, 2015.
10. Ann M. De Groote and Gilbert F. Froment. Simulation of the catalytic partial oxidation of methane to synthesis gas. *Applied Catalysis A: General*, 138(2):245–264, May 1996.
11. Nouredine Hajjaji, Marie-Noëlle Pons, Viviane Renaudin, and Ammar Houas. Comparative life cycle assessment of eight alternatives for hydrogen production from renewable and fossil feedstock. *Journal of Cleaner Production*, 44:177–189, April 2013.
12. J. D. Holladay, J. Hu, D. L. King, and Y. Wang. An overview of hydrogen production technologies. *Catalysis Today*, 139(4):244–260, January 2009.
13. Renika Baruah, Marm Dixit, Pratik Basarkar, Dhruvad Parikh, and Atul Bhargav. Advances in ethanol autothermal reforming. *Renewable and Sustainable Energy Reviews*, 51:1345–1353, November 2015.
14. Yaser Khojasteh Salkuyeh, Bradley A. Saville, and Heather L. MacLean. Techno-economic analysis and life cycle assessment of hydrogen production from natural gas using current and emerging technologies. *International Journal of Hydrogen Energy*, 42(30):18894–18909, July 2017.
15. R. Kirchhoff, K. H. van Heek, H. Jüntgen, and W. Peters. Operation of a semi-technical pilot plant for nuclear aided steam gasification of coal. *Nuclear Engineering and Design*, 78(2):233–239, April 1984.
16. Adnan Midilli, Haydar Kucuk, Muhammed Emin Topal, Ugur Akbulut, and Ibrahim Dincer. A comprehensive review on hydrogen production from coal gasification: Challenges and Opportunities. *International Journal of Hydrogen Energy*, 46(50):25385–25412, July 2021.
17. Hao Zhang, Binlin Dou, Hua Zhang, Jingjing Li, Chenjie Ruan, and Chunfei Wu. Study on non-isothermal kinetics and the influence of calcium oxide on hydrogen production during bituminous coal pyrolysis. *Journal of Analytical and Applied Pyrolysis*, 150:104888, September 2020.
18. R. D. Cortright, R. R. Davda, and J. A. Dumesic. Hydrogen from catalytic reforming of biomass-derived hydrocarbons in liquid water. *Nature*, 418(6901):964–967, August 2002. Number: 6901 Publisher: Nature Publishing Group.
19. F. Frusteri and G. Bonura. 5 - Hydrogen production by reforming of bio-alcohols. In Velu Subramani, Angelo Basile, and T. Nejat Veziroğlu, editors, *Compendium of Hydrogen Energy*, Woodhead Publishing Series in Energy, pages 109–136. Woodhead Publishing, Oxford, January 2015.
20. Z. L. Wang, G. F. Naterer, K. S. Gabriel, R. Gravelins, and V. N. Daggupati. Comparison of sulfur–iodine and copper–chlorine thermochemical hydrogen production cycles. *International Journal of Hydrogen Energy*, 35(10):4820–4830, May 2010.

21. J. E. Funk and R. M. Reinstrom. Energy Requirements in Production of Hydrogen from Water. *Industrial & Engineering Chemistry Process Design and Development*, 5(3):336–342, July 1966. Publisher: American Chemical Society.
22. Kr Schultz. USE OF THE MODULAR HELIUM REACTOR FOR HYDROGEN PRODUCTION. Technical report, General Atomics, San Diego, CA (United States), September 2003.
23. Roxanne Pinsky, Piyush Sabharwall, Jeremy Hartvigsen, and James O’Brien. Comparative review of hydrogen production technologies for nuclear hybrid energy systems. *Progress in Nuclear Energy*, 123:103317, May 2020.
24. Seiji Kasahara, Shinji Kubo, Ryutaro Hino, Kaoru Onuki, Mikihiro Nomura, and Shin-ichi Nakao. Flowsheet study of the thermochemical water-splitting iodine–sulfur process for effective hydrogen production. *International Journal of Hydrogen Energy*, 32(4):489–496, March 2007.
25. J. H. Norman, G. E. Besenbruch, L. C. Brown, D. R. O’Keefe, and C. L. Allen. Thermochemical water-splitting cycle, bench-scale investigations, and process engineering. Final report, February 1977–December 31, 1981. Technical Report DOE/ET/26225-1; GA-A-16713, GA Technologies, Inc., San Diego, CA (USA), May 1982.
26. S Satyapal. DOE Hydrogen Program 2009 Annual Merit Review and Peer Evaluation Report. *US Department of Energy*, page 813, 2009.
27. Benjamin Russ, G. Naranjo, R. Moore, W. Sweet, M. Hele, and N. Pons. Nuclear Hydrogen Initiative, Results of the Phase II Testing of Sulfur-Iodine Integrated Lab Scale Experiments. Technical Report DOE/ID/14899, General Atomics, San Diego, CA (United States), October 2009.
28. Farid Safari and Ibrahim Dincer. A review and comparative evaluation of thermochemical water splitting cycles for hydrogen production. *Energy Conversion and Management*, 205:112182, 2020.
29. Lee E. Brecher and Christopher K. Wu. Electrolytic decomposition of water, June 1975.
30. Onur Oruc and Ibrahim Dincer. Assessing the potential of thermo-chemical water splitting cycles: A bridge towards clean and sustainable hydrogen generation. *Fuel*, 286:119325, February 2021.
31. L. C. Brown, J. F. Funk, and S. K. Showalter. Initial Screening of Thermochemical Water-Splitting Cycles for High Efficiency Generation of Hydrogen Fuels Using Nuclear Power. Technical Report GA-A23373, General Atomics, San Diego, CA (US); University of Kentucky, Lexington, KY (US); Sandia National Lab. (SNL-NM), Albuquerque, NM (United States), December 1999.
32. Robert Varrin Jr., Kenneth Reifsneider, David Sandborn, Patricia Irving, and Gregory Rolfson. NGNP Hydrogen Technology Down-Selection- Results of the Independent Review Team (IRT) Evaluation. Technical Report R-6917-00-01, Dominion Engineering Inc., 2011.
33. M. Gorenssek, W. Summers, C. Boltrunis, E. Lahoda, D. Allen, and R. Greyvenstein. HYBRID SULFUR PROCESS REFERENCE DESIGN AND COST ANALYSIS. Technical Report SRNL-L1200-2008-00002, Savannah River Site (SRS), Aiken, SC (United States), May 2009.
34. Yong Hoon Jeong and Mujid S. Kazimi. Optimization of the Hybrid Sulfur Cycle for Nuclear Hydrogen Generation. *Nuclear Technology*, 159(2):147–157, August 2007. Publisher: Taylor & Francis eprint: <https://doi.org/10.13182/NT07-A3861>.

35. Michele A. Lewis and Joseph G. Masin. The evaluation of alternative thermochemical cycles – Part II: The down-selection process. *International Journal of Hydrogen Energy*, 34(9):4125–4135, May 2009.
36. Farid Safari and Ibrahim Dincer. A review and comparative evaluation of thermochemical water splitting cycles for hydrogen production. *Energy Conversion and Management*, 205:112182, February 2020.
37. T. Ohta and M. V. C. Sastri. Hydrogen energy research programs in Japan. *International Journal of Hydrogen Energy*, 4(6):489–498, January 1979.
38. F. Lemort, C. Lafon, R. Dedryvère, and D. Gonbeau. Physicochemical and thermodynamic investigation of the UT-3 hydrogen production cycle: A new technological assessment. *International Journal of Hydrogen Energy*, 31(7):906–918, June 2006.
39. E. D. Teo, N. P. Brandon, E. Vos, and G. J. Kramer. A critical pathway energy efficiency analysis of the thermochemical UT-3 cycle. *International Journal of Hydrogen Energy*, 30(5):559–564, April 2005.
40. Dorottya Guban, Ibrahim Kolawole Muritala, Martin Roeb, and Christian Sattler. Assessment of sustainable high temperature hydrogen production technologies. *International Journal of Hydrogen Energy*, 45(49):26156–26165, October 2020.
41. T. Nakayama, H. Yoshioka, H. Furutani, H. Kameyama, and K. Yoshida. MASCOT—a bench-scale plant for producing hydrogen by the UT-3 thermochemical decomposition cycle. *International Journal of Hydrogen Energy*, 9(3):187–190, January 1984.
42. M. Lewis and J. Masin. An assessment of the efficiency of the hybrid copper-chloride thermochemical cycle. 2005, January 2005.
43. H. Ishaq and I. Dincer. A comparative evaluation of three CuCl cycles for hydrogen production. *International Journal of Hydrogen Energy*, 44(16):7958–7968, March 2019.
44. Mehmet F. Orhan, Ibrahim Dincer, and Marc A. Rosen. Efficiency analysis of a hybrid copper–chlorine (Cu–Cl) cycle for nuclear-based hydrogen production. *Chemical Engineering Journal*, 155(1):132–137, December 2009.
45. Maan Al-Zareer, Ibrahim Dincer, and Marc A. Rosen. Development and assessment of a novel integrated nuclear plant for electricity and hydrogen production. *Energy Conversion and Management*, 134:221–234, February 2017.
46. G. Naterer, S. Suppiah, M. Lewis, K. Gabriel, I. Dincer, M. A. Rosen, M. Fowler, G. Rizvi, E. B. Easton, B. M. Ikeda, M. H. Kaye, L. Lu, I. Pioro, P. Spekkens, P. Tremaine, J. Mostaghimi, J. Avsec, and J. Jiang. Recent Canadian advances in nuclear-based hydrogen production and the thermochemical Cu–Cl cycle. *International Journal of Hydrogen Energy*, 34(7):2901–2917, April 2009.
47. Greg F. Naterer, Ibrahim Dincer, and Calin Zamfirescu. Hybrid Copper–Chlorine Cycle. In Greg F. Naterer, Ibrahim Dincer, and Calin Zamfirescu, editors, *Hydrogen Production from Nuclear Energy*, pages 273–438. Springer, London, 2013.
48. Ahmet Ozbilen, Ibrahim Dincer, and Marc A. Rosen. Environmental evaluation of hydrogen production via thermochemical water splitting using the Cu–Cl Cycle: A parametric study. *International Journal of Hydrogen Energy*, 36(16):9514–9528, August 2011.
49. Nuclear Energy Agency, OECD. *Nuclear Production of Hydrogen: Third Information Exchange Meeting, Oarai, Japan*. Nuclear Science. OECD, June 2006.

50. IEA. The Future of Hydrogen – Analysis. Technical report, 2019.
51. K W Harrison, R Remick, and G D Martin. Hydrogen Production: Fundamentals and Case Study Summaries; Preprint. page 21, Essen, Germany, 2010.
52. Martín David, Carlos Ocampo-Martínez, and Ricardo Sánchez-Peña. Advances in alkaline water electrolyzers: A review. *Journal of Energy Storage*, 23:392–403, June 2019.
53. Marcelo Carmo, David L. Fritz, Jürgen Mergel, and Detlef Stolten. A comprehensive review on PEM water electrolysis. *International Journal of Hydrogen Energy*, 38(12):4901–4934, April 2013.
54. Ramchandra Bhandari, Clemens A. Trudewind, and Petra Zapp. Life cycle assessment of hydrogen production via electrolysis – a review. *Journal of Cleaner Production*, 85:151–163, December 2014.
55. Jan Christian Koj, Andrea Schreiber, Petra Zapp, and Pablo Marcuello. Life Cycle Assessment of Improved High Pressure Alkaline Electrolysis. *Energy Procedia*, 75:2871–2877, August 2015.
56. Cummins Inc. Cummins hydrogen technology powers the largest proton exchange membrane (PEM) electrolyzer in operation in the world.
57. O. Schmidt, A. Gambhir, I. Staffell, A. Hawkes, J. Nelson, and S. Few. Future cost and performance of water electrolysis: An expert elicitation study. *International Journal of Hydrogen Energy*, 42(52):30470–30492, December 2017.
58. Kay Bareiß, Cristina de la Rúa, Maximilian Möckl, and Thomas Hamacher. Life cycle assessment of hydrogen from proton exchange membrane water electrolysis in future energy systems. *Applied Energy*, 237:862–872, March 2019.
59. Charles Forsberg and Mujid Kazimi. Nuclear hydrogen using high temperature electrolysis and light water reactors for peak electricity production. pages 155–164, June 2010. Publisher: OECD.
60. J. Sigurvinsson, C. Mansilla, P. Lovera, and F. Werkoff. Can high temperature steam electrolysis function with geothermal heat? *International Journal of Hydrogen Energy*, 32(9):1174–1182, June 2007.
61. J. A. O’Brien, J. T. Hinkley, S. W. Donne, and S-E. Lindquist. The electrochemical oxidation of aqueous sulfur dioxide: A critical review of work with respect to the hybrid sulfur cycle. *Electrochimica Acta*, 55(3):573–591, January 2010.
62. Jarosław Milewski, Jakub Kupecki, Arkadiusz Szcześniak, and Nikolaï Uzunow. Hydrogen production in solid oxide electrolyzers coupled with nuclear reactors. *International Journal of Hydrogen Energy*, 46(72):35765–35776, October 2021.
63. Toshio Nakagiri, Takeshi Kase, Shoichi Kato, and Kazumi Aoto. Development of a New Thermochemical and Electrolytic Hybrid Hydrogen Production System for Sodium Cooled FBR. *JSME International Journal Series B Fluids and Thermal Engineering*, 49(2):302–308, 2006.
64. Yoshitaka Chikazawa, Mamoru Konomura, Shouji Uchida, and Hiroyuki Sato. A Feasibility Study of a Steam Methane Reforming Hydrogen Production Plant with a Sodium-Cooled Fast Reactor. *Nuclear Technology*, 152(3):266–272, December 2005. Publisher: Taylor & Francis. eprint: <https://doi.org/10.13182/NT05-A3675>.
65. João G. O. Marques, Antonella L. Costa, and Cláudia Pereira. NaOH thermochemical water splitting cycle: A new approach in hydrogen production based on sodium cooled fast reactor. *International Journal of Hydrogen Energy*, 43(16):7738–7753, April 2018.

66. Internationale Atomenergie-Organisation, editor. *Hydrogen production using nuclear energy*. Number NP-T-4.2 in IAEA nuclear energy series. IAEA, Vienna, 2013.
67. Larry Demick and Doug Vandell. Next Generation Nuclear Plant Pre-Conceptual Design Report. Technical Report INL/EXT-07-12967, 923515, November 2007.
68. Nicholas R. Brown, Volkan Seker, Shripad T. Revankar, and Thomas J. Downar. Transient simulation of an endothermic chemical process facility coupled to a high temperature reactor: Model development and validation. *Nuclear Engineering and Design*, 248:1–13, July 2012.
69. Bosong Lin, Theodore Wiesner, and Mahdi Malmali. Performance of a small-scale haber process: A techno-economic analysis. *ACS Sustainable Chemistry & Engineering*, 8(41):15517–15531, 2020.
70. George W. Huber and James A. Dumesic. An overview of aqueous-phase catalytic processes for production of hydrogen and alkanes in a biorefinery. *Catalysis Today*, 111(1):119–132, January 2006.

## Task 4: Economics of heat exchanger integration

### 1 Introduction

Nuclear reactors could be utilized to provide heat for applications such as manufacturing, chemical processes, district heating, and other industrial uses [1]. Recently, with the increasing need to make the next generation advanced microreactors economically feasible, various designs have been under consideration in order to utilize the process heat dispatched by such reactors. The process heat has to be dispatched to the final application through a heat transport loop that features a heat exchanger as the interface between the reactor and the end process [2]. The typical approach of dispatching process heat from a nuclear reactor involves transferring heat between primary and secondary, or secondary and tertiary, mediums using fluid circuits. For advanced reactor applications, the Intermediate Heat Exchanger (IHX) has to dispatch process heat at high temperatures. There are several designs for IHX with a variety of flow configurations and heat transfer mechanisms. The shell-and-tube heat exchanger is the most commonly used design due to its high technological maturity compared to other designs. In order to achieve the optimal heat exchange, the tubes in the shell-and-tube heat exchanger can exhibit different configurations in terms of the primary and secondary fluid flow, including, a parallel configuration, a counterflow configuration, and a cross-flow configuration. Furthermore, the optimum design and configuration of the heat exchanger for a given application is highly dependent on the choice of coolant used.

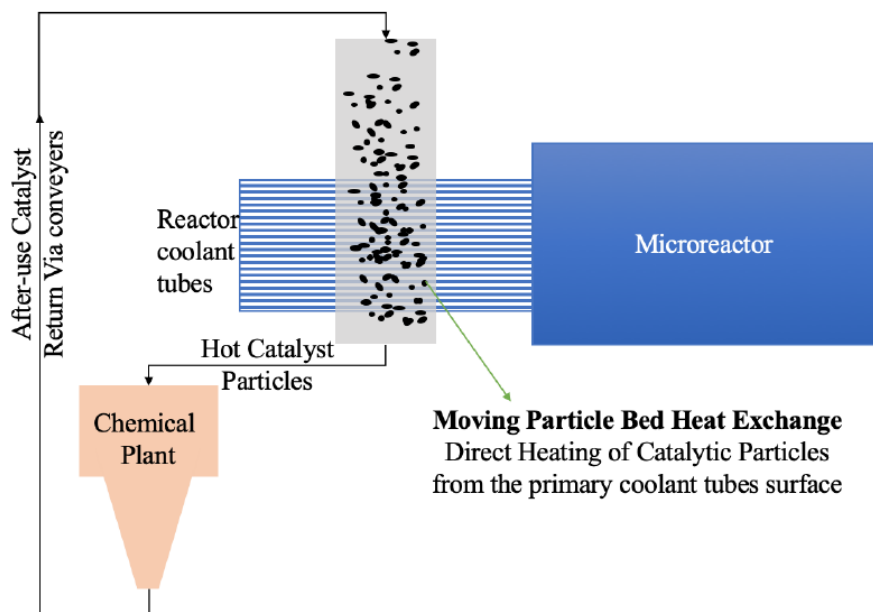


Figure 1. A generic schematic of microreactor heat transfer fluid heating catalytic particles, which enter into the chemical reactor.

There are several types of coolants that can be considered for heat transportation, the choice of the most suitable coolant depends on different parameters that are application-specific. Advanced reactors, for example, utilize helium or molten salts to transport heat at high temperatures. Recently, moving particles have been under consideration for heat transportation and energy storage in a variety of end-process applications, such as for the application of coupling a nuclear plant to a Hydrogen production facility (Figure 1). Moving particles exhibit the advantage of acting as a heat transfer fluid, an energy storage medium, and a catalyst carrier, especially for the Steam Methane Reforming (SMR) hydrogen production process. To evaluate the design requirements of a heat exchanger that utilizes moving particles as a coolant, an assessment needs to be performed.

A heat transfer system that utilizes moving particles as a Heat Transfer Fluid (HTF), called a Moving Packed Bed Heat Exchanger (MPBHX), is widely employed in solar energy applications [3]. In this system, the particles (acting as the HTF) receive the concentrated solar energy at high temperatures, both, directly through irradiation and indirectly through walls/tubes. These particles are tightly packed and flow along with the gaseous phase within the system, thereby constituting a two-phase flow of a solid-gas mixture. The solid particles absorb heat from the concentrated solar irradiation while they transport between a cold particle storage tank and a hot particle storage tank. The particles move from the cold storage tank to the hot storage tank through a passive gravity-driven flow. The hot particles can be dispatched and used as process heat either through a continuous flow loop or through a Thermal Energy Storage (TES). Once the thermal energy is extracted from the hot particles by the end application (either through gas fluidization or through use as chemical catalysts) they are recirculated back through the system using mechanical conveyor belts.

## 2 Thermal design process for a cross-flow heat exchanger

In the cross-flow configuration of the heat exchanger, the primary fluid flows in the tubes whereas the secondary fluid flows over the tubes in a direction perpendicular to the tubes. The design of the heat exchanger is constrained by typical end-process requirements, such as a specified heat load and a specified operating temperature. Under these conditions, where the heat load and the operating temperatures are defined, the geometry needed for a given combination of coolants can be determined. There are three degrees of freedom for the geometric parameters: tube diameter, tube length, and the number of tubes. Here, the tubes are assumed to be arranged in a staggered configuration with longitudinal and transverse pitches equal to 1.5 times the outer diameter of the tube. The tube thickness is considered as 0.005 m. The heat exchanger is in a balanced state, ie  $(\dot{m}C_p)_1 = (\dot{m}C_p)_2$ , where the subscripts 1 and 2 represent primary and secondary sides, respectively,  $\dot{m}$  is the coolant mass flow rate, and  $C_p$  is the specific heat capacity of the coolant.

The flow arrangement is illustrated in Figure 2. The relation for the system parameters of the heat exchanger is given as follows:

$$Q = UA_s\theta_{LMTD} \quad (1)$$

where  $Q$  is the heat duty,  $U$  is the overall heat transfer coefficient,  $A_s$  is the surface area of heat transfer, and  $\theta_{LMTD}$  is the log-mean-temperature-difference. In the analysis, the heat load is considered to be 10 MW. The overall heat transfer coefficient is given in terms of the primary side heat transfer coefficient,  $h_1$ , and the secondary side heat transfer coefficient,  $h_2$ , as follows:

$$\frac{1}{U} = \frac{1}{h_1} + \frac{1}{h_2} \quad (2)$$

In this relation, the conduction effects of the tube material are assumed to be negligible. The heat transfer

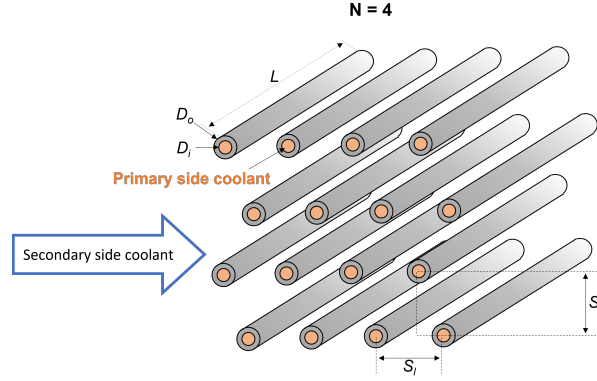


**Figure 2. Tube bundle arrangement in cross flow considered in this analysis.**

coefficient for both the primary and secondary sides follows the generic form:

$$h = C Re^m Pr^n k / D \quad (3)$$

where  $Re$  is the Reynolds number,  $Pr$  is the Prandtl number,  $k$  is the thermal conductivity of the coolant, and  $D$  is the diameter of the tube. The constants  $C$ ,  $m$ , and  $n$  are determined from empirical correlations, such correlations can be found in the literature for a variety of conditions. For this study, the value of the constant  $n$  is considered 0.4 if the fluid is being heated and 0.3 if the fluid is being cooled. The values of the other constants are summarized in Table ?? for different values of Reynolds number. Here, the Reynolds number, which is a non-dimensional form of velocity, is calculated from the mass flow rate and the flow area. The flow area for the primary side is given by:

$$A_{f1} = \frac{\pi}{4} D_i^2 N_t N_r \quad (4)$$

where  $N_t$  is the number of tubes in a row,  $N_r$  is the number of rows,  $D_i$  is the inner diameter of the tube and  $L$  is the tube length. The Reynolds number for the secondary side over the tube bundle is calculated using the maximum velocity, which occurs between the tubes, as follows:

$$Re_{D,max} = \frac{\rho V_{max} D_o}{\mu} \quad (5)$$

$$V_{max} = \frac{S_l}{S_l - D_o} V \quad (6)$$

where  $V$  is the approach velocity of coolant on the secondary side,  $D_o$  is the outer diameter of the tube and  $S_l$  is the pitch of the tube lattice. The heat transfer coefficient between the tubes is calculated using the Dittus-Boelter correlation [4] for flow inside a tube.

**Table I. Coefficients used in Equation 3 for varying Reynolds numbers.**

Re	C	m
10 - 1000	0.9	0.4
1000 - $2 \times 10^5$	0.27	0.63
$2 \times 10^5$ - $2 \times 10^6$	0.022	0.84

The thermal design of the heat exchanger involved several steps as illustrated by the flow diagram in Figure 3. Using the standard heat transfer models described earlier, the size of the heat exchanger is determined

in an iterative manner by outlet fluid temperatures. The thermal design process was performed to calculate coolant outlet temperatures using the  $\epsilon - NTU$  method. First, an initial size of the heat exchanger is assumed. If the calculated outlet temperature is found to be within a specified tolerance ( $\pm 0.1^\circ\text{C}$ ) of the design outlet temperature, the given design is deemed to be thermally appropriate. On the other hand, if the outlet temperature falls outside the tolerance bounds, the geometry is tweaked and the process is repeated. This process is reiterated until a thermally appropriate design is achieved.

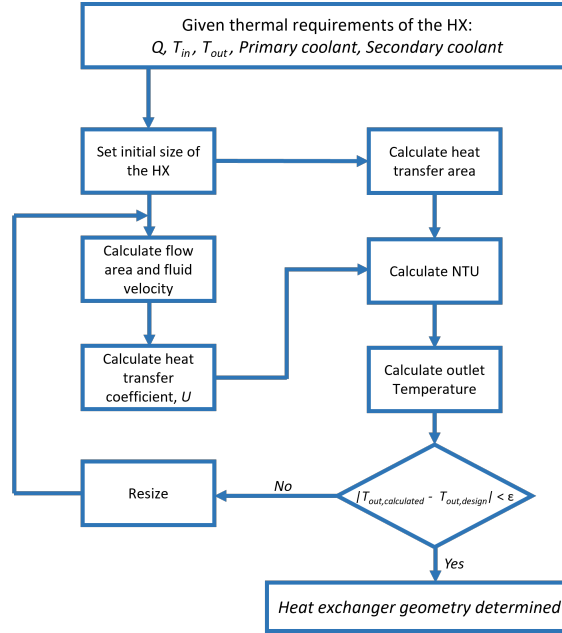


**Figure 3. Thermal design process.**

Once a geometry matching the thermal constraints is obtained, a pressure drop analysis is applied to the design to calculate the total work that needs to be imposed for coolant circulation. A higher pumping work corresponds to higher operational costs. Through cost analysis, a choice is made for an optimum design that exhibits the right balance between the operational cost and the capital cost. Upon achieving an optimum geometry that exhibits the lowest total cost possible, the design parameters of the heat exchanger for various coolant combinations are determined.

### 3 Economic analysis of heat exchanger

The overall total cost of a heat exchanger, also referred to as lifetime costs, encompasses capital, installation, operational, and sometimes disposal costs. The capital cost comprises expenses related to design, materials, manufacturing (including machinery, labor, and overhead), testing, shipping, installation, and depreciation. The operational costs encompass various expenditures, including fluid pumping power, warranty, insurance, maintenance, repairs, cleaning, and energy expenses associated with utilities [5]. In the early design phase, accurately estimating all the above-mentioned costs can be challenging. In the present economic model, the capital cost ( $C_C$ ) is estimated based on the raw material cost, while the operating cost ( $C_O$ ) is evaluated considering the expenses associated with pumping power. The total cost ( $C_{total}$ ) is modeled as follows:

$$C_{total} = C_C + C_O \quad (7)$$

The capital cost depends on the structural material and the size of the heat exchanger. The total mass of the heat exchanger is given by:

$$M_{HX} = \rho_{HX} V_{HX} \quad (8)$$

where  $V_{HX}$  is the volume of the heat exchanger, calculated from the tube bundle geometry as follows:

$$V_{HX} = \frac{\pi}{4} (D_o - D_i)^2 L N_t N_r \quad (9)$$

in this equation,  $D_o$  is the outer diameter of the tube,  $D_i$  is the inner diameter of the tube,  $N_t$  is the number of tubes in a row and  $N_r$  is the number of rows, and  $L$  is the length of a single tube. The capital cost associated with the material cost of the heat exchanger is given by:

$$C_C = C_M M_{HX} \times CRF \quad (10)$$

where  $C_M$  is the cost of the material per unit mass (\$200/kg), and CRF stands for Capital Recovery Factor, which is used to annualize the capital cost. The CRF is given by:

$$CRF = \frac{i (i + 1)^x}{(i + 1)^x - 1} \quad (11)$$

where  $i$  is the fractional interest rate per year (%), and  $x$  is the total lifetime of the heat exchanger (20 yrs).

To estimate the operating cost, the required pumping power is calculated. The pumping power, for both the primary and the secondary sides, can be calculated as follows:

$$\dot{W} = \frac{\dot{m} \Delta P}{\rho} \quad (12)$$

where  $\dot{m}$  is the coolant mass flow rate,  $\Delta P$  is the pressure drop, and  $\rho$  is the density of the coolant. Upon calculating the pumping power for both sides, the operating cost is calculated as follows:

$$C_O = C_E (\dot{W}_1 + \dot{W}_2) \quad (13)$$

where  $C_E$  is the cost of electricity in \$/Wh.

## 4 Heat transfer performance with geometric variation and economic assessment

The results outlined in this section illustrate the variation of parameters, namely overall heat transfer coefficient and costs, concerning two geometric parameters: tube outer diameter and the number of tubes in a row. The variation of the calculated overall heat transfer coefficient for the heat exchanger when helium is used on both the primary and the secondary sides is shown in Figure 4.

Increasing the tube diameter leads to a reduction in flow velocity. Consequently, the heat transfer coefficient is decreased. This reduction in heat transfer coefficient requires a larger surface area in order to meet the thermal requirements of the system. For a given tube diameter and number of tubes, the increase in surface area necessary to meet the thermal requirements is accounted for by using longer tubes. The total cost of the heat exchanger over a period of 20 years was determined as a summation of the capital and operational costs as shown in Figure 5.

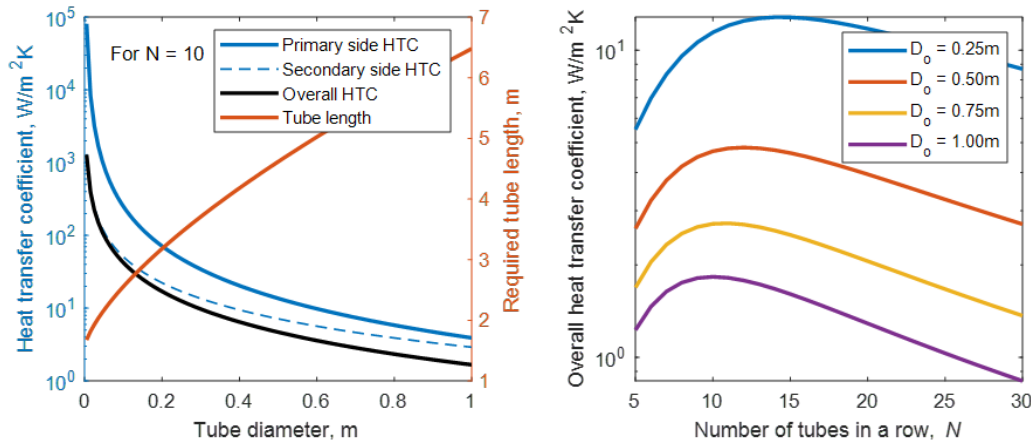


**Figure 4. Variation of the overall heat transfer coefficient with various geometric parameters for a He-He cross-flow heat exchanger with the number of tubes.**

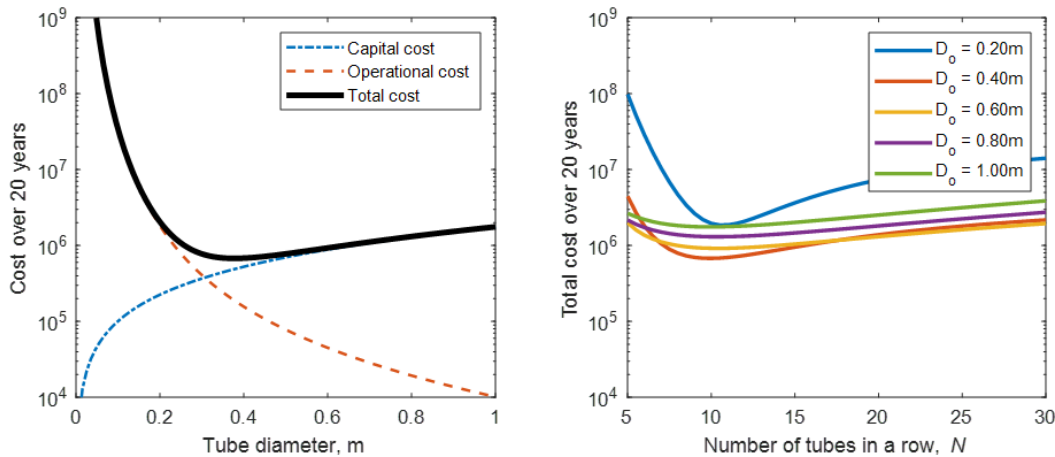


**Figure 5. Variation of the total cost of the heat exchanger with geometric parameters (He-He).**

Increasing the diameter of the tube leads to increasing the total volume of the heat exchanger’s material, consequently, increasing the capital cost. Nevertheless, as the pipe diameter is increased, the pressure drop incurred in the tube reduces, leading to a decrease in the work exerted by the pump for coolant circulation, consequently, decreasing the operational cost. Combining the capital and operational costs, there exists an optimal geometry (diameter) at which the total cost is lowest. This cost optimization can be performed in terms of both, tube diameters and number of tubes in a row. The color map shown in Figure 6 illustrates the variation in the total cost due to variations in the two aforementioned parameters, it also shows the optimal geometry at which the total cost is lowest, as shown by the red mark.

It is worth mentioning that the optimal geometry changes based on primary-secondary coolant combinations, hence, the methodology discussed in this section can be applied to determine such optimal geometries for different combinations of primary-secondary coolants. Nevertheless, the heat transfer model applied in this section doesn’t apply when moving particles are considered, and the methodology to determine optimal geometries is different. More details on the systems that utilize moving particles are discussed in the next sections.

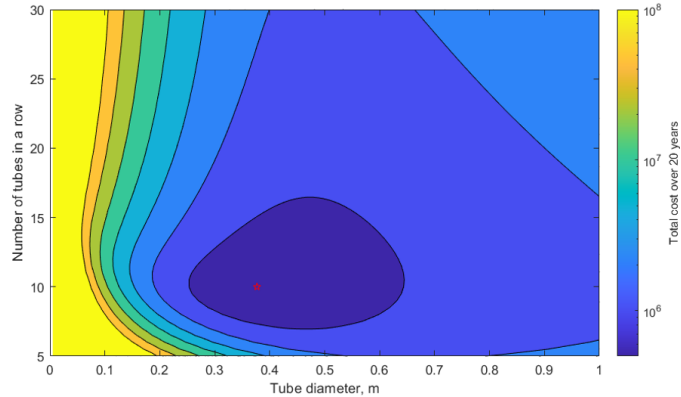


**Figure 6. Variation of the total cost over 20 years with geometric parameters. The optimum geometry with the lowest cost is also plotted.**

**Modeling moving packed bed heat exchanger** When moving particles are considered, modeling of heat transfer coefficients has been performed through different approaches in the literature. A continuum approximation, in which the moving particles are considered as a single continuous fluid, has been shown to be an appropriate approximation for the evaluation of the heat transfer coefficient. Numerical and experimental data can be found in the literature. Nevertheless, there seems to be a lack of mathematical models to address the heat transfer coefficient of moving particles across a bundle of tubes. Therefore, experimental data of granular particles moving across a tube bundle were utilized to perform the analysis presented in this paper [6]. These measurements were performed at low velocities, causing a minimal void zone below an individual heater rod. This void zone is expected at high particle velocities, analogous to the wake region downstream of an immersed body in a moving fluid. This effect of the void zone downstream of a rod at high particle velocities on the heat transfer coefficient has not been considered in this analysis.

## 5 Comparison of various coolants

Several coolant combinations on the primary and secondary sides were considered to assess the optimal geometric characteristics of a heat exchanger. Results of the total cost over 20 years for different coolant combinations are presented in Table II. It has been found that when helium is employed as both the primary and secondary fluids in a heat exchanger, the overall costs tend to be considerably higher. This is primarily due to the low volumetric heat density of helium, which necessitates large volumes of helium to achieve effective heat transfer. Consequently, this large volume of helium must be pumped at high flow rates, resulting in increased pumping requirements. The combination of large volumes and high flow rates leads to higher capital and operational costs. However, employing liquid metals on both the primary and secondary sides presents the most cost-effective combination. The findings also indicate that using particles may be economically feasible compared to the use of traditional high-temperature coolants like helium.

## 6 Economic comparison of He-molten salt-air IHX with moving packed bed heat exchanger

An economic analysis has also been conducted for the combination of helium (primary media), molten salt (secondary media), and air (tertiary media) for process heat application, with a heat duty of 10 MW (Figure

**Table II. Total cost of heat exchanger for different coolant combinations and heat duty of 10 MW.**

Cost, \$	Primary	
	He	Na
He	6.74E + 05	3.22E + 05
NS	6.14E + 05	3.62E + 04
Na	3.87E + 05	2.78E + 04
Particles	4.91E + 05	7.68E + 04

7). It is found that the total cost is nearly 2.57 times higher than the moving packed bed heat exchanger, which utilizes helium as the primary media and granular particles as the secondary media. The distribution of capital and operating costs in the annual cost of these heat exchangers is presented in Figure 8. For estimating the annualized capital cost, a fractional interest rate of 5% is considered.

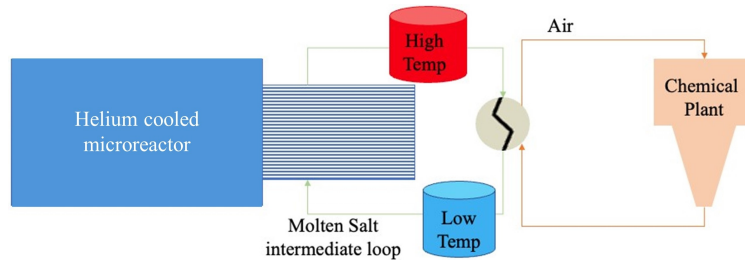


**Figure 7. Schematic of molten salt loop with traditional two-tank thermal storage to supply process heat.**

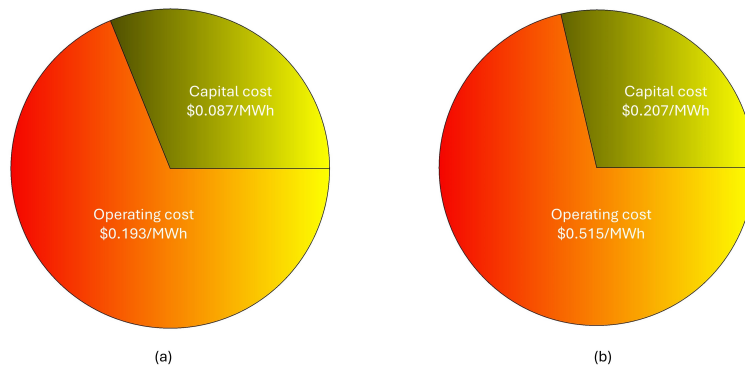


**Figure 8. Annualized cost distribution: (a) He-particles, and (b) He-molten salt-air.**

In addition to the aforementioned financial benefits, moving particles exhibit several other attractive benefits as well. These particles exhibit the benefit of being inert in nature, thus preventing the corrosion and chemical reactivity that can be found in applications where molten salts and liquid metals are used. Furthermore, due to their capability of storing energy, these particles can be used as an energy storage media, similar to the solar technology under development at Sandia National Lab. Additionally, the particles can be used as catalyst carriers for applications such as SMR for hydrogen production. All in all, the inert nature of the particles, their high chemical stability at high temperatures, their high energy storage density, and their good heat transfer characteristics make them a very suitable candidate to be considered as a heat transfer fluid.

## 7 Conclusions

In this report section, a detailed techno-economic assessment of the shell and tube exchanger for advanced nuclear applications has been conducted. The analysis takes into consideration both the design aspects (tube size and number of tubes) and the choice of working fluids, including helium, molten salts, liquid metals, and granular particles. From an economic point of view, the analysis demonstrated that as the tube diameter increases, the capital cost also increases, while the operating cost decreases due to reduced pressure drop. However, the increase in tube diameter leads to a decline in the thermal performance of the heat exchanger as the heat transfer coefficient decreases. Consequently, longer tubes are required to offset this effect, resulting in increased capital and operating costs. Considering these factors, an optimal geometry of the heat exchanger is proposed at which the total cost is minimal. The analysis also demonstrated that utilizing helium as the working fluid for both primary and secondary sides results in higher costs compared to employing liquid metal for both primary and secondary side working fluids. Furthermore, the utilization of granular particles as a heat transfer fluid proves to be an economically viable option.

## References

1. Hitesh Bindra and Shripad Revankar. *Storage and Hybridization of Nuclear Energy: Techno-Economic Integration of Renewable and Nuclear Energy*. Academic Press, 2018.
2. Vivek Utgikar, Xiaodong Sun, Richard Christensen, and Piyush Sabharwall. Advanced reactors-intermediate heat exchanger (ihx) coupling: Theoretical modeling and experimental validation. Technical report, Battelle Energy Alliance, LLC, Idaho Falls, ID (United States), 2016.
3. Kevin Albrecht, Hendrik Laubscher, Christopher Bowen, and Clifford Ho. Performance evaluation of a prototype moving packed-bed particle/sco2 heat exchanger. Technical report, Sandia National Lab.(SNL-NM), Albuquerque, NM (United States), 2022.
4. Theodore L Bergman. *Fundamentals of heat and mass transfer*. John Wiley & Sons, 2011.
5. Dusan P Sekulic and Ramesh K Shah. *Fundamentals of heat exchanger design*. John Wiley & Sons, 2023.
6. Julian D Hertel and Stefan Zunft. Experimental validation of a continuum model for local heat transfer in shell-and-tube moving-bed heat exchangers. *Applied Thermal Engineering*, 206:118092, 2022.

## **Task 5: Techno-economic feasibility of sustainable agriculture using micro reactors**

### **1 Introduction**

Ammonia is gaining recognition as a sustainable energy storage and carrier attributed to its high hydrogen content. According to available data, global ammonia production in 2019 totaled 235Mt, ranking it the second most-produced chemical commodity behind sulfuric acid [1]. The major portion of global ammonia production is utilized for fertilizer production, with the remaining serving diverse industrial applications like pharmaceuticals, plastics, textiles, fibers, explosives, and other chemicals [2]. Nitrogen-based fertilizer is pivotal in enhancing agricultural productivity and fostering crop growth that substantially contributes to the global food supply. Conventionally, ammonia is manufactured at the plants using the Haber-Bosh process at a production rate of 1000- 1500 tons per day, which uses H<sub>2</sub> produced via steam methane reforming (SMR) or coal gasification [1]. The CO<sub>2</sub> emissions (kg) for every kg of H<sub>2</sub> produced via SMR and coal gasification are around 8-12 and 18-20, respectively [3]. In biomass gasification, biomass is converted into hydrogen and other valuable products in a controlled environment using heat, oxygen, and steam [4]. The alternative pathway of H<sub>2</sub> generation from biomass is considered an environment-friendly and sustainable energy source. Compared to fossil fuels, it supports decarbonization efforts by relying on renewable feedstocks, offering carbon neutrality, reducing greenhouse gas emissions, and promoting diverse, sustainable energy options [5,6].

Koroneos et al. [7] conducted a life cycle assessment of different H<sub>2</sub> production methods. The findings underscore the potential of using biomass as a feedstock, revealing a noteworthy 63% reduction in CO<sub>2</sub> gas emissions compared to those from natural gas reforming processes. Biomass- to-H<sub>2</sub> conversion involves two main pathways: thermochemical (pyrolysis, gasification) and biological. Biological H<sub>2</sub> production uses microorganisms, including bacteria and algae, to convert organic matter into H<sub>2</sub>. The primary biological pathways for biomass-to- H<sub>2</sub> conversion are anaerobic digestion, fermentation, and photofermentation. Compared to biological processes, thermochemical processes result in a more efficient and substantial H<sub>2</sub> yield [8].

Corn and wheat are primary crops cultivated extensively worldwide, resulting in the abundant availability of agricultural residues such as corn stover and wheat straw. These residues, characterized by their cellulose and lignocellulosic composition, serve as valuable biomass resources with diverse applications [9]. Numerous studies have provided substantial evidence supporting the use of corn stover, wheat straw, and wood chips as promising feedstocks for biomass gasification, particularly in the context of H<sub>2</sub> production [10–13]. These feedstocks have significant energy potential for hydrogen generation due to their high cellulose and lignocellulosic content, which can be efficiently converted into hydrogen rich syngas. The thermochemical conversion of biomass to H<sub>2</sub>, utilizing steam as a gasification agent, demonstrates superior efficiency compared to air gasification, resulting in an increased H<sub>2</sub> yield [14]. This enhanced performance is attributed to the promotion of the water gas shift reaction, reduction in tar formation, improved process control, and the generation of a syngas composition favorable for H<sub>2</sub> production. The endothermic nature of the steam

gasification process necessitates an external energy source to facilitate the progression of the reaction. Various suggested energy sources for this process include partial combustion of organic matter, the utilization of concentrated solar energy, or nuclear energy. Numerous studies have been performed to investigate H<sub>2</sub> production using the steam gasification of biomass [15–18]. Ishaq and Dincer [19] presented an innovative biomass gasification system designed for both ammonia and power generation, featuring a process for recovering heat from high-temperature gases to supply steam for gasification. Flórez-Orrego et al. [20] carried out an exergy analysis comparing ammonia production plants based on natural gas and biomass. It is estimated that carbon emissions from the combustion of biomass are quite significant which is the heat source in the conventional biomass gasification process [21]. Sahu et al. [22] conducted a techno-economic analysis for a process that uses an electrolyte membrane water electrolyzer for hydrogen synthesis and H-B for ammonia production.

Nuclear energy is acknowledged as a clean energy source as the energy production process in nuclear power plants does not generate direct carbon emissions. Microreactors, with a thermal capacity below 20 MW, represent innovative nuclear energy technologies which have the potential to generate low-carbon electricity and process heat, presenting a distinctive advantage in efficiently delivering these benefits to remote communities through a simplified installation process [23–28]. To progress toward sustainable carbon-neutral farming, it is imperative to adopt ammonia production processes that have significantly lower greenhouse gas emissions. It is pointed out here that ammonia production requires 1/3rd of total energy consumption in the agriculture sector.

The techno-economic analysis for ammonia production based on integrated conventional biomass gasification and H-B process is available in the literature [6, 29–31]. A similar approach is used in the present work to perform the energy requirement and economic assessment of small-scale ammonia production through the Haber-Bosch (H-B) method at the local depots using a nuclear microreactor as a process heat source. Three different biomass feedstocks (corn stover, wood, and wheat straw) are considered for H<sub>2</sub> production. The economic model estimates the Levelized cost of Ammonia *LCOA* for the proposed process using the considered feedstocks. Moreover, a detailed sensitivity analysis is carried out to identify the significant parameters influencing the *LCOA*.

## 2 Process description

The primary goal of the current study is to sustainably manage a farm by converting the agriculture waste residue into hydrogen and ammonia without using carbon-emitting energy resources. The schematic of the ammonia production process used in the present study is depicted in Figure 1. The proposed process consists of various unit operations, encompassing biomass gasification, syngas cleaning and conditioning, air separation and thermochemical H-B synthesis. The energy needed for these operations is supplied by nuclear microreactor, as illustrated in Figure 1.

### 2.1 Biomass to H<sub>2</sub> production process

Biomass gasification is a thermochemical process wherein biomass undergoes conversion into a gaseous fuel known as syngas. In the present study, corn stover, wheat straw, and wood were considered as the feedstocks for the gasification process. The composition of corn stover includes stalks, leaves, and cobs, whereas wheat straw consists of stems and leaves after the harvest. Gasification can be carried out with various gasifier designs, including fixed beds, fluidized beds, and entrained bed reactors. Fluidized bed gasifiers

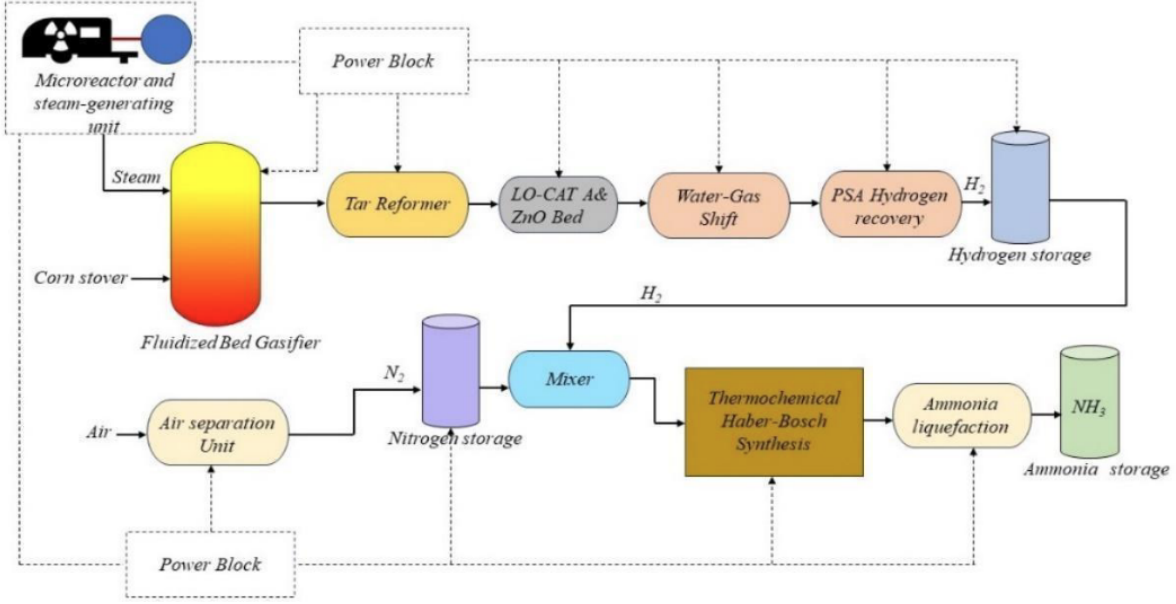
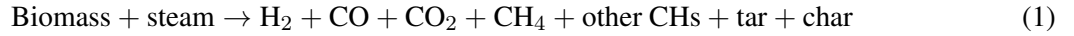


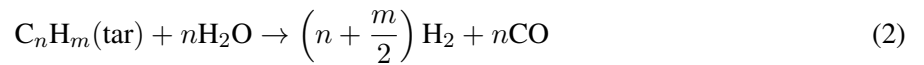
**Figure 1. Ammonia production flow diagram.**

are often preferred due to their flexibility in handling diverse feedstock qualities, high carbon conversion efficiency, minimal tar-related challenges, and the ability to maintain uniform temperature distribution. Given the unpredictable composition and moisture content of biomass, a fluidized bed gasifier was chosen to address these concerns. Steam assisted biomass gasification has demonstrated its advantages over air-blown gasification, particularly in yielding a higher amount of H<sub>2</sub> [32]. Due to the endothermic nature of this process, thermal energy is required. With the energy sourced from the nuclear microreactor, the thermochemical process of converting agriculture feedstock to hydrogen adopted is constrained by the temperature limitations of the microreactor. Therefore, the proposed gasification process is set to operate at a temperature of 650 °C. Based on the heating value of the feedstock and the gasifier efficiency presented in the literature [10], the estimated energy requirement for gasifying each kilogram of corn stover, wheat straw, and wood is approximately 2.39, 2.32 and 3.24 kWh (th), respectively. Eq. 1 represents the conversion of biomass into syngas through its reaction with steam.



The gas composition used in this analysis is drawn from the pilot-scale experiments conducted by Carpenter et al. [10], as outlined in Table I.

Upon examination of the gas composition data derived from the gasification process, it has been deduced that the H<sub>2</sub> yield is approximately 0.0133 kg per kg of corn stover, 0.0124 kg per kg of wheat straw, and 0.0196 kg per kg of wood. The gas coming out from the gasifier is directed to the tar reformer, where hydrocarbon compounds undergo conversion into CO and H<sub>2</sub>, as shown in Eq. 2.



The percentage conversion values used for each compound are shown in Table II. The overall H<sub>2</sub> yield per kilogram of biomass resulting from the catalytic steam tar reforming process was estimated to be approxi-

**Table I. Gasifier operating parameters, yields, and gas compositions in a pilot experimental study [10].**

<b>Gasifier Type</b>	<b>Fluidized Bed</b>		
<b>Temperature</b>	<b>650°C</b>		
<b>Steam/biomass feed</b>	<b>1 kg/kg</b>		
<b>Gas Composition, % Volume</b>	<b>Corn Stover</b>	<b>Wheat Straw</b>	<b>Vermont Wood</b>
H <sub>2</sub>	26.9	25.4	28.6
CO	24.7	27.5	23.5
CO <sub>2</sub>	23.7	22.0	24.0
CH <sub>4</sub>	15.3	16.3	15.5
He (tracer)	1.6	1.6	1.2
C <sub>2</sub> H <sub>4</sub>	4.2	4.3	3.9
C <sub>2</sub> H <sub>2</sub>	0.45	0.31	0.38
C <sub>3</sub> H <sub>8</sub>	0.40	0.81	0.61
C <sub>3</sub> H <sub>6</sub>	0.12	0.10	0.09
1-C <sub>4</sub> H <sub>8</sub>	0.08	0.08	0.06
2-cis-C <sub>4</sub> H <sub>8</sub>	0.02	0.00	0.00
2-trans-C <sub>4</sub> H <sub>8</sub>	0.00	0.00	0.01
H <sub>2</sub> S	-	0.08	0.00
Gas yield on a dry basis, kg/kg	0.54		
Gas yield on a dry basis, kg/kg		0.54	
Gas yield on a dry basis, kg/kg			0.74

mately 0.0374 kg for corn stover, 0.0384 kg for wheat straw, and 0.0535 kg for wood, respectively. The gas compositions, expressed in mol % on a dry basis, subsequent to the tar reforming process, are provided in Table III .

**Table II. Performance of tar reformer [12].**

<b>Compound</b>	<b>Conversion to CO and H<sub>2</sub></b>
CH <sub>4</sub>	80%
C <sub>2</sub> H <sub>4</sub>	90%
C <sub>2</sub> H <sub>2</sub>	90%
C <sub>3</sub> H <sub>8</sub>	90%
C <sub>3</sub> H <sub>6</sub>	90%

To increase the yield of H<sub>2</sub> and decrease the concentration of CO in the resulting product gas, a Water-Gas Shift (WGS) unit is utilized. The WGS reaction is shown in Eq. 3. With a CO conversion of 95% in the WGS unit [33], the overall H<sub>2</sub> yield reaches 0.0629 kg/kg of corn stover, 0.0657 kg/kg of wheat straw and 0.0876 kg/kg of wood.



A pressure Swing Absorption (PSA) unit is employed to purify the shifted gas stream, separating H<sub>2</sub> from the gas mixture containing CO<sub>2</sub> and other unreacted hydrocarbons. This purification step ensures a cleaner and more concentrated H<sub>2</sub> product. In the present study, it was assumed that the hydrogen recovery rate is

**Table III. Gas compositions after tar reformer.**

Gas composition, % mol dry basis	Feedstock type		
	Corn stover	Wheat straw	Vermont wood
H <sub>2</sub>	47.43	47.46	48.84
CO	34.06	35.58	32.81
CO <sub>2</sub>	14.87	13.26	14.99
CH <sub>4</sub>	1.92	1.97	1.94
He (tracer)	1.00	0.96	0.75
C <sub>2</sub> H <sub>4</sub>	0.53	0.52	0.49
C <sub>2</sub> H <sub>2</sub>	0.06	0.04	0.05
C <sub>3</sub> H <sub>8</sub>	0.05	0.10	0.08
C <sub>3</sub> H <sub>6</sub>	0.02	0.01	0.01
1-C <sub>4</sub> H <sub>8</sub>	0.05	0.05	0.04
2-cis-C <sub>4</sub> H <sub>8</sub>	0.01	0.00	0.00
2-trans-C <sub>4</sub> H <sub>8</sub>	0.00	0.00	0.01
H <sub>2</sub> S	0.00	0.05	0.00

85% [12], which resulted into the corresponding energy requirement of 5 kWh/kg H<sub>2</sub> for the purification process.

## 2.2 Ammonia synthesis process

The ammonia synthesis is based on the HB process, an exothermic equilibrium reaction between N<sub>2</sub> and H<sub>2</sub>, as represented by Eq 4.



The H<sub>2</sub> utilized in this process is sourced from the previously detailed biomass gasification process, while the N<sub>2</sub> is acquired through a system utilizing PSA technology. Within the PSA, surrounding air is directed through a bed of adsorbent material, notably carbon molecular sieves, and then desorbed by altering the pressure. The cavities and pores of the absorber bed facilitate a more rapid diffusion of oxygen than nitrogen. This characteristic plays a pivotal role in achieving the successful separation of nitrogen during the absorption phase. The PSA unit is estimated to consume around 0.11 kWh/kg N<sub>2</sub> [34].

The ammonia synthesis through the H-B process is conventionally executed within the temperature range of 400 to 500 °C and under a pressure ranging from 150 to 200 bar in the presence of an iron-based catalyst. These high operating conditions represent a balance between achieving faster reaction rates and adhering to Le Chatelier's principle, which states that a system in equilibrium shifts to counteract changes in pressure or temperature. In this case, while lower temperatures favor ammonia production, higher temperatures are needed for faster reaction rates. As a result, only 20-30% of the H<sub>2</sub> is converted to ammonia in each pass. To enhance the yield, a recycle loop is implemented, facilitating the reintroduction of unreacted components and promoting further reactions to maximize ammonia production. The overall cycle conversion was considered to be 97% in this study [35,36]. By taking into account this overall conversion efficiency of the H-B process,

the expected theoretical yield for ammonia is calculated to be 5.497 kg/kg H<sub>2</sub>. The energy requirement for the H-B unit is 0.725 MWh/tonne NH<sub>3</sub> [37].

Considering the overall hydrogen yield post-thermochemical gasification, encompassing the WGS reaction and gas purification via the PSA process, alongside the overall efficiency of the H-B process, energy requirements for each of these processes and a typical microreactor size of 5 MWe, annual ammonia yields are estimated to be 1811.31 tonnes, 1938.59 tonnes, and 1857.18 tonnes using corn stover, wheat straw, and wood as feedstocks, respectively, with annual feedstock requirements of approximately 5238.6 tonnes of corn stover, 5367.78 tonnes of wheat straw, and 3856.78 tonnes of wood.

### 3 Economic model

This section presents a comprehensive economic assessment of an ammonia synthesis plant employing a 5 MWe nuclear microreactor as its primary energy source. The plant utilizes corn stover, wheat straw, and wood as the feedstocks for gasification in hydrogen production and incorporates process heat and power generated by a nuclear microreactor. Figure 2 illustrates the categorization of total cost.

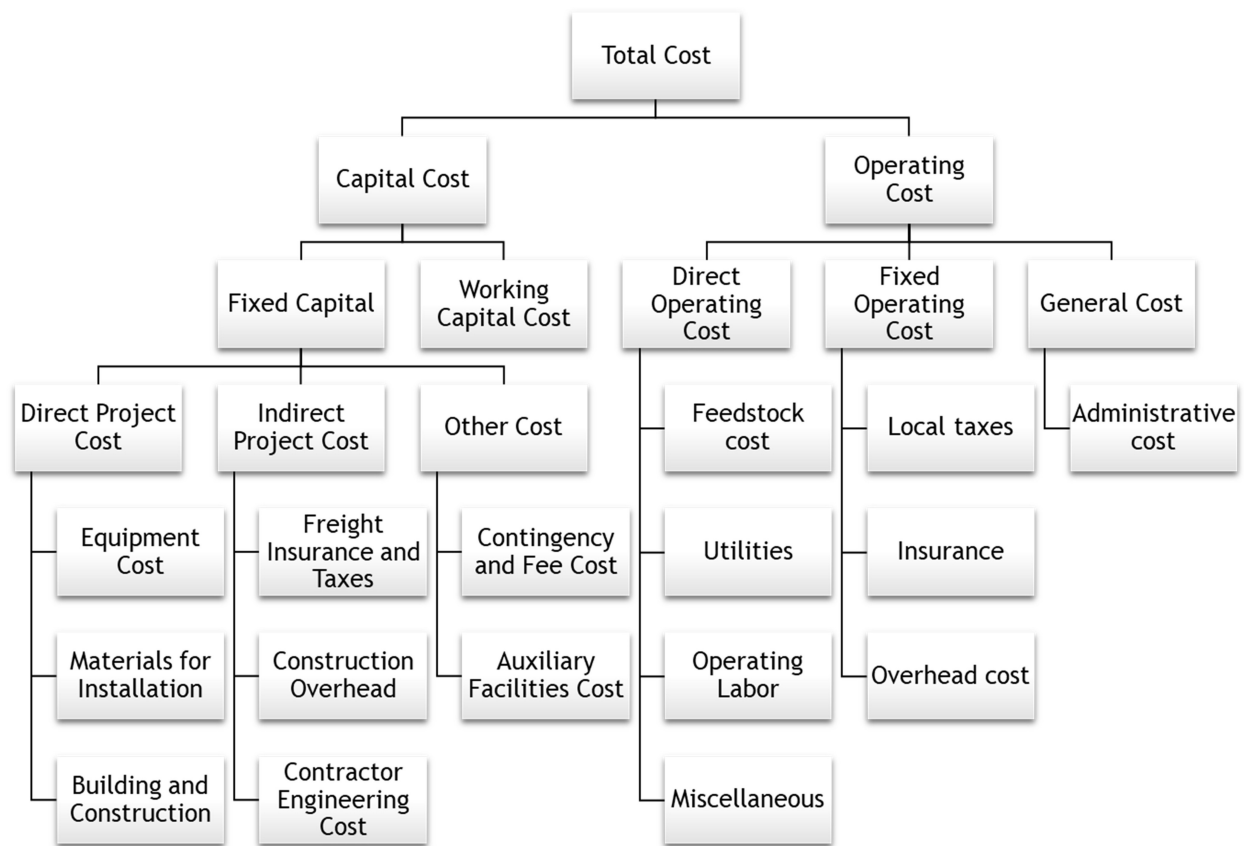


**Figure 2. Categorization of total cost. Inspiration for illustration from Refs. [38,39].**

The overall cost associated with ammonia production is composed of two high-level components: capital costs and operating costs. The total capital cost includes both fixed capital and working capital costs. The fixed capital costs encompass various components such as direct, indirect, contingency and auxiliary

costs. The direct costs constitute the principal expenses directly associated with acquiring and installing equipment. This includes the free on board cost of the equipment, the expenditure on materials required for installing the equipment, and the costs associated with labor during the installation process. The indirect costs are secondary expenses not directly linked to specific equipment but essential for the overall project. These costs include transportation expenses, construction overhead costs, and expenditures related to contractor engineering. The contingency costs represent additional funds set aside to account for unforeseen circumstances or changes that may arise during the project. The auxiliary costs are supplementary costs associated with supporting elements of the project, beyond the direct and indirect costs. The methodology adopted for the estimation of capital cost is presented in Table IV.

**Table IV. Methodology for estimating capital cost [38, 40].**

<b>Cost parameter</b>	<b>Basis</b>
Equipment cost (EC)	Exponential Economic Scaling [Eq. (5)]
Total Equipment cost (TEC)	$\sum_{i=1}^n EC_i$
Direct project cost (DPC)	1.55 TEC
Indirect project cost (IPC)	0.31 TEC
Contingency and fee cost (CFC)	0.18(DPC + IPC)
Auxiliary facilities cost (AFC)	0.3(DPC + IPC + CFC)
Fixed capital cost (FCC)	DPC + IPC + CFC + AFC
Working capital cost (WCC)	0.13 FCC
Total capital cost (TCC)	FCC + WCC

Due to the lack of precise data for evaluating the economic aspects of the designed scale plant, this study adopts an approach that involves leveraging information from available data. Considering the potential impact of inflation and deflation over time, it is essential to reevaluate and adjust all pertinent economic factors. The estimation of capital costs relies significantly on equipment costs (EC), which are computed with the help of the exponential scaling model, as shown in Eq. 5 [39].

$$EC_{2023 \text{ Aug}} = EC_{\text{ref}} \left( \frac{A}{A_{\text{ref}}} \right)^s \times \frac{CEPCI_{2023 \text{ Aug}}}{CEPCI_{\text{ref}}} \quad (5)$$

In Eq. 5, represents the  $EC_{2023 \text{ Aug}}$  anticipated equipment cost, associated with the attribute ( $A$ ) (e.g., production capacity). Moreover,  $EC_{\text{ref}}$  refers to the known equipment cost corresponding to the attribute . The CEPCI is the chemical engineering plant cost index, which ensures that the equipment cost is brought up to date and reflects the economic conditions at present (Aug 2023). The symbol ‘ $s$ ’ is the scaling scale exponent. For each process used in the study, the scaling exponent is detailed in Table V. The present economic model has been simplified by explicitly including equipment costs associated with hydrogen and ammonia production. This entails accounting for expenses associated with the gasifier, gas cleaning, tar removal, WGS reactor and PSA unit for hydrogen, as well as PSA for nitrogen and the H-B synthesis process for ammonia production (as detailed in Table VII). In the analysis, the values of  $EC_{\text{ref}}$  for gasifier, gas cleaning, tar removal, WGS reactor and PSA unit for hydrogen are taken from Spath et al. [12] while for the PSA for nitrogen and the H-B synthesis process, the values are taken from Bose et al. [37]

The integration of equipment costs related to the nuclear microreactor has been facilitated by incorporating the capital cost of the 5 MWe nuclear microreactor, as reported in the NEI report [42] and ref [43].In

**Table V. Scaling exponents for each process [41].**

Process	Scaling factor
Gasification	0.65
Reforming	0.60
Synthesis process	0.62
Separation process	0.62
Other process	0.68

the present analysis, the capital cost of an Nth-of-a-kind (NOAK) nuclear microreactor has been utilized, obtained with the help of Eq. 6 [43]:

$$\text{Cost of NOAK} = \text{Cost of FOAK} \times (1 - LR)^{\log_2 N} \quad (6)$$

Here, *FOAK* denotes first-of-a-kind, *LR* is the learning rate and *N* is the number of microreactor deployments. Corresponding parameter values used in estimating the NOAK capital cost are presented in Table VI.

**Table VI. Input parameters for estimating NOAK nuclear microreactor capital costs [42].**

Parameter	Value
Number of microreactor deployments ( <i>N</i> )	50
Cost of FOAK microreactor deployment	\$15,000
LR	10%

Operating costs constitute essential expenditures for plant operations and are incurred annually. Operating costs are typically broadly categorized into direct operating costs *DOC*, fixed operating costs *FOC*, and general and administrative costs *GAC* [39]. The *DOC* in ammonia production, encompassing items like feedstock, fuel costs, utilities, operating labor, supplies, and related costs, are directly influenced by production levels. As production increases or decreases, these costs vary accordingly. In contrast, *FOC*, which involves expenditures like taxes, insurance, and facility depreciation, remains constant irrespective of the production capacity. These costs are incurred annually and do not vary with the production volume. *GAC*, covering management, sales, financing, and research functions, are essential components necessary for the overall functioning of the business but remain independent of production levels.

The operating cost *OPC* is estimated as follows [39]:

$$OPC = DOC + FOC + GAC \quad (7)$$

$$DOC = RMC + UTC + 1.33LC + 0.069FCC + 0.03OPC \quad (8)$$

$$FOC = 0.708LC + 0.068FCC \quad (9)$$

$$GAC = 0.177LC + 0.009FCC + 0.16OPC \quad (10)$$

$$OPC = 0.180FCC + 2.73LC + 1.23(UTC + RMC) \quad (11)$$

In the above equations,  $LC$ ,  $UTC$ , and  $RMC$  represent labor cost, utility cost, and raw material cost, respectively. The cost of operating supplies, laboratory charges, insurance, taxes, and other overhead expenses are considered as factors of  $FCC$ ,  $LC$ ,  $UTC$ , and  $RMC$ .

The Levelized Cost of Ammonia  $LCOA$  serves as a critical metric for evaluating the economic aspects of the cost of producing ammonia over the lifetime of a project. Expressed as a standardized measure, the  $LCOA$  facilitate a comprehensive evaluation of the cost of ammonia production. This standardized approach enables a more straightforward comparison of various technologies or projects within the ammonia production industry. This metric takes into account both the initial capital costs and the ongoing operating costs associated with ammonia production. As shown in Eq. 12, the calculation normally entails adding the net present value of these costs and then dividing the result by the present value of total ammonia production throughout the course of the project [44]. The parameters and assumptions considered in estimating  $LCOA$  are provided in Table VII.

$$LCOA = \frac{\sum_{t=0}^{n_{life}} \frac{TCC_t + OPC_t + DC_t}{(1+r)^t}}{\sum_{t=0}^{n_{life}} \frac{P_t}{(1+r)^t}} \quad (12)$$

where the variable  $TCC_t$  is the capital cost in year  $t$ ,  $OPC_t$  is the operating cost in year  $t$ ,  $DC_t$  is the decommissioning cost associated with the nuclear microreactor in year  $t$ ,  $P_t$  corresponds to the ammonia production in year  $t$ ,  $n_{life}$  denotes the plant's operational lifespan and  $r$  is the interest rate.

## 4 Results and discussions

This section presents the economic assessment of an ammonia production facility that incorporates biomass gasification and utilizes thermal/electrical energy sourced from a 5 MWe nuclear microreactor. Utilizing the experimental findings of Carpenter et al. [10] and accounting for conversion efficiencies in key processes such as the WGS reaction and PSA as detailed in Subsection 2.1, the estimated hydrogen yield in the overall gasification process is found to be 0.0629 kg per kg of corn stover, 0.0657 kg per kg of wheat straw, and 0.0876 kg per kg of wood. Based on a theoretical yield of 5.497 kg of ammonia per kg of  $H_2$  in the H-B process and considering the energy requirements associated with each biomass feedstock and microreactor size (5 MWe), it is determined that the plant's annual ammonia production would amount to 1811.31 tonnes from corn stover, 1938.59 tonnes from wheat straw, and 1857.18 tonnes from wood. Based on the typical ammonia requirement per acre of a farm field for corn stover cultivation, which ranges from 147 to 173 pounds, [45] and the ammonia yield of the proposed process, a 5 MWe nuclear microreactor could potentially support the cultivation of corn stover on a 50×500-acre farm fields or 50 farms of 500 acres which is the typical size of a corn or wheat crop producing farm in United States.

Figure 3 illustrates the estimated ammonia production costs ( $LCOA$ ), obtained using Eq. 12, which considers the capital cost, operating cost of the plant, and decommissioning cost of the microreactor, along with the production capacity of the plant and the discount rate, from different biomass feedstocks for two different capital costs of the microreactor: Figure 3(a) is based on a capital cost of \$8276/kWe for the 50th reactor deployment, derived from a FOAK reactor cost of \$15,000/kWe and a learning rate ( $LR$ ) of 10%

**Table VII. Parameters and assumptions for the estimation of LCOA.**

<b>Parameter</b>	<b>Value</b>
Money value	US \$ (Aug 2023)
CEPCI <sub>2023 Aug</sub>	798.7
Plant lifespan	40 years
Construction year	1 year
Interest rate	8%
Inflation rate	2%
Working hours	52 weeks in a year, 6 days in a week, 8 hours per day for one shift
No of operating labor	2 laborers per shift
Efficiency of microreactor	36%
Fuel cost	\$10/MWh
Feedstock cost	\$80/tonne
Operating labor cost	\$20/h
Decommissioning cost	\$5/MWh
<b>Equipment cost estimation</b>	
<b>Equipment</b>	<b>Attribute / Designed capacity</b>
Gasifier, including gas cleaning and tar	Feedstock, tonne/day:
	Corn stover: 16.79
	Wheat straw: 17.20
WGS reactor	Vermont wood: 12.36
	Producer gas entering the shift reactor, kg/h:
	Corn stover: 816.79
PSA for hydrogen	Wheat straw: 866.95
	Vermont wood: 815.13
	kg/h (H <sub>2</sub> ):
PSA for nitrogen	Corn stover: 44
	Wheat straw: 47.10
	Vermont wood: 45.12
H-B synthesis process	kg/h (NH <sub>3</sub> ):
	Corn stover: 205.37
	Wheat straw: 219.80
	Vermont wood: 210.57
	kg/h (NH <sub>3</sub> ):
	Corn stover: 241.89
	Wheat straw: 258.89
	Vermont wood: 248.02

using Eq. 6, while Figure 3(b) is based on a capital cost of \$3996/kWe for the 50th reactor deployment, derived from a FOAK reactor cost of \$10,000/kWe and an LR of 15%. It can be observed that when wheat straw is employed as a biomass feedstock for hydrogen production, the *LCOA* is the most economical compared to other feedstocks. This cost advantage can be attributed to the higher yield of ammonia production for fixed energy input, as the energy required for wheat straw gasification is relatively lower compared to other biomass feedstocks. Although gasifying wood results in a higher hydrogen yield, requiring a smaller capacity gasifier, the mass balance analysis shows that the WGS reactor also needs a smaller capacity when using wood compared to other feedstocks (see Table VII). These reduced capacity requirements lead to a

lower unit price for both the gasifier and the WGS reactor. However, the *LCOA* for wood is still higher than for wheat straw, primarily due to the higher energy requirement.

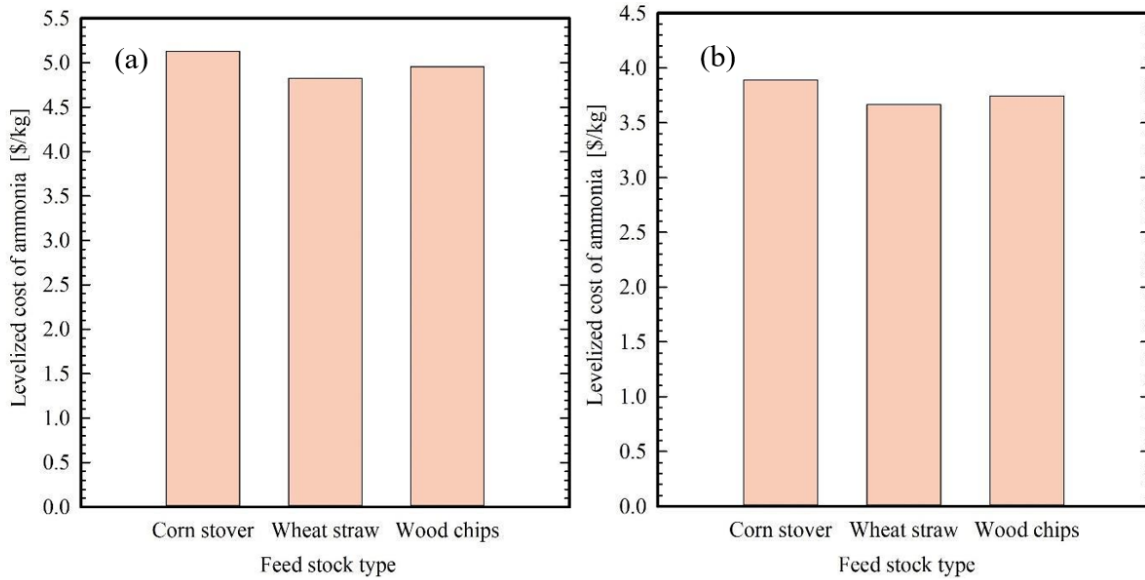


**Figure 3. Estimated levelized costs of ammonia production for different biomass feedstocks: (a) based on a capital cost of \$8276/kWe for the 50th reactor deployment, and (b) based on a capital cost of \$3996/kWe for the 50th reactor deployment.**

Table VIII presents the costs of the key process equipment used in the ammonia production process for each feedstock.

**Table VIII. Costs of the process equipment.**

Equipment	Cost, K\$		
	Corn stover	Wheat straw	Vermont wood
Gasifier, including gas cleaning and tar reformer	923.35	938.09	756.70
WGS reactor	27.45	28.45	27.41
PSA for hydrogen	104.50	111.17	106.91
PSA for nitrogen	43.43	46.19	44.43
Ammonia synthesis process	1549.06	1615.68	1573.27

To comprehend the cost contribution of individual items in each of the analyzed cases, Figure 4 showcases the breakdown of annualized total costs for ammonia production based on the capital cost of \$8276/kWe for the 50th reactor deployment. For the calculation of the annualized TCC ( $TCC_{an}$ ) presented in Figure 4, the concept of the capital recovery factor (CRF) is utilized, as illustrated in Eq.13 and 14

$$TCC_{an} = CRF \times TCC \quad (13)$$

$$CRF = \frac{r(1+r)^{n_{life}}}{(1+r)^{n_{life}} - 1} \quad (14)$$

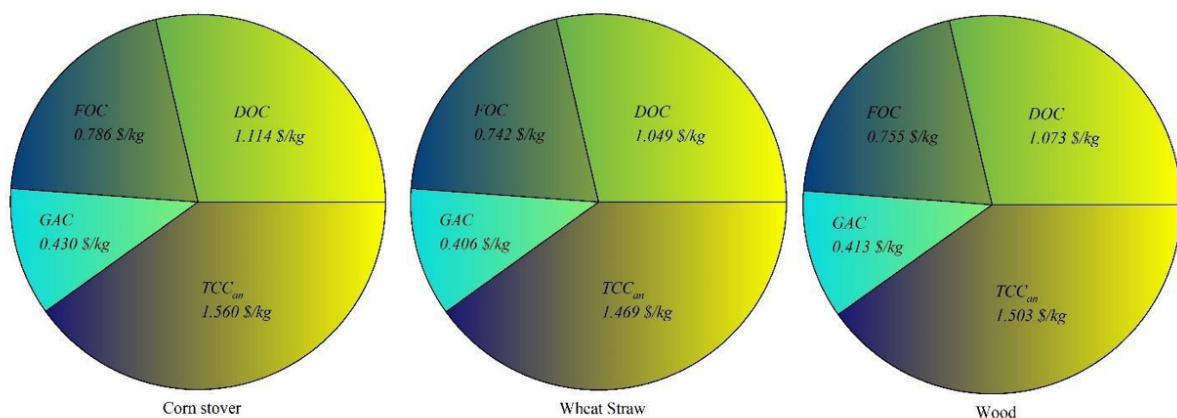


**Figure 4. Breakdown of annualized total costs associated with ammonia production.**

It is observed that the dominant cost component across all cases is the annualized  $TCC$ , which constitutes approximately 35% of the overall expenses. Following closely is the  $DOC$ , contributing around 32%. The  $FOC$  and  $GAC$  each represent approximately 19% and 13% of the overall expenses, respectively. A detailed breakdown of the capital cost of equipment shows that the microreactor cost stands out as the primary factor driving the capital cost, representing approximately 88-90% of the total. Following this, the cost share of the ammonia synthesis loop amounts to nearly 6-7% of the total equipment cost. The gasifier cost, which includes drying and tar removal processes, contributes approximately 3-4% to the total equipment cost. The remaining portion encompasses equipment costs associated with the shift reactor and the PSA unit. The breakdown of the  $DOC$  for the plant reveals that operating and supervisory labor costs constitute approximately 29%, followed by biomass feedstock costs and fuel costs, each representing 27% and 25% respectively. Maintenance and repair costs make up approximately 17% of the  $DOC$ , with the remaining portion allocated to laboratory charges.

A comprehensive sensitivity analysis has been conducted on the calculations pertaining to ammonia synthesis, specifically focusing on discerning the influence of various key parameters and underlying assumptions on the  $LCOA$ . Table IX displays the key parameters considered in the analysis, along with their corresponding upper and lower bounds values. Each parameter, such as total process equipment cost, interest rate, labor cost, and feedstock cost, is subject to a variation of  $\pm 30\%$ . However, the parameters associated with the nuclear microreactor, including the fuel cost, cost of the FOAK nuclear microreactor, and learning rate, which are pivotal factors in the analysis, undergo a slightly different adjustment as specified in the NEI report [42]. Figure 5 displays the results of the sensitivity analysis in the form of tornado charts.

The outcomes from the sensitivity analysis revealed a consistent pattern across all biomass feedstocks, underscoring the predominant influence of the financial parameters of the microreactors, such as the cost of FOAK reactor deployment and the learning rate. The process equipment cost component within the fixed capital cost, alongside the interest rate, also significantly impacts the levelized cost of ammonia. In contrast, the impact of the remaining parameters, including feedstock cost, fuel cost, and labor cost rate, was found to be relatively modest, indicating a secondary role in affecting the levelized cost of ammonia. This emphasizes the critical importance of infrastructure and operational expenses in driving economic considerations

**Table IX. Details of the parameters considered in the sensitivity analysis.**

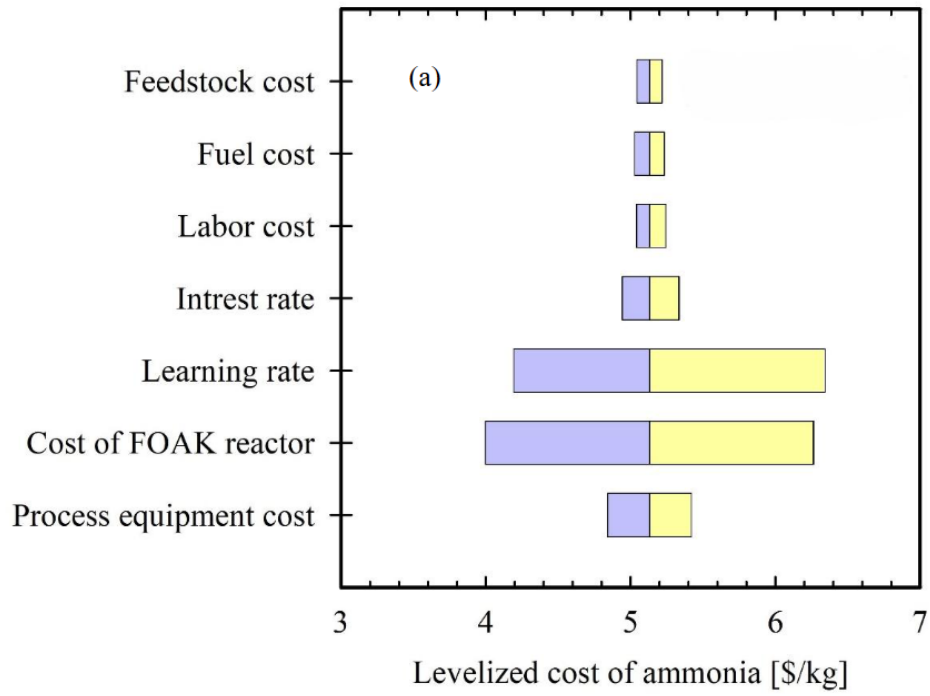
Key Parameters	Base Value	Lower Value		Upper Value	
		CS	WS	CS	WS
Total Process Equipment Cost (K\$)	938.6	657.0	650.3	1220.2	1207.7
Cost of FOAK Nuclear Microreactor (K\$/kWe)	15	10	10	20	20
Learning Rate (%)	10	15	15	5	5
Interest Rate (%)	8	5.6	5.6	10.4	10.4
Labor Cost (\$/h)	20	14	14	26	26
Fuel Cost (\$/MWh)	10	6	6	14	14
Feedstock Cost (\$/t)	80	56	56	104	104

for ammonia production from diverse biomass sources using a nuclear microreactor as an energy source. A pivotal factor in reducing the total cost of ammonia production from biomass using present technology is making nuclear microreactor technology cost-competitive with conventional energy sources.

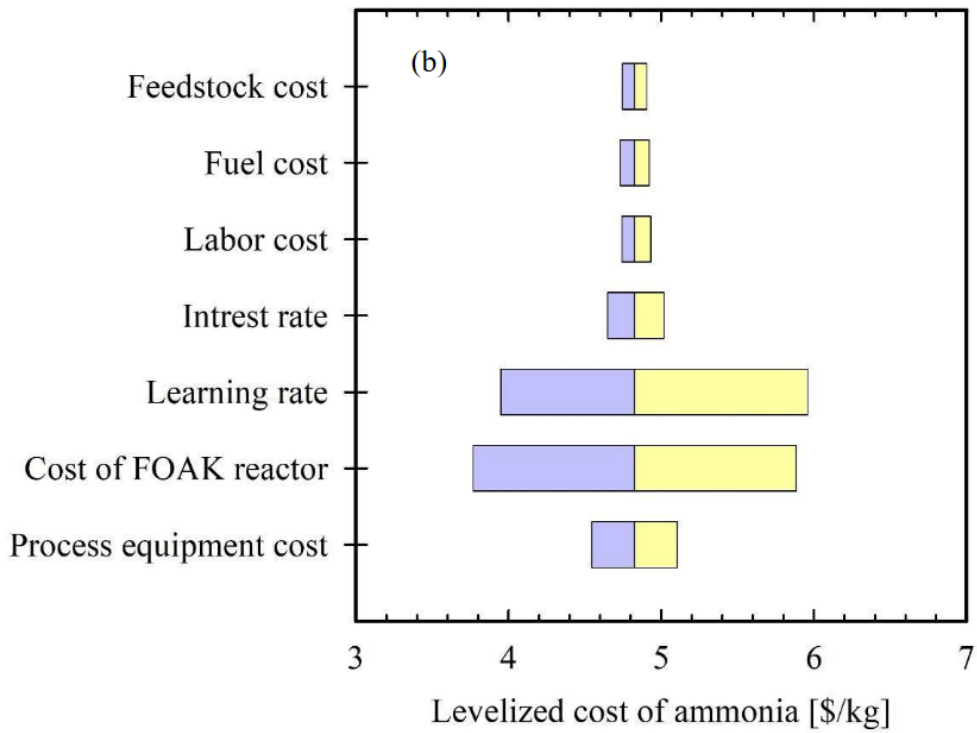
The predicted results indicate that when the cost of the *FOAK* reactor deployment is reduced from \$20,000/kWe to \$15,000/kWe, such that the cost of the 50th reactor deployment at a learning rate of 10% becomes \$8276/kWe using Eq. 6, the *LCOA* is significantly reduced. For corn stover, wheat straw, and wood as feedstocks, the *LCOA* (\$/kg) decreases from 6.264 to 5.131, 5.884 to 4.825, and 6.059 to 4.995, respectively. Furthermore, by further reducing the cost of *FOAK* reactor deployment to \$10,000/kWe, the *LCOA* for corn stover, wheat straw, and wood as feedstocks are; reduced to \$3.998/kg, \$3.767/kg, and \$3.850/kg, respectively.

As previously mentioned, the learning rates of nuclear microreactors also significantly impact the *LCOA*. These learning rates are expected to range between 5% and 15% [42]. By maintaining a learning rate of 15% and the cost of the *FOAK* at \$10,000/kWe, the cost of the 50th reactor deployment is \$3996/kWe and *LCOA* is estimated to be \$3.890/kg for corn stover, \$3.666/kg for wheat straw, and \$3.744/kg for wood as feedstocks. In addition to the microreactor capital cost, the results are highly sensitive to the capital cost assumptions of the process equipment. In particular, a 30% decrease in process equipment cost corresponds to a roughly 6-10% reduction in the *LCOA*. To further examine the influence of individual process equipment cost assumptions on *LCOA*, a sensitivity analysis was conducted by varying individual process equipment costs by  $\pm 30\%$  relative to the base value. This analysis specifically targeted prominent process equipment, namely the gasifier and ammonia synthesis loop, which collectively contribute significantly to the total process equipment cost. The results of this analysis are illustrated in Figure 6. For a  $\pm 30\%$  variation in gasifier prices, the *LCOA* for corn stover, wheat straw, and wood ranges from \$5.03 to \$5.232/kg, \$4.729 to \$4.921/kg, and \$4.874 to \$5.035/kg, respectively. Similarly, the *LCOA* for each biomass feedstock experiences a variation of  $\pm \$0.17/\text{kg}$ ,  $\pm \$0.165/\text{kg}$ , and  $\pm \$0.169/\text{kg}$  from the base values (\$5.131/kg, \$4.825/kg, and \$4.955/kg for corn stover, wheat straw, and wood, respectively) when the ammonia synthesis capital cost is adjusted by  $\pm 30\%$ . This variation in *LCOA* due to the cost variation of the ammonia synthesis process equipment is nearly double the variation in *LCOA* resulting from the cost variation of the gasifier.

The *LCOA* obtained from the current technology was compared with the findings of other studies analyzing the economic aspects of ammonia production from biomass using conventional techniques, as illustrated in Table X. In conventional biomass gasification, the energy required for the reactions is derived from the combustion of char [29]. Additionally, Table X presents the predicted *LCOA* based on the integrated ammonia synthesis loop process and hydrogen production through a conventional electrolysis process using



(a)



(b)

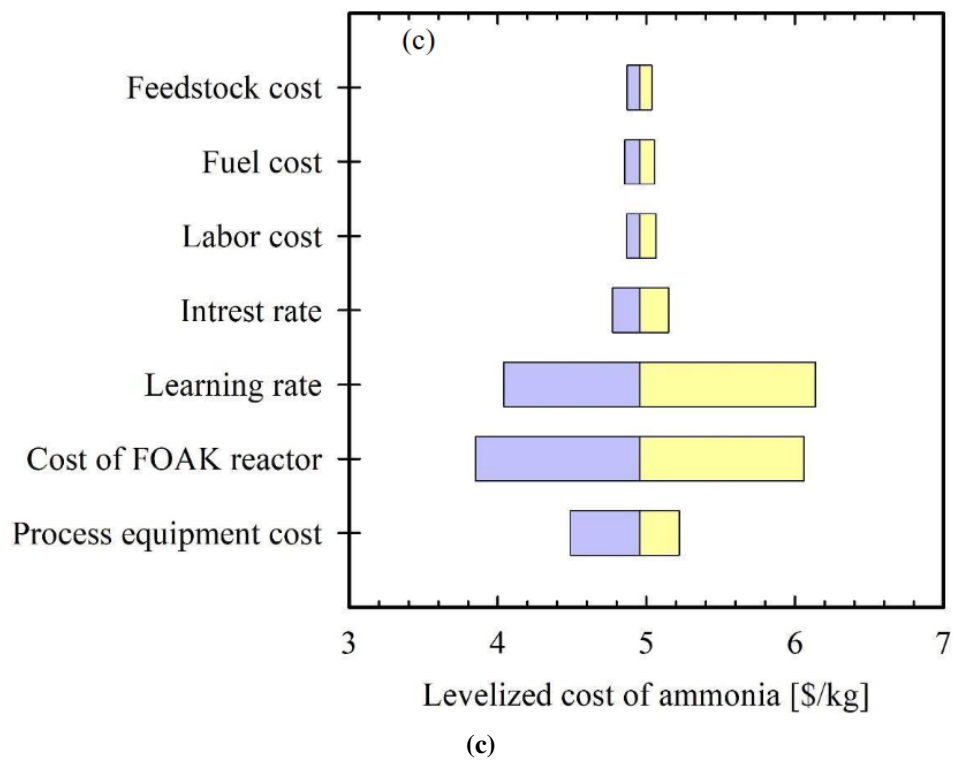


**Figure 5. Sensitivity analysis of LCOA based on low and high values for key model inputs, considering different feedstocks—(a) corn stover, (b) wheat straw, and (c) wood. Purple color represents values lower than the base value, and yellow color represents values higher than the base value.**

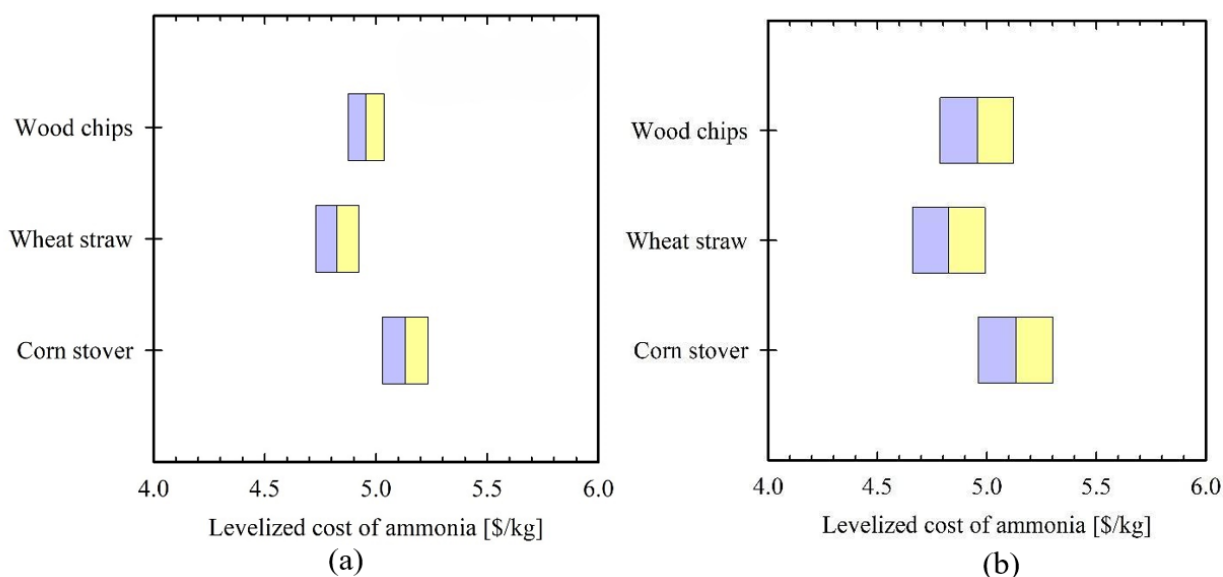


**Figure 6. Sensitivity analysis of LCOA with  $\pm 30\%$  equipment cost variations for (a) gasifier, gas cleaning, and tar reformer; (b) H-B ammonia synthesis loop. Purple colour represents values lower than the base value, and yellow colour represents values higher than the base value.**

nuclear power. For the estimation of *LCOA* in this scenario, the initial step involved is acquiring the cost of hydrogen production from the conventional electrolysis process. This was achieved through the utilization of the HydCalc tool developed by the International Atomic Energy Agency (IAEA) [46]. Within this tool, the hydrogen requirement is set at 329.5 tonnes, 353.6 tonnes and 337.9 tonnes. These values correspond to the equivalent hydrogen produced from the gasification of corn stover, wheat straw, and wood, respectively. In addition to hydrogen, the unit cost of electricity was set at \$0.21/kWh [42]. The total cost of hydrogen was estimated to be \$ 4.72M, \$ 5.06M and \$ 4.84M for the respective hydrogen requirements of 329.5 tonnes, 353.6 tonnes and 337.9 tonnes. Once the cost of hydrogen production was determined, it served as the feedstock cost for the subsequent ammonia synthesis process. The remaining operating parameters, encompassing operating labor, electrical power for PSA for  $N_2$ , and the H-B process, remained consistent with those utilized in previous analyses. The equipment cost for this case included PSA for  $N_2$  and the ammonia synthesis loop. The economic assumptions also remained consistent with those used previously. It can be seen that the cost of ammonia produced from the proposed concept is currently more economical than that of integrated conventional electrolysis using nuclear power and the Haber-Bosch process. However, the higher cost is largely due to the estimated hydrogen demand cost. Although ammonia production from the proposed technology is not yet competitive with conventional methods, there is potential for cost reduction through standardization and supply chain improvements in the microreactor, which in turn can make the proposed technology directly competitive with conventionally produced ammonia.

## 5 Conclusions

The escalating threat of climate change and environmental degradation is driving renewed interest in nuclear energy as a reliable, low-carbon power source. Among emerging nuclear technologies, microreactors show significant promise for providing low-carbon energy, capable of generating between 1 and 20 MW of heat or electricity. Traditional ammonia production through the Haber-Bosch process, involving thermochemical

**Table X. Comparison of LCOA from various technologies.**

Technology	LCOA (\$/kg)	Remarks
Based on integrated conventional biomass gasification and H-B process [?]	1.519 (2008)	Ammonia production capacity: 10 t/d; biomass type: eucalyptus; biomass price: \$16.5/t
Based on integrated conventional biomass gasification and H-B process [?]	1.153 (2016)	Ammonia production capacity: 65 t/d; biomass price: \$100/t
Based on integrated conventional electrolysis using nuclear power and H-B process	5.014 <sup>a</sup> (2023)	<sup>a</sup> Ammonia production capacity: 5.81 t/d; <sup>b</sup> Ammonia production capacity: 6.21 t/d; <sup>c</sup> Ammonia production capacity: 5.95 t/d; electricity feedstock price: \$0.21/kWh; estimated hydrogen demand cost: \$14.34/kg
This work	4.930 <sup>b</sup>	
	4.960 <sup>c</sup>	
	3.890 <sup>a</sup>	<sup>a</sup> Ammonia production capacity: 5.81 t/d; biomass type: corn stover
	3.666 <sup>b</sup>	<sup>b</sup> Ammonia production capacity: 6.21 t/d; biomass type: wheat straw
	3.744 <sup>c</sup>	<sup>c</sup> Ammonia production capacity: 5.95 t/d; biomass type: wood; biomass price: \$80/t; cost of 50 <sup>th</sup> reactor deployment: \$3966/kWe

conversion of biomass for hydrogen production, is highly energy-intensive. This paper presents the economic analysis of ammonia production by integrating a 5 MWe nuclear microreactor as the energy source within the Haber-Bosch process, along with thermochemical biomass gasification. Three different biomass feedstocks—corn stover, wheat straw, and wood—were considered. The findings indicate that the anticipated yield of ammonia production using a 5 MWe nuclear microreactor is sufficient to meet the annual ammonia requirements for a 50×500-acre farm field. The current estimate suggests that LCOA based on the proposed technology is higher than integrated conventional biomass gasification and H-B process. However, the ammonia production route presented here is conceived to be lower in carbon emissions. The economic analysis highlighted the significant sensitivity of the LCOA to the capital cost of the nuclear microreactor, with the microreactor’s capital expenses representing nearly 86% of the total plant cost. In order to make the LCOA competitive with conventional technology, the cost of microreactor needs significant reduction. There exists a potential for this reduction through supply chain, and technology maturity. Moreover, the cost of the proposed approach is significantly lower than the conventional electrolysis using nuclear power and H-B process.

## References

1. Seyedehhoma Ghavam, Maria Vahdati, IA Grant Wilson, and Peter Styring. Sustainable ammonia production processes. *Frontiers in Energy Research*, 9:580808, 2021.
2. International Energy Agency. Executive summary – ammonia technology roadmap – analysis - iea, 2021. Accessed: December 8, 2024.

3. Thomas Koch Blank and Patrick Molly. Hydrogen's decarbonization impact for industry. *Near-term challenges and long-term potential*. Rocky Mountain Institute, 2020.
4. Haris Ishaq and Curran Crawford. Review of ammonia production and utilization: Enabling clean energy transition and net-zero climate targets. *Energy Conversion and Management*, 300:117869, 2024.
5. Prakash Parthasarathy and K Sheeba Narayanan. Hydrogen production from steam gasification of biomass: influence of process parameters on hydrogen yield—a review. *Renewable energy*, 66:570–579, 2014.
6. Paul Gilbert, Sarah Alexander, Patricia Thornley, and John Brammer. Assessing economically viable carbon reductions for the production of ammonia from biomass gasification. *Journal of cleaner production*, 64:581–589, 2014.
7. C Koroneos, Aris Dompros, George Roubas, and Nicolas Moussiopoulos. Life cycle assessment of hydrogen fuel production processes. *International journal of hydrogen energy*, 29(14):1443–1450, 2004.
8. Nowilin James Rubinsin, Nabila A Karim, Sharifah Najiha Timmiati, Kean Long Lim, Wan Nor Roslam Wan Isahak, and Manoj Pudukudy. An overview of the enhanced biomass gasification for hydrogen production. *International journal of hydrogen energy*, 49:1139–1164, 2024.
9. G Ginni, S Kavitha, Yukesh Kannah, Shashi Kant Bhatia, Adish Kumar, M Rajkumar, Gopalakrishnan Kumar, Arivalagan Pugazhendhi, Nguyen Thuy Lan Chi, et al. Valorization of agricultural residues: Different biorefinery routes. *Journal of Environmental Chemical Engineering*, 9(4):105435, 2021.
10. Daniel L Carpenter, Richard L Bain, Ryan E Davis, Abhijit Dutta, Calvin J Feik, Katherine R Gaston, Whitney Jablonski, Steven D Phillips, and Mark R Nimlos. Pilot-scale gasification of corn stover, switchgrass, wheat straw, and wood: 1. parametric study and comparison with literature. *Industrial & Engineering Chemistry Research*, 49(4):1859–1871, 2010.
11. Luis M Gandia, Gurutze Arzamedi, and Pedro M Diéguez. *Renewable hydrogen technologies: production, purification, storage, applications and safety*. Newnes, 2013.
12. P Spath, A Aden, T Eggeman, M Ringer, B Wallace, and J Jechura. Biomass to hydrogen production detailed design and economics utilizing the battelle columbus laboratory indirectly-heated gasifier. Technical report, National Renewable Energy Lab.(NREL), Golden, CO (United States), 2005.
13. Ziyin Zhang and Shusheng Pang. Experimental investigation of tar formation and producer gas composition in biomass steam gasification in a 100 kw dual fluidised bed gasifier. *Renewable Energy*, 132:416–424, 2019.
14. Yohanes Andre Situmorang, Zhongkai Zhao, Ping An, Tao Yu, Jenny Rizkiana, Abuliti Abudula, and Guoqing Guan. A novel system of biomass-based hydrogen production by combining steam bio-oil reforming and chemical looping process. *Applied energy*, 268:115122, 2020.
15. J Barco-Burgos, J Carles-Bruno, U Eicker, AL Saldana-Robles, and V Alcántar-Camarena. Hydrogen-rich syngas production from palm kernel shells (pks) biomass on a downdraft allothermal gasifier using steam as a gasifying agent. *Energy Conversion and Management*, 245:114592, 2021.
16. Sylvain Fremaux, Sayyed-Mohsen Beheshti, Hojat Ghassemi, and Rasoul Shahsavan-Markadeh. An experimental study on hydrogen-rich gas production via steam gasification of biomass in a research-scale fluidized bed. *Energy Conversion and Management*, 91:427–432, 2015.

17. Hilal Sayhan Akci Turgut and Ibrahim Dincer. Novel hydrogen and biomethanol production from pinecone biomass using an integrated steam gasification system. *Energy Conversion and Management*, 310:118474, 2024.
18. Jingang Yao, Michael Kraussler, Florian Benedikt, and Hermann Hofbauer. Techno-economic assessment of hydrogen production based on dual fluidized bed biomass steam gasification, biogas steam reforming, and alkaline water electrolysis processes. *Energy Conversion and Management*, 145:278–292, 2017.
19. H Ishaq and I Dincer. A novel biomass gasification based cascaded hydrogen and ammonia synthesis system using stoichiometric and gibbs reactors. *Biomass and Bioenergy*, 145:105929, 2021.
20. Daniel Flórez-Orrego, François Maréchal, and Silvio de Oliveira Junior. Comparative exergy and economic assessment of fossil and biomass-based routes for ammonia production. *Energy Conversion and Management*, 194:22–36, 2019.
21. John D Serman, Lori Siegel, and Juliette N Rooney-Varga. Does replacing coal with wood lower co2 emissions? dynamic lifecycle analysis of wood bioenergy. *Environmental Research Letters*, 13(1):015007, 2018.
22. Saket Sahu, Nitish Srivastava, Pratham Arora, Indraneel Natu, Amit C Bhosale, Rhythm Singh, Dhirendra Tiwari, and Vineet Saini. Techno-enviro-economic evaluation of decentralized solar ammonia production plant in india under various energy supply scenarios. *Energy Conversion and Management*, 318:118908, 2024.
23. Geoffrey Black, David Shropshire, Kathleen Araújo, and Alike van Heek. Prospects for nuclear microreactors: a review of the technology, economics, and regulatory considerations. *Nuclear Technology*, 209(sup1):S1–S20, 2023.
24. Anshuman Chaube, Zayed Ahmed, Broderick Sieh, Caleb S Brooks, and Hitesh Bindra. Nuclear microreactors and thermal integration with hydrogen generation processes. *Nuclear Engineering and Design*, 419:112968, 2024.
25. Ruaridh Macdonald and John E Parsons. *The Value of Nuclear Microreactors in Providing Heat and Electricity to Alaskan Communities*. JSTOR, 2021.
26. T-Ying Lin, Ketan Ajay, and Hitesh Bindra. Numerical simulations of passive heat removal from mobile microreactors. *Nuclear Science and Engineering*, pages 1–15, 2024.
27. Molly Ross, T-Ying Lin, Isaiah Wicoff, Broderick Sieh, Piyush Sabharwall, Donald E McEligot, and Hitesh Bindra. Passive heat removal in horizontally oriented micro-htgrs. *Progress in Nuclear Energy*, 156:104530, 2023.
28. Kaeley Stevens, Joseph Oncken, Ronald Boring, Thomas Ulrich, Megan Culler, Haydn Bryan, Jeren Browning, and Izabela Gutowska. Opportunities, challenges, and research needs for remote microreactor operations. *Nuclear Technology*, pages 1–17, 2024.
29. Pratham Arora, Andrew FA Hoadley, Sanjay M Mahajani, and Anuradda Ganesh. Small-scale ammonia production from biomass: a techno-enviro-economic perspective. *Industrial & Engineering Chemistry Research*, 55(22):6422–6434, 2016.

30. Pratham Arora, Andrew FA Hoadley, Sanjay M Mahajani, and Anuradda Ganesh. Multi-objective optimization of biomass based ammonia production-potential and perspective in different countries. *Journal of cleaner production*, 148:363–374, 2017.
31. Jeffrey Ralph Bartels. *A feasibility study of implementing an Ammonia Economy*. Iowa State University, 2008.
32. Shweta Sharma Shweta Sharma and PN Sheth. Air-steam biomass gasification: experiments, modeling and simulation. 2016.
33. John Klaehn, Eric Peterson, Christopher Orme, Dhaval Bhandari, Scott Miller, Anthony Ku, Kimberly Polishchuk, Kristi Narang, Surinder Singh, Wei Wei, et al. Water-gas-shift membrane reactor for high-pressure hydrogen production. a comprehensive project report (fy2010-fy2012). Technical report, Idaho National Lab.(INL), Idaho Falls, ID (United States), 2013.
34. Bosong Lin, Theodore Wiesner, and Mahdi Malmali. Performance of a small-scale haber process: A techno-economic analysis. *ACS Sustainable Chemistry & Engineering*, 8(41):15517–15531, 2020.
35. René Bañares-Alcántara, Gerard Dericks III, Maurizio Fiaschetti, Philipp Grünewald, J Masa Lopez, Edman Tsang, Aidong Yang, Lin Ye, and Shangyi Zhao. Analysis of islanded ammonia-based energy storage systems. *University of Oxford*, 2015.
36. Kevin HR Rouwenhorst, Aloijsius GJ Van der Ham, and Leon Lefferts. Beyond haber-bosch: the renaissance of the claude process. *international journal of hydrogen energy*, 46(41):21566–21579, 2021.
37. Abhishek Bose, Nikifar Lazouski, Michal L Gala, Karthish Manthiram, and Dharik S Mallapragada. Spatial variation in cost of electricity-driven continuous ammonia production in the united states. *ACS Sustainable Chemistry & Engineering*, 10(24):7862–7872, 2022.
38. Hakkwan Kim, Prem B Parajuli, Fei Yu, and Eugene P Columbus. Economic analysis and assessment of syngas production using a modeling approach. In *2011 Louisville, Kentucky, August 7-10, 2011*, page 1. American Society of Agricultural and Biological Engineers, 2011.
39. Richard Turton, Richard C Bailie, Wallace B Whiting, and Joseph A Shaeiwitz. *Analysis, synthesis and design of chemical processes*. Pearson Education, 2008.
40. DongWon Choi, David C Chipman, Scott C Bents, and Robert C Brown. A techno-economic analysis of polyhydroxyalkanoate and hydrogen production from syngas fermentation of gasified biomass. *Applied biochemistry and biotechnology*, 160:1032–1046, 2010.
41. In Seop Gwak, Jong Ha Hwang, Jung Min Sohn, and See Hoon Lee. Economic evaluation of domestic biowaste to ethanol via a fluidized bed gasifier. *Journal of Industrial and Engineering Chemistry*, 47:391–398, 2017.
42. Marcus Nichol and H Desai. Cost competitiveness of micro-reactors for remote markets. *Nuclear Energy Institute (NEI): Washington, DC, USA*, 2019.
43. Abdalla Abou-Jaoude, Linyu Lin, Chandrakanth Bolisetti, Elizabeth Kirkpatrick Worsham, Levi Morin Larsen, and Aaron S Epiney. Literature review of advanced reactor cost estimates. 2023.
44. Ola Osman, Sgouris Sgouridis, and Andrei Sleptchenko. Scaling the production of renewable ammonia: A techno-economic optimization applied in regions with high insolation. *Journal of cleaner production*, 271:121627, 2020.

45. Gary Schnitkey, Sarah Sellars, Laura Gentry, and Carl Zulauf. Fall anhydrous ammonia application practices and profitability on fields enrolled in precision conservation management. *farmdoc daily*, 12(158), 2022.
46. IAEA. Nuclear hydrogen production. <https://www.iaea.org/topics/non-electric-applications/nuclear-hydrogen-production>, 2024. Retrieved February 14, 2024.

## **Task 5: (Contribution from Illinois) Coupling and economic analysis of nuclear microreactor enabled ammonia production – Demand side analysis**

### **1. Introduction**

Nuclear microreactors are gaining interest as the need for smaller, distributed energy sources becomes more prevalent. Compared to the current gigawatt-scale facilities, microreactors are much smaller and can be easily transported, allowing for the reduction of logistical challenges associated with large construction projects [1, 2]. As the need for carbon-free energy solutions increases, the anticipated streamlined deployment and lower capital cost of nuclear microreactors provides an opportunity for increased investment into nuclear technology amidst wavering support for its revival due to stalled projects and cost overruns in traditional nuclear construction [3, 4]. Microreactors also produce high-temperature process heat which enables their coupling with industrial processes and the potential to produce higher value products than the historical role of electricity generation.

A variety of proposed uses for microreactors have been studied in depth, from integration into existing microgrids to the powering of industrial facilities. Wodrich et al. [5] modeled a representative microgrid with heating steam and electrical loads fulfilled by fossil fueled and renewable generation and tested the deployment of a microreactor for electrical generation, direct integration into existing steam infrastructure as a nuclear boiler, and as a load conditioning device. They determined that the greatest cost savings were obtained from using a microreactor for electrical generation but noted that these benefits would be present with comparable conventional power generation methods. Lovering [6] investigated off-grid deployment of microreactors through case studies involving diesel-dependent communities such as hospitals. Their study determined that microreactors can be competitive with applications where diesel cost is high but noted that microreactors are not competitive on the U.S. electrical grid and particularly with natural gas. They suggested that the application of microreactors for industrial applications in desalination and chemical production should be evaluated. Testoni et al. [7] reviewed a study of proposed nuclear

microreactor costs and determined that microreactors are cost-competitive with diesel generators particularly due to the cost of fuel and its transportation. They also compared microreactors with distributed renewable generation and found renewables to have lower LCOEs but not being completely carbon-free due to the use of backup fossil-fuel generation. Chaube et al. [8] have studied various hydrogen production methods and microreactor designs, and the possibilities of integrating the two for nuclear microreactor hydrogen production. They concluded that all proposed microreactor designs can act as process heat sources for low-temperature hydrogen production methods, but that only select designs could provide heat at temperatures above 700 °C and that external heating might be required for optimal hydrogen producing conditions in mature thermochemical processes. Meanwhile, Kalinichenko et al. [9] modeled the pairing of a microreactor with two mature hydrogen production technologies and compared their economic viability to existing estimates of microreactor cost. They determined that at longer plant operating periods the natural gas reforming method was more competitive than the high temperature electrolysis method due to the reduced energy requirements as a result of stored chemical energy in the methane reactant. Comparing to existing microreactor cost estimates, they found that the natural gas reforming method could provide a return on investment in 21 years and the high temperature electrolysis method required above average hydrogen sale prices to provide a return on investment within 25 years.

Of the reviewed microreactor applications, hydrogen production appears to be promising for recuperating the high capital cost of the nuclear technology. However, the market for hydrogen is not well developed, with its main proposed use being as a fuel for transportation. As hydrogen fueled transportation is currently in the early stages of mass deployment, it is not likely that a large uninterrupted demand for hydrogen will exist to make a nuclear microreactor based hydrogen production facility feasible. Furthermore, the use of hydrogen for transportation requires compression to pressures between 350 bar and 700 bar, which requires significant energy [10]. One possible alternative end-product is ammonia which uses hydrogen as a precursor followed by the bonding of nitrogen and hydrogen at moderate pressure and temperature through the Haber-Bosch process. This process combines nitrogen and hydrogen at 150-200

bar, thus requiring less compression energy [11]. In contrast to hydrogen, ammonia has a well-developed market in its use in agricultural fertilizers such as urea [12]. This means that there will be a demand that can allow a microreactor-powered ammonia production facility to operate continuously at its rated output. Furthermore, ammonia is a higher value product than hydrogen and can be a more promising economic opportunity for investment in the deployment of nuclear microreactors. This is particularly true considering that ammonia pricing has been significantly elevated in recent years as observed in the ammonia market pricing shown in Figure 1.

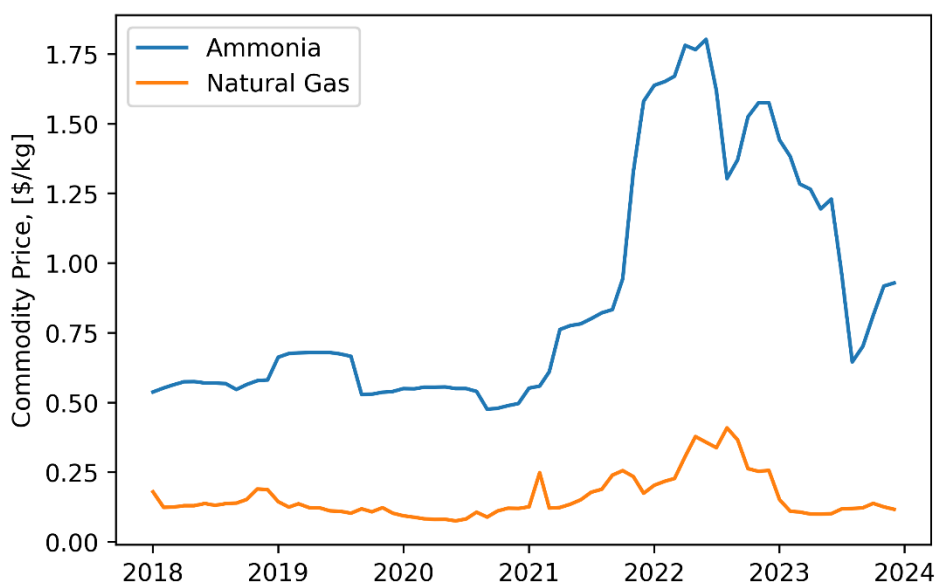


Figure 1 Historic ammonia market prices in Illinois and natural gas prices, indicating a significant rise during 2022 and 2023 [13, 14].

In the commodity pricing trends in Figure 1, the prices of ammonia and natural gas are correlated, which helps explain the rise in ammonia pricing during 2022 and 2023. For comparison, estimates for the levelized cost of hydrogen are between \$1.06-\$3.64/kg<sub>H2</sub> [15]. However, using stoichiometric ratios in the conventional Haber-Bosch process, a kilogram of hydrogen can be used to produce 11.3 kg of ammonia, which means that while hydrogen has higher price per kilogram, there is a greater economic return with ammonia production since a greater mass of ammonia can be produced.

Ammonia production has been discussed extensively in the existing literature, particularly with regard to green ammonia production. Tunå et al. [16] performed a techno-economic evaluation of ammonia production from wind electricity, biogas, and woody biomass to investigate the usage of non-fossil energy sources. They determined that with the possible exception of the biomass gasification, the methods were not cost competitive with existing fossil-fueled production, with production costs ranging from \$970/tonne for biomass to \$1725/tonne for a 3 MW electrolysis plant using wind electricity. In a more recent study, Campion et al. [17] developed a model to perform techno-economic analyses of ammonia produced using electricity from the grid or wind and photovoltaic technologies for various electrolyzers and weather profiles. They determined that the lowest production cost is achieved using solar technology in Chile, with a cost of \$926/tonne. Furthermore, they noted that production costs can be further reduced with a grid connection, achieving as low as \$835/tonne. Armijo and Philibert [18] studied the specific case of electrolyzer ammonia production from green wind and photovoltaic electricity in Chile and Argentina with regard to the challenges presented by the variability of the renewables. They determined that the ammonia producing loop required hydrogen storage to deal with the fluctuation in hydrogen production due to the fluctuating energy supply, and that increased flexibility in the Haber-Bosch process significantly decreases the amount of hydrogen that needs to be stored which decreases the corresponding cost. Considering this increased flexibility, a levelized production cost as low as \$462/tonne was achieved. Cinti et al. [19] studied the integration of solid oxide electrolyzers into ammonia production powered by renewable electricity. By modelling the system in AspenPlus and comparing to the existing natural gas method and conventional electrolysis, they determined that the electricity requirements can be significantly decreased compared to conventional electrolyzers (i.e., down to 8.30 kWh<sub>e</sub>/kg<sub>NH<sub>3</sub></sub>) but that this was still higher than that of the natural gas process at 1.77 kWh<sub>e</sub>/kg<sub>NH<sub>3</sub></sub>. Meanwhile, Wood et al. [20] considered the integration of a high temperature gas cooled nuclear reactor (HTGR) with a variety of ammonia producing cycles. They determined that using nuclear heat in the conventional gas-to-ammonia process reduced the natural gas consumption by 18% and CO<sub>2</sub> emissions by 70%, while four 600 MW<sub>th</sub> HTGRs coupled with high temperature steam electrolysis were required to achieve the same plant output as a single 450 MW<sub>th</sub> HTGR

coupled to a gas-to-ammonia process. They further determined that the integration of an HTGR with the conventional gas-to-ammonia process produced a comparable urea price to the conventional process and the U.S. urea sale price, indicating that this pathway could be promising for the reduction of natural gas usage and carbon emissions, while noting that the steam electrolysis appeared economically unviable.

With the high outlet temperatures of proposed designs, nuclear microreactors are well poised for integration with ammonia production cycles requiring high quality heat sources. The baseload operation of microreactors can help alleviate the difficulties experienced with the volatility of renewables in the search for green ammonia production technologies. Furthermore, while the economics of large-scale nuclear based ammonia production have been studied, the translation of these results to smaller scales that can be powered by microreactors requires further attention. In this work, an investigation into powering ammonia production systems based on natural gas reforming and high-temperature electrolysis with a microreactor was performed, with the two studied methods varying in the hydrogen production process. Each system configuration was optimized with the goal of maximizing the rate of ammonia production considering the assumed constraints of the microreactor and the conditions required for each of the reactions to proceed. Historic ammonia prices [13] were analyzed to generate a range of revenue estimates for each system and a theoretical gross margin (TGM) was determined by similarly analyzing historical pricing of the input feedstocks for each reaction. The TGM was used to determine the monthly income for use in a reverse amortization formula with the aim of determining the achievable principal loan (APL) for a given system configuration. Cost relations for the hydrogen and ammonia producing loops as a function of system size were used to calculate APLs representing only the microreactor and associated operating costs. This study aims to specify a range of APLs for ammonia producing systems that operate between 7-25 years to quantify the economic return of such configurations, investigate the impact of interest rates on the results, use available estimates for microreactor capital and operating costs [21] to interpret the results, and analyze the performance of the microreactor based production methods against their non-nuclear counterparts with

regard to specific energy requirements and production costs, thereby informing the extent to which ammonia production can aid in the economic viability of nuclear microreactors.

## 1. System coupling

Hydrogen production is the first key step in the production of ammonia through the Haber-Bosch cycle where hydrogen is combined with nitrogen under high pressures and with the help of catalysts [22]. Various approaches to microreactor-driven hydrogen generation have been explored in previous work [9], including natural gas reforming (NGR) and high-temperature electrolysis (HTE). Both methods work by using energy to produce hydrogen from steam (and methane in the case of NGR), with heat and some chemical reaction energy in the NGR process and electrical energy in HTE. Natural gas reforming has been shown to be the most cost competitive solution due to the considerably lower energy input due to energy chemically derived via the exothermic formation of carbon dioxide [23]. The NGR process reacts natural gas and steam under high temperatures to produce hydrogen and is currently the state-of-the-art method for commercial hydrogen and ammonia production [22]. Because NGR produces carbon dioxide, carbon capture and sequestration have to be considered in order to reduce its emissions impact. Such carbon capture and sequestration processes require energy which has to be included in the energy balance of the system. Meanwhile, HTE features lower electricity inputs than conventional low temperature electrolysis as a result of higher electrolysis efficiencies at temperatures above 650 °C [22]. At these higher temperatures heat can be used for some of the reaction input energy, bypassing losses related to the thermodynamic efficiency of electricity generation [24]. Nuclear reactors produce high temperature process heat that can be used to supply the necessary thermal energy and their coupling with industrial processes is an area of active research [9].

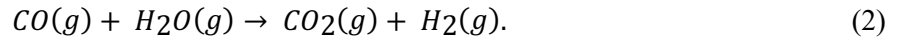
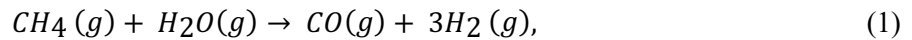
In this work, the production of ammonia using the microreactor-driven NGR and HTE processes is explored. A representative electricity conversion efficiency of 33.3% is assumed for the microreactor, modelled as a technologically agnostic source supplying thermal energy at 560 °C [9]. The ammonia synthesis is identical between the two systems and is achieved through the Haber-Bosch process. In this

process, hydrogen and nitrogen are combined at temperatures around 400 °C and pressures of about 150 bar to produce ammonia [22, 25]. This process is the main method of industrial scale ammonia production currently in use [22].

## 2.1 Natural Gas Reforming Coupled with the Haber-Bosch Process

The modelling of a microreactor coupled to natural gas reforming for hydrogen production has been investigated in detail in previous work [9], including the optimization of the system. The system for hydrogen production is modified for ammonia production by integrating a Haber-Bosch loop downstream of the produced hydrogen. A brief summary of the hydrogen producing natural gas reforming loop is provided along with the necessary modifications to obtain an ammonia producing system.

In natural gas reforming, methane is reacted with water in the Steam Methane Reforming (SMR) and Water-Gas Shift (WGS) reactions to obtain hydrogen, represented by Eq. (1) and (2) respectively,



The simplified process flow of the microreactor-driven NGR and Haber-Bosch processes in this work is presented in Figure 2, with the modifications to the system in previous work [9] highlighted.

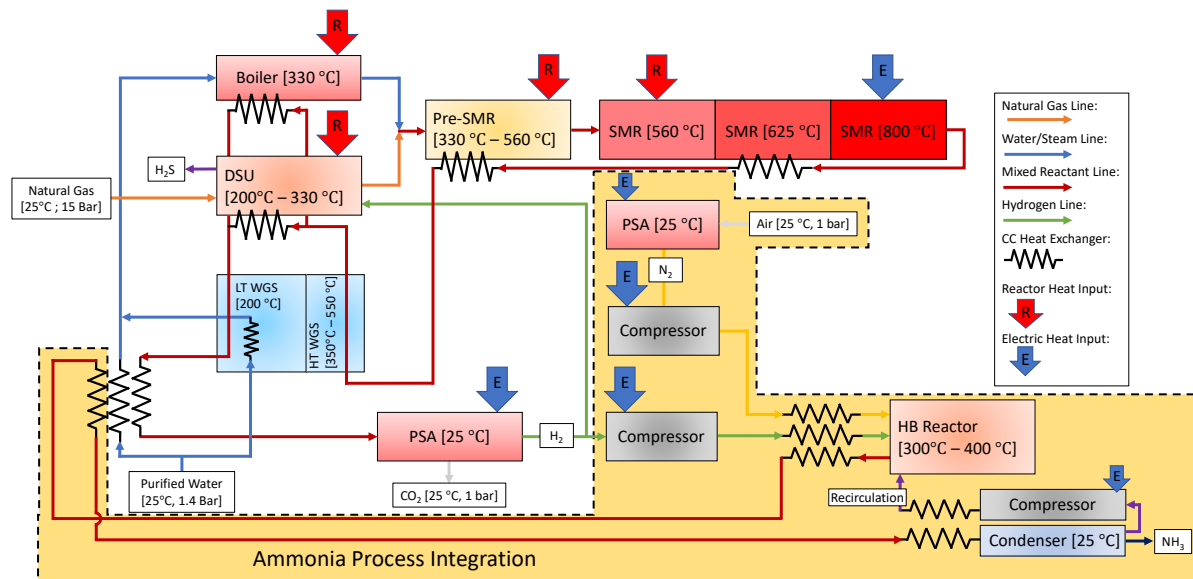
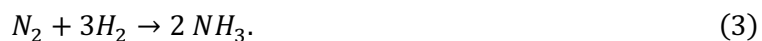


Figure 2 Process flow diagram of the microreactor driven ammonia production system with hydrogen generation via the natural gas reforming process described in the previous work [9, 26, 27, 28]. The ammonia process integration components are highlighted by the dashed area. In the ammonia generation system, the hydrogen stream enters a Haber-Bosch (HB) loop along with nitrogen separated from air through PSA. The exothermic HB reaction is used to heat the reactants for both processes through the recycling of thermal energy of the hot products using counter-current heat exchangers.

In Figure 2, pressurized streams of natural gas and purified water are fed into the plant to be heated by the reactor to the SMR reaction temperature. Pressurization occurs via isothermal compression with an assumed 50% efficiency [9]. The two streams are combined once the natural gas is desulfurized and are heated by the microreactor up to 560°C to initiate the SMR reaction. Additional energy input occurs in the form of thermal and electrical energy to drive the endothermic ( $\Delta H = 206\text{kJ/mol}$ ) reaction forward, with electrical heating used for temperatures above the microreactor process heat temperature. Multiple stages of the SMR are illustrated in Figure 2 to model reactions driven by the microreactor heat (SMR 1), by recovered heat from the hot SMR products (SMR 2), and by electrical heating at higher temperature for greater completion (SMR 3). Previous work found electrical heating to be inefficient and the optimal configuration involved only the first SMR stage [9].

Heat recovery from the hot SMR products heats the reactants using counter-current heat exchangers with an assumed recovery of 90% of the thermal energy [9]. The cooled products undergo the WGS reaction and enter Pressure Swing Adsorption (PSA) to separate the hydrogen. The hydrogen is passed into the Haber-Bosch loop at 150 bar [25] and at 200 °C, while the carbon is separated from the effluent via another PSA system for sequestration as a liquid at 140 bar [9].

The ammonia producing portion makes use of the exothermic reaction ( $\Delta H = -92\text{kJ/mol}$ ) [29] represented by,



In the ammonia production process, ambient air is first supplied to a pressure swing adsorption component to obtain nitrogen. The nitrogen is then compressed to 150 bar [25] and heated to the reactant inlet temperature of 300 °C [29]. The hydrogen from the NGR is similarly compressed and heated, with the

heating for both streams provided by the thermal energy recovered from the products of the Haber-Bosch (HB) reaction and supplemented by the nuclear microreactor. The HB reaction is exothermic, thereby raising the temperature of the exiting products to 400 °C [25], which proceed to heat the reactants for the HB and NGR reactions via heat recovery. The mixed reactant stream is then cooled to 25 °C to condense ammonia into the liquid phase for separation and storage while the unreacted gaseous nitrogen and hydrogen are returned to the HB reactor. The ammonia production reaction can proceed further towards completion at higher pressures and lower temperatures. However, the analysis performed in this work found that the electrical energy used in compression to achieve higher pressures significantly lowered the overall efficiency. Therefore, the lowest possible pressure and temperature were used when calculating the equilibrium constant [30].

Thermodynamic analysis of the processes in Figure 2 was performed according to the enthalpies of formation of the chemical species in each stream, calculated using their reference and relative values [31]. The heat input required for a process is then determined as the enthalpy difference between the outlet and inlet. The analysis was simplified by lumping heating and cooling for processes below the microreactor process heat temperature (560 °C), as appropriate for counter-current heat exchangers where the cold reactant stream is always at lower temperatures than the hot products [9].

A summary of the energy of the natural gas reformation and Haber-Bosch processes in Figure 2 is presented in Table 1 for 1 mol of natural gas at the optimal steam and natural gas mix determined in previous work [9]. The ammonia production rate of 40.1 g/s per  $MW_{th}$  can be used to scale the production rate to the desired reactor size.

Table 1 Thermodynamic summary of the energy used by the processes in Figure 2 assuming the previously determined optimal inlet mix of steam and natural gas for NGR [9] and a 1 mol natural gas input. Blue processes require electricity input, green processes recover heat, and red processes are driven by recovered heat and reactor thermal energy as needed.

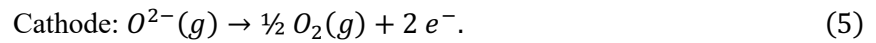
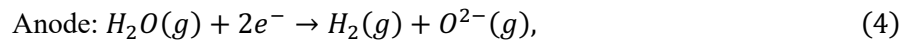
Process	$\Delta H$ (kJ)	Type	Efficiency	Process Energy (kJ)
Water Purification	0.42	Electric	1	0.42
Inlet Compression	6.77	Electric	0.5	13.5
Pre-SMR	460	Recovery + Heat	1	460
SMR 1	130	Recovery + Heat	1	130
SMR 2	0	Recovery	1	0
SMR 3	0	Electric	0.95	0
SMR 3 to SMR 2 Recovery	0	Recovery	0.9	0
SMR 3 to Lumped Recovery	-91.3	Recovery	0.9	-82.2
WGS Reaction	-69.3	Recovery	0.9	-62.4
WGS Products Recovery	-370	Recovery	0.9	-333
H <sub>2</sub> Compression	15.9	Electric	0.5	31.8
Pre CC-Compression	2.01	Electric	0.5	4.02
Carbon Capture (CC)	1.80	Electric	1	1.80
CO <sub>2</sub> Compression	5.38	Electric	0.5	10.8
Nitrogen PSA	10.1	Electric	1	10.1
Nitrogen Compression	6.24	Electric	0.9	6.93
HB Reactant Preheat	8.55	Recovery + Heat	1	8.55
HB Reaction Heat Recovery	-33.4	Recovery	0.9	-30.0
HB Products Recovery	-29.0	Recovery	0.9	-26.1
<b>Total Reactor Heat Required</b>				<b>598.01</b>
<b>Recoverable Heat</b>				<b>533.76</b>
<b>Net Reactor Heat Required</b>				<b>64.25</b>
<b>Total Electricity Required</b>				<b>79.36</b>
<b>Ammonia Produced (mol)</b>				<b>0.71</b>

## 2.2 High-Temperature Electrolysis

A microreactor-coupled high-temperature electrolysis process for hydrogen production has been modeled and optimized in previous work [9]. Similar to NGR, the system can be modified for ammonia

production by integrating a Haber-Bosch loop. A brief summary of the main steps in the HTE process is provided.

In the HTE process, steam electrolysis is performed at temperatures of 650 °C to 1000 °C, increasing the hydrogen yield relative to conventional electrolysis processes. The elevated temperature reduces the electrical energy requirements in the solid oxide electrolysis cells (SOECs) to separate hydrogen from steam [9]. The half-cell reactions are given by the following [24],



A Haber-Bosch loop was integrated into the HTE process for the production of ammonia, as illustrated by the highlighted portions in Figure 3 which represent the modifications to the HTE system from the previous work [9].

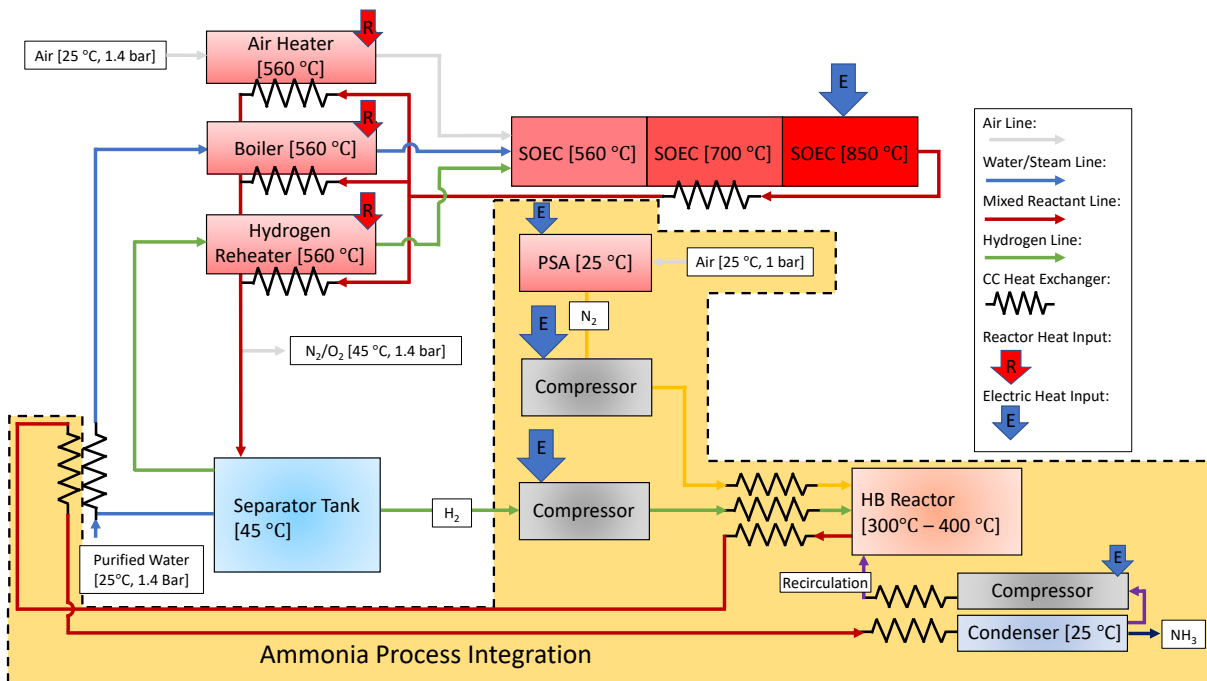


Figure 3 Process flow diagram of the microreactor driven ammonia production system with hydrogen generation via the high temperature electrolysis (HTE) process described in the previous work [9]. The ammonia process integration components are highlighted by the dashed area and are identical to that in the NGR-based process with similar process heat recovery.

In Figure 3, purified water is combined with recirculated water and heated in a heat recuperator to produce steam for the SOEC reaction. A small amount of hydrogen, used to maintain reduction conditions during electrolysis, and air, used to safely remove oxygen, are also heated in the recuperator using recovered thermal energy from hot SOEC products and supplemental reactor heat input [9]. The reactants enter the SOECs to undergo electrolysis in three stages with the aim of balancing inefficient electrical heating with lower reaction voltages at higher temperatures [9]. SOEC 1 minimizes additional heating by reacting at the microreactor process temperature but at a high electrolysis voltage. Heat generated in the SOEC 1 reaction and heat recovered from hot products raises the temperature to that of SOEC 2 which reduces the electrolysis voltage. Additional electrical heating is performed to reach a temperature of 850 °C in SOEC 3, where a thermoneutral reaction takes place. Previous optimizations of the multistage SOEC yielded a single stage operating at 850 °C as the most efficient system configuration [9].

After the SOECs, counter-current heat exchangers minimize electrical heating by heating the reactants with recovery heat as the electrolysis products are cooled. The products consist of a nitrogen-oxygen mix and a hydrogen-steam mix due to incomplete conversion of the steam, shown as a single stream in Figure 3 for simplicity.

Following the heat recuperator, the hydrogen is separated by first exhausting the nitrogen-oxygen mix and then separation of water via condensation. The hydrogen is then compressed to 150 bar [25] and reheated to the HB reactant temperature of 300 °C [29]. The HB loop is identical to that discussed for the NGR-based process where the excess thermal energy from the exothermic reaction is similarly recovered for heating the process reactants.

A summary of the energy of the HTE and Haber-Bosch processes in Figure 3 is presented in Table 2 with 1 mol of steam-hydrogen input mix [9]. In the analyzed process, no net reactor heat is required as excess heat is recovered from both the HB loop and hot SOEC products, which is simply wasted. This differs from hydrogen generated as an end product via HTE in the previous work where net reactor heat

was required due to the absence of recoverable heat from a HB process. The energy tally implies that the HTE system is not as good of a fit for the HB method of ammonia production as the NGR system, as the recovered thermal heat cannot be fully utilized due to HTE loop's already low thermal requirements. The ammonia production rate of 9.44 g/s per MW<sub>th</sub> can be used to scale the production rate to the desired reactor size.

Table 2 Thermodynamic summary of the energy used by the processes in Figure 3 assuming a 1 mol steam-hydrogen input into the cell and an SOEC reaction temperature of 850 °C. The processes are grouped by type as in Table 1.

Process	$\Delta H$ (kJ)	Type	Efficiency	Process Energy (kJ)
Water Purification	0.16	Electric	1	0.16
Recycle Compression	1.12	Electric	0.5	2.25
Inlet Air Compression	0.79	Electric	0.9	0.88
Reactant Heating	74.0	Recovery + Heat	1	74.0
SOEC 1 Power	0	Electric	1	0
SOEC 1 Heat Recovery	0	Recovery	1	0
SOEC 2 Power	0	Electric	1	0
SOEC 2 Heat Recovery	0	Recovery	1	0
SOEC 2 Reactant Heating	10.2	Recovery	1	10.2
SOEC 3 Power	233	Electric	1	233
SOEC 3 Reactant Heating	10.5	Recovery	1	10.5
SOEC 3 Reaction Heat	-33.8	Recovery	0.9	-30.5
SOEC 3 to SOEC Heating	-11.3	Recovery	0.9	-10.2
Lumped Recovery	-52.1	Recovery	0.9	-46.9
H <sub>2</sub> Compression	10.6	Electric	0.5	21.2
Nitrogen PSA	8.49	Electric	1	8.49
Nitrogen Compression	4.88	Electric	0.9	5.42
HB Reactant Preheat	9.75	Recovery + Heat	1	9.75
HB Reaction Heat Recovery	-20.9	Recovery	0.9	-18.8
HB Products Recovery	-19.3	Recovery	0.9	-17.4
<b>Total Reactor Heat Required</b>				<b>83.79</b>
<b>Recoverable Heat</b>				<b>103.05</b>
<b>Net Reactor Heat Required</b>				<b>0.00</b>
<b>Total Electricity Required</b>				<b>271.12</b>
<b>Ammonia Produced (mol)</b>				<b>0.45</b>

## 2. Economics of Microreactor-Driven Ammonia Production

A method for economic analysis of microreactor-driven industrial processes has been developed in the previous work [9] and is applied in this study. Rather than assume a price on the energy supplied by the microreactor and evaluating the cost of producing the commodity of interest, this method utilizes the market pricing of the produced commodity to estimate the revenue produced by the microreactor system. Known capital costs such as the cost of the hydrogen and ammonia producing loops are subtracted to yield a bounding Achievable Principal Loan (APL) value for the microreactor. The APL represents the loan for the microreactor's construction and operation that could be paid off with the revenue it generates. Estimates for the costs associated with a reactor between first- and nth-of-a-kind (BOAK) are presented in Table 3 and can be used to determine the viability of a given configuration according to its APL.

Table 3 Available cost estimate models for costs associated with a between first- and nth-of-a-kind (BOAK) microreactor [21].

BOAK	Nominal	Range
Overnight Capital Cost [\$/kWe]	\$8,000.00	[\$5,500 - \$10,000]
Fixed O&M Cost [\$/kWe-yr]	\$136	[\$118 - \$216]
Fuel Cost [\$/MWh]	\$11	[\$10 - \$12.10]
Variable O&M [\$/MWh]	\$2.60	[\$2.20- \$2.80]

The APL is determined by inverting the amortization formula to produce the following relation,

$$P_L = \frac{M \times n \times \left(1 - \left(1 + \frac{r}{n}\right)^{-nt}\right)}{r}, \quad (6)$$

where the  $M$  is the monthly payment in dollars,  $r$  is the interest rate over the selected period of years,  $n$  is the number of months within a year,  $t$  is the time in years, and  $P$  is the total principal loan [9]. Relations for the NGR plant cost [32] and HTE plant cost [33] as a function of the plant size have been developed, and a relation for Haber-Bosch plant cost was developed by constructing a characteristic function from values discussed by Bartels [34] in reviewing the economics of ammonia production. These relations are captured within the following,

$$Plant\ Cost\ HTE\ \left(\frac{\$}{kW_{dc}}\right) = 1.795 \times (862.9 \times k_1^{-0.501} + 570.7 \times k_1^{-0.052}), \quad (7)$$

$$Plant\ Cost\ NGR\ (\$M) = 17.896 \times s_1^{0.6773}, \text{ and} \quad (8)$$

$$Plant\ Cost\ Ammonia\ (\$M) = 2.8911 \times s_2^{0.6499}, \quad (9)$$

for the HTE, NGR, and Haber-Bosch systems, respectively. The parameters are the SOEC electrical power use  $k_1$  in  $MW_{dc}$ , the production rate of hydrogen  $s_1$  in tonnes/day, and the production rate of ammonia  $s_2$  in tonnes/day, in the ammonia loop [9]. The APL is the remaining portion of the principal loan once the known plant costs are subtracted.

### 3.1 Method for Determining Achievable Principal Loan

A method for determining the APL was developed in the previous work for hydrogen production [9] and is modified in this work for ammonia production. The APL depends on Eq. (6), which requires knowledge of the monthly payments, and the plant cost correlations in Eq. (7) to Eq. (9). The monthly payments are based on the theoretical gross margin (TGM), or ammonia spread, determined by subtracting the cost of reactant feedstock from the sale price of the produced product. This is determined separately for each plant and depends on natural gas and ammonia market pricing data.

Ammonia sold prices from 2018-2023 were analyzed, with the lowest sold price of ammonia occurring in September 2020 at \$432 per short ton or \$0.48/kg<sub>NH3</sub> and the highest sold price of ammonia occurring in June 2022 at \$1636 per short ton or \$1.80/kg<sub>NH3</sub> [13]. Similarly for natural gas cost, the lowest and highest cost during this period were \$0.0757/kg<sub>n</sub> and \$0.409/kg<sub>n</sub> in June 2020 and August 2022 respectively [14]. As with carbon capture in a previously considered NGR system for hydrogen production [9], carbon capture would allow the NGR system to benefit from a tax credit of \$85 per million tonnes of CO<sub>2</sub> for the first 12 years of operation [35, 36]. The low and high ammonia spread for the HTE and NGR is then generated by subtracting the price of the natural gas feed (if applicable) from the ammonia sale price. The NGR spread is modified by adding the tax credit based on the amount of CO<sub>2</sub> produced per kilogram of ammonia. These values are presented in Table 4.

The price of ammonia is inherently reliant on the price of natural gas, as is evident by the fact that the extremes in pricing of each commodity from 2018-2023 occur around the same time. Therefore, the range for the spread is determined by evaluating the ammonia spread at each data point in this six-year span and selecting the maximum and minimum spreads. This results in a more realistic range than simply using the maximum ammonia price and minimum natural gas price for the maximum spread, and vice versa for the minimum spread.

Table 4 Range of ammonia spreads for each production method using historical sale prices of ammonia and natural gas [13, 14]. The carbon capture tax credit is included for the NGR.

Production Method	Nominal Ammonia Spread (\$/kg <sub>NH3</sub> )	Range (\$/kg <sub>NH3</sub> )
High-Temperature Electrolysis	1.14	[0.48 – 1.80]
Natural Gas Reforming	1.44	[0.81 – 2.07]

The NGR spread needs to be modified from Table 4 if the plant lifetime is longer than 12 years to account for the expiration of the tax credit, which amounts to a decrease of \$0.47/kg<sub>NH3</sub>. This is done by evaluating a representative average spread over the entire operating period for use in Eq. (6) as determined by the following relation,

$$M_{avg} = \frac{M_{high} \times t_{high} + M_{low} \times t_{low}}{t} \quad (10)$$

where  $M_{avg}$  is the average monthly payment over the plant lifetime,  $M_{high}$  and  $M_{low}$  are the spreads during the tax credit period and after the tax credit period, respectively,  $t_{high}$  and  $t_{low}$  are the corresponding years of operating in each period, and  $t$  is the total plant lifetime which is a sum of  $t_{high}$  and  $t_{low}$  [9].

The APL used to service the microreactor costs is evaluated by first determining the spreads using Table 4 and Eq. (10). These are used as  $M$  in Eq. (6) to determine the total principal loan for the range of considered combinations of operating periods and interest rates. The APL for the microreactor is then found by using Eq. (7) to Eq. (9) to determine the portion of the total principal loan devoted to known facility

costs. For comparison across different microreactor sizes, the APLs are normalized by the microreactor capacity [9].

### **3.2 Economic Simulation of Industrial Ammonia Production Methods**

Economic simulation was done in a similar manner to that performed in the previous work for hydrogen production [9]. Accordingly, the proposed system layouts were studied for interest rates from 1% to 4%, for microreactors between 1 and 20 MW<sub>th</sub>, and for operating periods from 7 to 25 years. Similar to the results for hydrogen production, a microreactor capacity of at least 10 MW<sub>th</sub> was required to produce reasonable APL values. The principal loans for microreactors from 10 to 20 MW<sub>th</sub> at varying interest rates are presented in Figure 4, where the APL can be interpreted as the maximum project cost for the system to break even in the given amount of time.

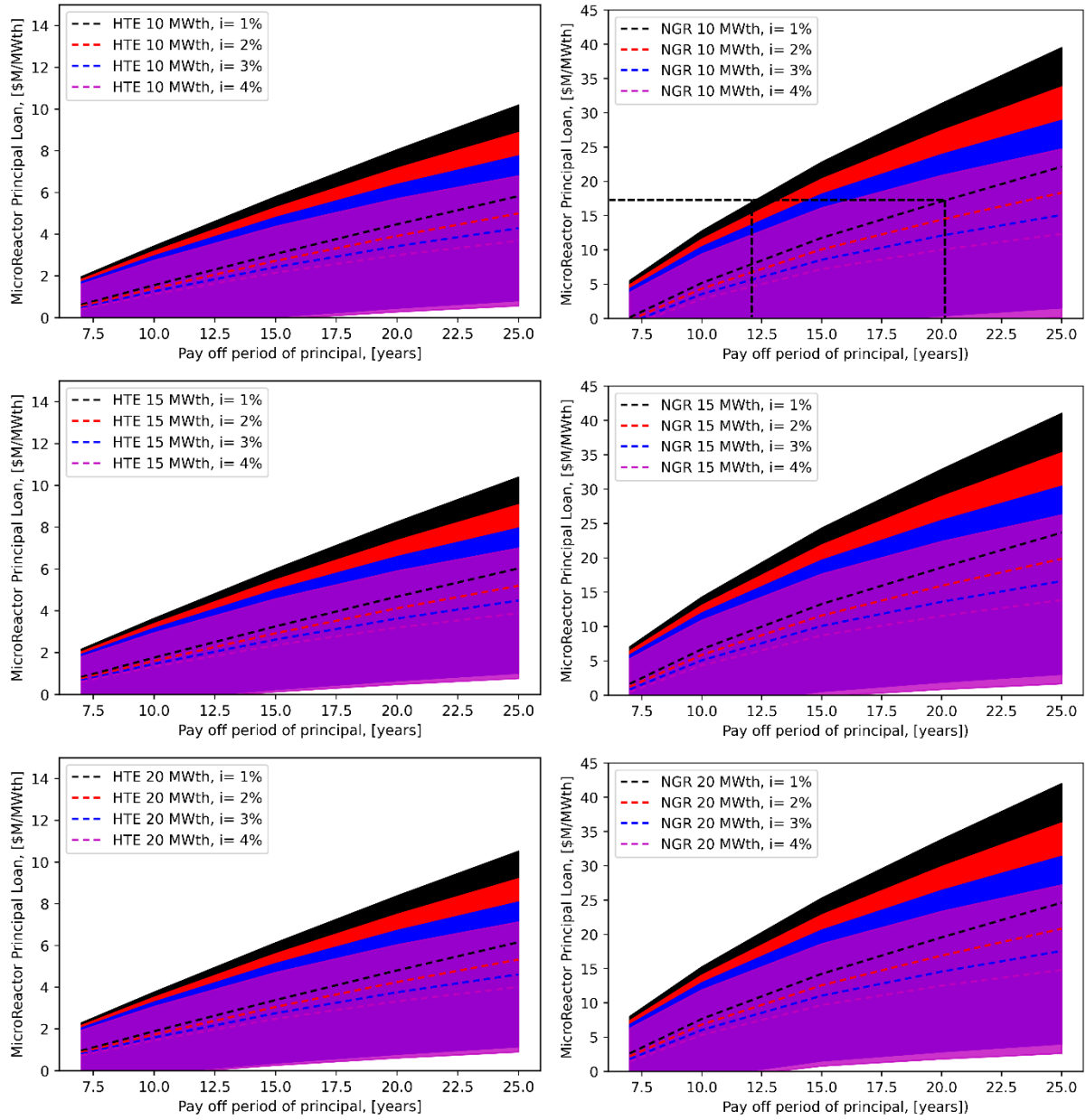


Figure 4 Achievable principal loans for various sizes of microreactor integrated HTE (left) and NGR (right) systems for multiple interest rates. The range of estimates is represented by the shaded region with a dashed line indicating the nominal values. The APLs are valid for  $\pm 1.5$  MW<sub>th</sub> relative to the considered microreactor size due to small effects from the cost of scale [9].

In Figure 4, the average APL denoted by the dashed line is the APL if the nominal ammonia spread is used, while the shaded region denotes the variation of the spread due to the variation in the commodity pricing. The APL represents the portion of the principal loan that is devoted to both the overnight capital cost of the microreactor and the operations of the microreactor throughout its operating life and is indicative

of the break-even period for various interest rates. The costs that are serviced by the APL must be lower than the APL to provide a return on investment for a chosen operating period [9].

For example, if the loan interest is 1% with a 20-year operating period for a 10 MW<sub>th</sub> microreactor coupled to an NGR-based ammonia plant, the microreactor costs must be below \$17.5M/MW<sub>th</sub> as indicated on Figure 4. If the maximum value of the spread is used, this same APL can be produced at a 12.5 operating period instead.

The trends in Figure 4 observed for ammonia production are similar to those observed for hydrogen production in previous work [9] but with larger APLs due to ammonia being a higher value product. HTE produces less ammonia than the NGR and, as a result, has less variation in the APLs. The HTE APLs do not change significantly with microreactor size while the NGR benefits greatly from economies of scale. The HTE system has a lower investment cost than the NGR system which translates to higher APLs for HTE as compared with NGR for short operating periods and smaller microreactor sizes, just as in hydrogen production [9]. For both systems, an increase in microreactor size has a positive effect, with more capital per unit of reactor energy available to break even on the project. The NGR offers the best option for the most ammonia production out of a given microreactor size which results in the larger APL, while the HTE produces fully carbon-free ammonia due to the lack of reliance on the natural gas feedstock, unlike in the NGR process.

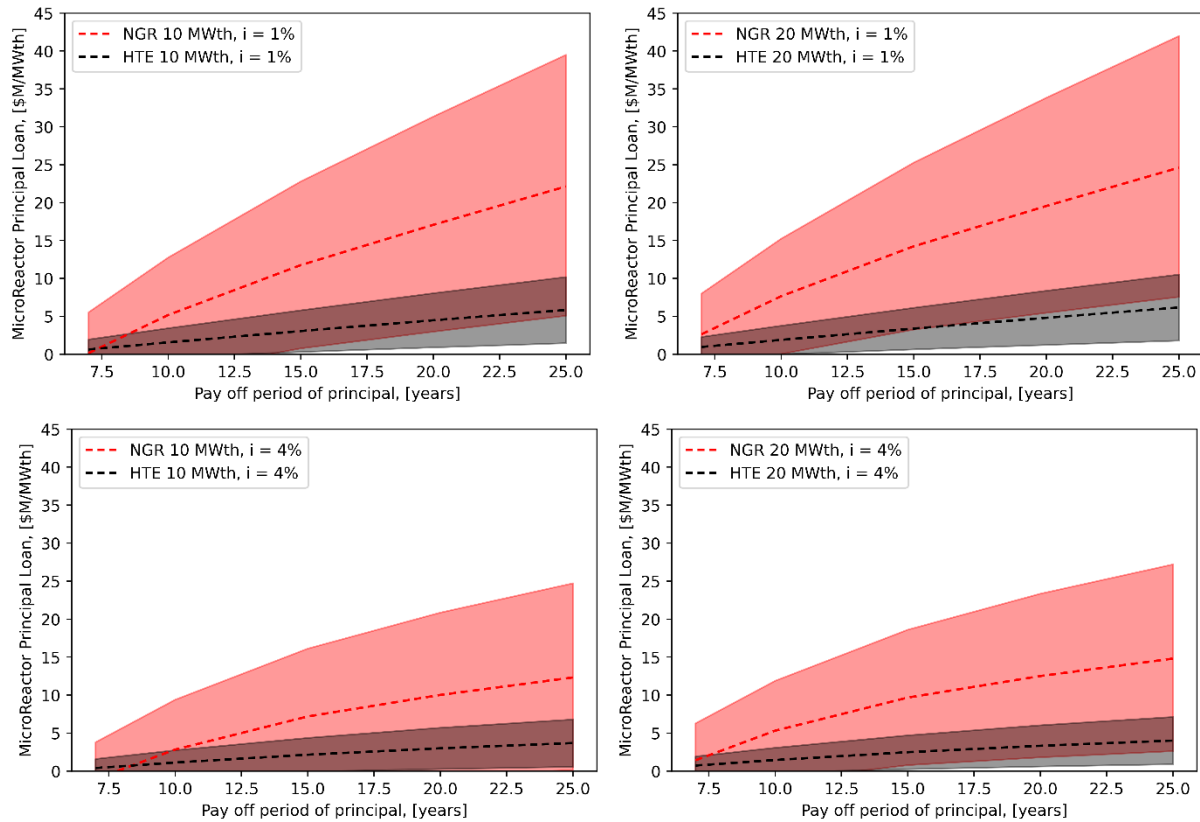


Figure 5 APLs for the NGR and HTE compared for the 10 MW<sub>th</sub> cases (left) and the 20 MW<sub>th</sub> cases (right) at 1% (top) and 4% (bottom) interest rates.

Figure 5 presents a comparison between the HTE and NGR APLs across microreactor sizes and interest rates, exhibiting similar system behavior as previously observed for microreactor-based hydrogen production [9]. Larger ammonia producing facilities produce a noticeable increase in the NGR APLs without a noticeable effect on the HTE APLs. Increasing the interest rate decreases the NGR APL more significantly than for HTE since the NGR system has a higher investment cost. At 10 MW<sub>th</sub> and 1% interest rates, the intersection of the dashed lines indicate 7.5 years of operation as the crossover after which NGR is more competitive than HTE. This moves to under 7 years when a 20 MW<sub>th</sub> microreactor is used. As the interest rate increases the intersection moves rightwards and longer operating periods are required for NGR to be more competitive. Higher interest rates and lower capacities increase the competitiveness of HTE at the nominal spreads, but NGR is more competitive for any period over 7.5 years when the maximum ammonia spread is considered due to the higher production rate of ammonia.

Table 5 shows the nominal APLs for the HTE and NGR systems, respectively, for various microreactor sizes and operating periods and using a 1% interest rate. Similar to previous work on hydrogen production [9], the HTE APL scales negligibly with plant size, as opposed to the NGR APL which benefits noticeably from increase microreactor size. The NGR system has a greater range of APLs over the 7-to-25 years operating period, which shows that the system is unable to recuperate its high cost as well as the lower-cost HTE system at shorter periods of operation but is able to do so rapidly at longer operating periods due to the high production rates. This causes the NGR to have great economic potential for longer operating periods.

Table 5 APLs at the nominal ammonia spread for the selected methods across different microreactor capacities and operating periods and at 1% interest rate.

System	Microreactor Size (MW <sub>th</sub> )	APL at 7 years (\$M/MW <sub>th</sub> )	APL at 15 years (\$M/MW <sub>th</sub> )	APL at 25 years (\$M/MW <sub>th</sub> )
HTE	10	0.62	3.05	5.83
	15	0.82	3.25	6.03
	20	0.95	3.38	6.16
NGR	10	0.14	11.7	22.1
	15	1.66	13.3	23.6
	20	2.62	14.2	24.6

To determine the feasibility of industrial ammonia microreactor systems, available cost estimate models [21] were compared against the APL estimates for 20 MW<sub>th</sub> arrangements in Figure 6. The largest studied capacity was selected since it achieved the largest APL for each respective system. Using a 1% interest rate, the NGR plant generated an APL capable of covering the cost of a microreactor at around 7.5 years of operation, while the HTE required 17.5 years. Increasing the interest rate to 4% caused the NGR to take 8.5 years and the HTE to require spreads above the nominal value to provide a return on investment in 25 years.

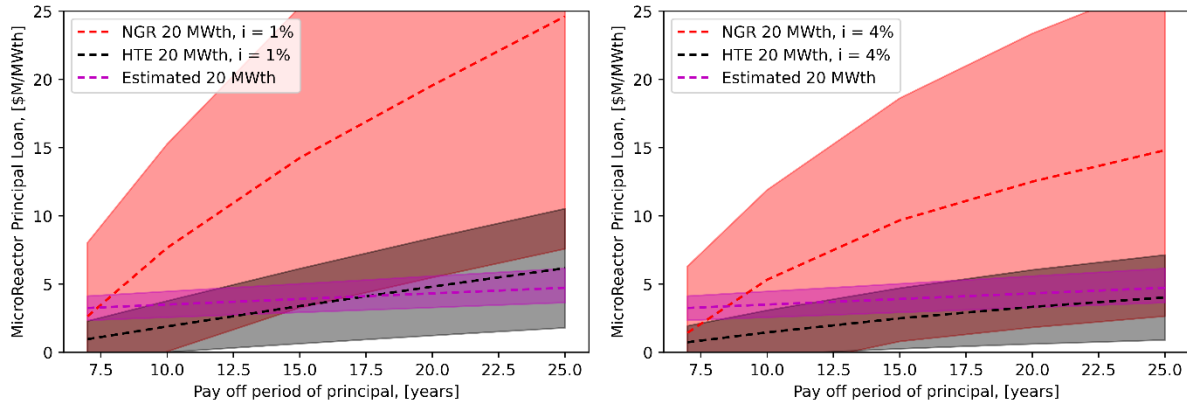


Figure 6 Available cost estimate models for a BOAK microreactor [21] and generated APLs for interest rates of 1% (left) and 4% (right).

The results in Figure 6 rely heavily on the current ammonia spread, with the upper boundary being dictated by the recent jump in prices. If prices were to trend back to their relatively stable pre-2021 values, the ammonia spread would be reduced and the breakeven point would shift rightwards in accordance with the decreased APLs. The ammonia spread for these pre-2021 price levels is close to that represented by the lower boundary for both systems. At a 1% interest rate, the breakeven point for the NGR-coupled system would be around 17 years, which is significantly shorter than the expected lifetime of the microreactor and associated ammonia production facilities, while the HTE system would take significantly longer than 25 years to break even. At a 4% interest rate, it is unlikely that either system could break even at these lower APLs as indicated by the slope of the lower boundary being essentially the same or less than that of the estimated reactor costs.

Additional costs associated with the practical construction of an integrated ammonia production facility are likely to exist, such as those related to grid interconnection for auxiliary power. Additionally, a practical system would likely need to not only provide a return on investment but also make a profit. Such considerations are outside the scope of this work. Nonetheless, the NGR's breakeven point occurring earlier than the expected lifetime of the facility makes the system promising even in light of these considerations.

### 3.3 Comparison to non-nuclear ammonia production

To better understand the coupling of a nuclear microreactor to an ammonia producing cycle, the systems studied in this work are compared with comparable non-nuclear ammonia production methods,

specifically with regard to the cost of production. The microreactor-NGR system represents the state-of-the-art fossil-fueled ammonia production method through steam methane reforming. The NGR based microreactor system in this study has a specific energy requirement of 25.0 GJ/tonne<sub>NH<sub>3</sub></sub> and emits negligible CO<sub>2</sub> due to the included carbon capture. The best available technology of fossil-fueled NGR with carbon capture requires 33.0 GJ/tonne<sub>NH<sub>3</sub></sub> and emits 0.4 tonne<sub>CO<sub>2</sub></sub>/tonne<sub>NH<sub>3</sub></sub>, while fossil-fueled NGR without carbon capture requires 26.0 GJ/tonne<sub>NH<sub>3</sub></sub> and emits 1.6 tonne<sub>CO<sub>2</sub></sub>/tonne<sub>NH<sub>3</sub></sub> [29]. Due to the extensive thermal energy recovery in the proposed system, the microreactor-NGR coupled system achieves lower energy requirements with lower CO<sub>2</sub> emissions. Using a 25-year operating period and 20 MW<sub>th</sub> system, the microreactor-NGR pairing has a production cost of \$456/tonne<sub>NH<sub>3</sub></sub> (including the nuclear microreactor cost), while estimates of fossil-fueled NGR ammonia production costs are about \$220-450/tonne<sub>NH<sub>3</sub></sub> and \$300-530/tonne<sub>NH<sub>3</sub></sub> when carbon capture is considered [37]. Using the nominal cost estimate, this means that the microreactor-NGR pairing costs \$121 more per tonne of NH<sub>3</sub> than fossil-fueled NGR and \$41 more per tonne when considering carbon capture. Using the CO<sub>2</sub> emissions of each process, a carbon price can be determined at which the microreactor-NGR pairing becomes competitive with the fossil-fueled alternatives. To be competitive with the fossil-fueled NGR, the carbon tax needs to exceed \$75.6/tonne<sub>CO<sub>2</sub></sub>, while a value of \$102.5/tonne<sub>CO<sub>2</sub></sub> is needed to compete with fossil-fueled NGR with carbon capture.

The comparable system to the microreactor-HTE coupling is a state-of-the-art green ammonia system using renewable electricity and solid oxide electrolysis cells. In such a system the lack of a high temperature heat source such as a nuclear microreactor requires electrical heating to reach the process temperatures required by the SOECs. The specific energy requirement of the HTE system in this work is 35.3 GJ/tonne<sub>NH<sub>3</sub></sub> as compared with 30.0 GJ/tonne<sub>NH<sub>3</sub></sub> for the renewable electricity driven system optimized for efficiency and 30.5 GJ/tonne<sub>NH<sub>3</sub></sub> when optimized for production cost [22]. This is likely due to the large amount of wasted thermal recovery energy in the microreactor-HTE pairing and suggests that there are further optimizations to be made in the HTE loop to allow for increased thermal energy requirements and decreased electrical energy requirements. The cost of production of these two systems can be compared by

using 25-year operating periods and the nominal reactor cost for the 20 MW<sub>th</sub> microreactor-HTE system from the available estimate [21]. For the microreactor-HTE pairing, the cost of production is \$815/tonne<sub>NH3</sub> (including the nuclear microreactor cost) as compared to \$666/tonne<sub>NH3</sub> for the renewable electricity system operating at maximum efficiency or \$544/tonne<sub>NH3</sub> for a renewable electricity system optimized to reduce production cost at the expense of efficiency [22]. Meanwhile, other studies on solar photovoltaic and wind-powered ammonia production estimate a production cost of \$835-926/tonne<sub>NH3</sub> [17].

### **3.4 Effect of microreactor process heat temperature**

The selected microreactor was assumed to have a process heat temperature of 560 °C as this value aligns with the process heat temperature from some proposed microreactor designs, as well as being approximately equal to the temperature of the secondary loop of historic and proposed high temperature gas cooled reactors (HTGRs) – a nuclear reactor technology whose high temperature enables its integration with industrial processes [38]. However, the HTGR core and primary loop can reach temperatures of up to 950 °C and if process heat could be delivered at these temperatures, it would result in more efficient systems with higher outputs. To investigate the effect that the process heat temperature has on the results of this study, the nominal APLs for a 20 MW<sub>th</sub> microreactor operating for 25 years were calculated for the two methods across various process heat temperatures and are presented in Figure 7 for the NGR system. For the HTE system, an increase in reactor process heat temperature has no effect on the APLs as the system optimized for 560 °C already operates at the maximum cell reaction temperature of 850 °C such that a higher process heat temperature does not enable the reaction to occur at higher temperatures as it does for the NGR. Furthermore, since there is sufficient unused recoverable heat, electrical heating is not necessary in this system and the potential benefit to the process by being able to heat the reactants to higher temperatures are not utilized.

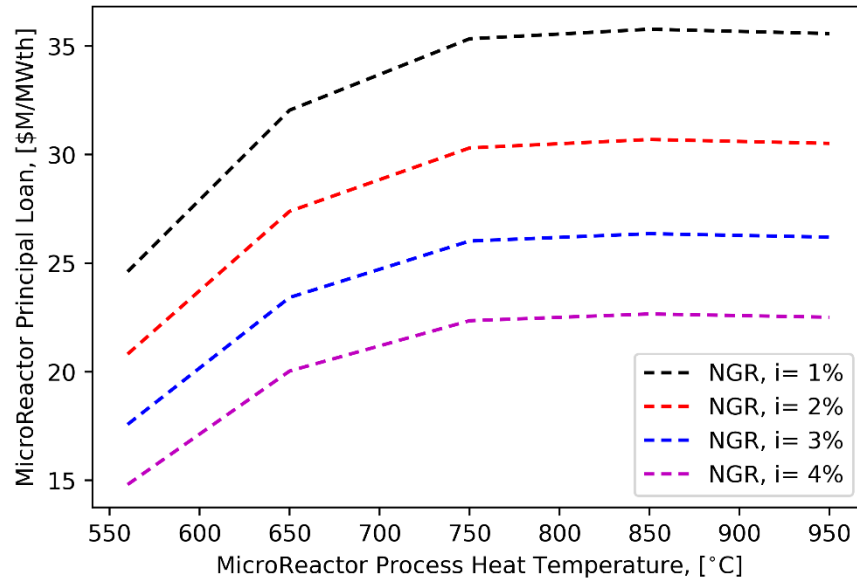


Figure 7 Variation of NGR APLs with microreactor process temperature at various interest rates.

Increasing the process heat temperature for the NGR system allows the reactions between steam and methane to occur at higher temperatures and proceed further towards completion. However, increasing the process heat temperature beyond 750 °C does not significantly increase the APL as the reaction is already proceeding to almost completion by this temperature, and when increased to 950 °C the APL decreased slightly due to the greater amount of thermal energy required to heat the reactants to such temperatures while yielding a negligible increase in the hydrogen output.

### 3. Conclusions

In this work, a method to estimate the economic performance of nuclear microreactor-driven ammonia production processes was developed. The production of hydrogen via Natural Gas Reforming (NGR) with carbon-capture, and High-Temperature Electrolysis (HTE) driven by a technology agnostic microreactor with a process heat temperature of 560 °C was analyzed thermodynamically to determine the specific (per unit MW<sub>th</sub>) production rates and resource consumption associated with these processes. The generated hydrogen was fed into a Haber-Bosch process to generate ammonia and the overall specific ammonia production rates and resource consumption were determined in a similar approach. Using the results of the thermodynamic analysis, the potential economic performance of ammonia production via a nuclear

microreactor was estimated by determining the theoretical gross margin (TGM) range associated with the production of ammonia (i.e., ammonia spread) via the NGR- and HTE-coupled processes, determining the net monthly revenue range, and calculating the Achievable Principal Loan (APL) amount under the various ammonia spreads and interest rates. The APL represents the greatest amount of loan principal that can be serviced by the net monthly revenue and was determined by an inverse of the amortization formula. The average APL associated with a 20 MW<sub>th</sub> nuclear microreactor under 1% interest rate exceeded the estimated cost of a between first-of-a-kind and nth-of-a-kind (BOAK) nuclear microreactor after 7.5 years and 17.5 years for NGR-coupled and HTE-coupled ammonia systems, respectively. At 4% interest rate, the NGR-coupled ammonia production system required only an additional year while the HTE-coupled system was unable to exceed the estimated nuclear microreactor cost in 25 years, indicating the greater economic feasibility of the NGR-coupled process under higher interest rate environments. While the results in this study were influenced by the recent jump in ammonia prices, the breakeven point associated with pre-2021 price levels for the NGR-coupled system would still only be 17 years. This indicated that ammonia production using a nuclear microreactor-driven NGR-coupled system would be economically feasible for a BOAK reactor. The two proposed systems were compared to their non-nuclear equivalent ammonia production method and it was found that the NGR required less energy per tonne than state-of-the-art fossil fueled systems but required a carbon tax of \$75.6/tonne<sub>CO2</sub> to be competitive; this increased to \$102.5/tonne<sub>CO2</sub> when comparing with systems equipped with carbon capture. The HTE based system was found to require significantly more energy to produce ammonia than comparable renewable solutions but the competitiveness in production cost was highly dependent on the assumptions about renewable electricity cost, which depended on location and the installed infrastructure. It was also determined that if higher temperature process heat from the reactor is available, the NGR based system would see a noticeable increase in its APLs, but that of the HTE based system would not be significantly changed.

## AKNOWLEDGEMENT

This material was based upon work supported by the Department of Energy Nuclear Energy University Program under Award Number DE-NE0009152 and was prepared as an account of work sponsored by an agency of the United States Government. Neither the United States Government nor any agency thereof, nor any of their employees, makes any warranty, express or implied, or assumes any legal liability or responsibility for the accuracy, completeness, or usefulness of any information, apparatus, product, or process disclosed, or represents that its use would not infringe privately owned rights. Reference herein to any specific commercial product, process, or service by trade name, trademark, manufacturer, or otherwise does not necessarily constitute or imply its endorsement, recommendation, or favoring by the United States Government or any agency thereof. The views and opinions of authors expressed herein do not necessarily state or reflect those of the United States Government or any agency thereof.

## References

- [1] Idaho National Laboratory, "Microreactors," 2024. [Online]. Available: <https://inl.gov/trending-topics/microreactors/>.
- [2] United States Department of Energy, "What is a Nuclear Microreactor," 2021. [Online]. Available: <https://www.energy.gov/ne/articles/what-nuclear-microreactor>.
- [3] United States Department of Energy, "Pathways to Commercial Liftoff: Advanced Nuclear," 2023.
- [4] C. A. Lloyd, T. Roulstone and R. E. Lyons, "Transport, constructability, and economic advantages of SMR modularization," *Progress in Nuclear Energy*, vol. 134, 2021.
- [5] L. Wodrich, A. J. H. Lee, T. Kozlowski and C. S. Brooks , "Modeling of an Energy-Diverse Embedded Grid for Microreactor Integration," *Nuclear Technology*, vol. 209, no. 6, pp. 809-834, 2022.
- [6] J. R. Lovering, "A Techno-Economic Evaluation of Microreactors for Off-Grid and Microgrid Applications," *Sustainable Cities and Society*, vol. 95, 2023.
- [7] R. Testoni, A. Bersano and S. Segantin, "Review of nuclear microreactors: Status, potentialities and challenges," *Progress in Nuclear Energy*, vol. 138, 2021.

- [8] A. Chaube, Z. Ahmed, B. Sieh, C. S. Brooks and H. Bindra, "Nuclear microreactors and thermal integration with hydrogen generation processes," *Nuclear Engineering and Design*, vol. 419, 2024.
- [9] D. Kalinichenko, L. Wodrich, A. J. H. Lee, T. Kozłowski and C. S. Brooks, "Analysis of nuclear microreactor efficacy with hydrogen production methods," *Progress in Nuclear Energy*, vol. 168, 2024.
- [10] United States Department of Energy Office of Energy Efficiency & Renewable Energy, "Dispensing Hydrogen Fuel to Vehicles," [Online]. Available: <https://www.energy.gov/eere/fuelcells/dispensing-hydrogen-fuel-vehicles>. [Accessed August 2024].
- [11] Australian Renewable Energy Agency, "Hydrogen to Ammonia Research and Development," 2018. [Online]. Available: <https://arena.gov.au/projects/hydrogen-to-ammonia/>. [Accessed August 2024].
- [12] thyssenkrupp AG, "Ammonia in agriculture: The engine of plant growth," 2024. [Online]. Available: <https://www.thyssenkrupp.com/en/stories/sustainability-and-climate-protection/ammonia-in-agriculture:-the-engine-of-plant-growth>. [Accessed September 2024].
- [13] United States Department of Agriculture, "Illinois Production Cost Report," United States Department of Agriculture.
- [14] United States Energy Information Administration, "Henry Hub Natural Gas Spot Price," United States Energy Information Administration, 2024.
- [15] E. Lewis, S. McNaul, M. Jamieson, M. S. Henriksen, H. S. Matthews, J. White, L. Walsh, J. Grove, T. Shultz, T. J. Skone and R. Stevens, "Comparison of commercial, state-of-the-art, fossil-based hydrogen production technologies," 2022.
- [16] P. Tunå, C. Hultberg and S. Ahlgren, "Techno-economic assessment of nonfossil ammonia production," *Environmental Progress & Sustainable Energy*, vol. 33, no. 4, pp. 1290-1297, 2014.
- [17] N. Campion, H. Nami, P. R. Swisher, P. V. Hendriksen and M. Münster, "Techno-economic assessment of green ammonia production with different wind and solar potentials," *Renewable and Sustainable Energy Reviews*, vol. 173, 2023.
- [18] J. Armijo and C. Philibert, "Flexible production of green hydrogen and ammonia from variable solar and wind energy: Case study of Chile and Argentina," *International Journal of Hydrogen Energy*, vol. 45, pp. 1541-1558, 2020.
- [19] G. Cinti, D. Frattini, E. Jannelli, U. Desideri and G. Bidini, "Coupling Solid Oxide Electrolyser (SOE) and ammonia production plant," *Applied Energy*, vol. 192, pp. 466-476, 2017.
- [20] R. A. Wood, R. D. Boardman and M. W. Patterson, "Nuclear-Integrated Ammonia Production Analysis," Idaho National Laboratory, 2010.

- [21] A.-J. Abdalla, L. M. Larsen, N. Guaita, I. Trivedi, F. Joseck, C. Lohse, E. Hoffman, N. Stauff, K. Shirvan and A. Stein, "Meta-Analysis of Advanced Nuclear Reactor Cost Estimations," Idaho National Laboratory, 2024.
- [22] H. Zhang, L. Wang, J. Van Herle, F. Maréchal and U. Desideri, "Techno-economic comparison of green ammonia production processes," *Applied Energy*, vol. 259, 2020.
- [23] M. U. Monir, A. A. Aziz, M. T. Ahmed and M. Y. Hasan, "Chapter 11 - Hydrogen energy—Potential in developing countries," in *Renewable Electricity and Sustainability: Prospects in Developing Economies*, 2022, pp. 299-325.
- [24] J. E. O'Brien, "Thermodynamic Considerations for Thermal Water Splitting Processes and High Temperature Electrolysis," *ASME 2008 International Mechanical Engineering Congress and Exposition*, vol. 8, pp. 639-651, 2008.
- [25] R. Steinberger-Wilckens and B. Sampson, "Chapter 8 - Market, Commercialization, and Deployment—Toward Appreciating Total Owner Cost of Hydrogen Energy Technologies," in *Science and Engineering of Hydrogen-Based Energy Technologies*, 2019, pp. 383-403.
- [26] L. O. Nord, A. Kothandaraman, H. Herzog, G. McRae and O. Bolland, "A modeling software linking approach for the analysis of an integrated reforming combined cycle with hot potassium carbonate CO<sub>2</sub> capture," *Energy Procedia*, vol. 1, no. 1, pp. 741-748, 2009.
- [27] C. Antonini, K. Treyer, A. Streb, M. van der Spek, C. Bauer and M. Mazzotti, "Hydrogen production from natural gas and biomethane with carbon capture and storage – A techno-environmental analysis," *Sustainable Energy Fuels*, no. 6, pp. 2967-2986, 2020.
- [28] R. A. Wood, R. D. Boardman, M. W. Patterson and P. M. Mills, "HTGR-Integrated Hydrogen Production via Steam Methane Reforming (SMR) Process Analysis," Idaho National Laboratory, 2010.
- [29] K. H. Rouwenhorst, P. M. Krzywda, N. E. Benes, G. Mul and L. Lefferts, "Chapter 4 - Ammonia Production Technologies," in *Techno-Economic Challenges of Green Ammonia as an Energy Vector*, 2021, pp. 41-83.
- [30] M. Mahmoud El-Gharbawy, F. Khalifa Gad and W. Mahmoud Shehata, "Simple new correlation for the prediction of equilibrium constant (KP) of Haber reaction covering the industrial conditions," *Egyptian Journal of Petroleum*, vol. 30, no. 1, pp. 11-15, 2021.
- [31] National Institute of Standard and Technology, "Thermophysical Properties of Fluid Systems," [Online]. Available: <https://webbook.nist.gov/chemistry/fluid/>. [Accessed 9 2022].
- [32] A. Oni, K. Anaya, T. Giwa, G. Di Lullo and A. Kumar, "Comparative assessment of blue hydrogen from steam methane reforming, autothermal reforming, and natural gas decomposition technologies for natural gas-producing regions," *Energy Conversion and Management*, vol. 254, no. 196, 2022.

- [33] D. S. Wendt, L. T. Knighton and R. D. Boardman, "High-Temperature Steam Electrolysis Process Performance and Cost Estimates," Idaho National Laboratory, 2022.
- [34] J. R. Bartels, "A feasibility study of implementing an Ammonia Economy," 2008.
- [35] Congress, "H.R.5376 - Inflation Reduction Act of 2022," 9 2021. [Online]. Available: <https://www.congress.gov/bill/117th-congress/house-bill/5376>. [Accessed 12 2022].
- [36] Gibson Dunn, "The Inflation Reduction Act Includes Significant Benefits for the Carbon Capture Industry," 9 2022. [Online]. Available: [https://www.gibsondunn.com/the-inflation-reduction-act-includes-significant-benefits-for-the-carbon-capture-industry/#\\_ftn5](https://www.gibsondunn.com/the-inflation-reduction-act-includes-significant-benefits-for-the-carbon-capture-industry/#_ftn5). [Accessed 2 2023].
- [37] IAEA, "The Future of Hydrogen," 2019.
- [38] K. Natesan, A. Purohit and S. W. Tam, "NUREG/CR-6824 Materials Behavior in HTGR Environments," 2003.